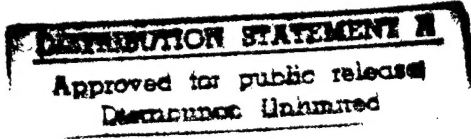


## REPORT DOCUMENTATION PAGE

Form Approved  
OMB No. 0704-0188

Public reporting burden for this collection of information is estimated to average 1 hour per response, including the time for reviewing instructions, searching existing data sources, gathering and maintaining the data needed, and completing and reviewing the collection of information. Send comments regarding this burden estimate or any other aspect of this collection of information, including suggestions for reducing this burden, to Washington Headquarters Services, Directorate for Information Operations and Reports, 1215 Jefferson Davis Highway, Suite 1204, Arlington, VA 22202-4302, and to the Office of Management and Budget, Paperwork Reduction Project (0704-0188), Washington, DC 20503.

1. AGENCY USE ONLY (Leave blank)	2. REPORT DATE 9 Jan 97	3. REPORT TYPE AND DATES COVERED	
4. TITLE AND SUBTITLE Gyrodynamic Effects of an energy Storage flywheel on the handling of a Hybrid-Electric Vehicle		5. FUNDING NUMBERS	
6. AUTHOR(S) James LaMonte Greer			
7. PERFORMING ORGANIZATION NAME(S) AND ADDRESS(ES) Purdue University		8. PERFORMING ORGANIZATION REPORT NUMBER  96-101	
9. SPONSORING/MONITORING AGENCY NAME(S) AND ADDRESS(ES) DEPARTMENT OF THE AIR FORCE AFIT/CI 2950 P STREET WPAFB OH 45433-7765		10. SPONSORING/MONITORING AGENCY REPORT NUMBER	
11. SUPPLEMENTARY NOTES			
12a. DISTRIBUTION AVAILABILITY STATEMENT Unlimited		12b. DISTRIBUTION CODE	
			
13. ABSTRACT (Maximum 200 words)			
SUBJECT TERMS		15. NUMBER OF PAGES 135	
		16. PRICE CODE	
17. SECURITY CLASSIFICATION OF REPORT	18. SECURITY CLASSIFICATION OF THIS PAGE	19. SECURITY CLASSIFICATION OF ABSTRACT	20. LIMITATION OF ABSTRACT

19970116 009

GYRODYNAMIC EFFECTS  
OF AN ENERGY STORAGE FLYWHEEL  
ON THE HANDLING  
OF A HYBRID-ELECTRIC VEHICLE

A Thesis

Submitted to the Faculty

of

Purdue University

by

James LaMonte Greer

In Partial Fulfillment of the

Requirements for the Degree

of

Master of Science in Mechanical Engineering

December 1996

## ACKNOWLEDGMENTS

I would like to dedicate this thesis to my wife Corrie, and my children, Kristin and Garrett. Without their willingness to pull up stakes and move off to West Lafayette, this would never have been possible. My success depends directly upon their patience and support. I would also like to thank my parents for their encouragement, which has always been a source of motivation for me.

Thank you Professor John Starkey, for your guidance and encouragement, especially when I was feeling dumb. I only hope that I can be as good a teacher and role model for others as you have been for me. Thank you Professor Al McDonald for your support in the completion of this thesis, and for your work in the area of flywheel gyrodynamics. And thank you Professor Ray Cipra for your efforts in getting me through to the completion of this thesis, and for your contribution to our publication for the ASME Design For Manufacturability conference.

In addition to these fine individuals who contributed so greatly to my success here at Purdue, I would also like to thank the faculty at the United States Air Force Academy, Department of Engineering Mechanics, for sponsoring me here to Purdue. I am grateful for the opportunity to have experienced graduate school at its finest. I look forward to the opportunity for continued service to my country, and to sharing the knowledge that I have gained here at Purdue with future Air Force Officers at the USAFA.

## TABLE OF CONTENTS

	Page
LIST OF FIGURES .....	vi
LIST OF TABLES .....	viii
ABSTRACT .....	ix
CHAPTER 1 INTRODUCTION AND ORGANIZATION .....	2
1.1 Introduction .....	2
1.2 Organization of the Thesis .....	5
CHAPTER 2 LITERATURE REVIEW - HYBRID ELECTRIC VEHICLES....	7
2.1 Hybrid Vehicles .....	7
2.1.1 Series and Parallel HEV .....	7
2.1.2 Merits of HEV Configurations .....	8
2.1.3 Disadvantages of HEV Configurations .....	9
2.1.4 Why HEV .....	9
2.1.5 Regenerative Braking .....	10
2.2 Flywheels in HEV .....	11
2.3 HEV Safety .....	14
2.3.1 Flywheel Burst Containment .....	15
2.3.2 Gyrodynamic Effects .....	16
2.3.3 Road Impact Effects .....	17
2.4 Competitions, Prototypes and Research .....	18
2.5 Closure .....	22
CHAPTER 3 LITERATURE REVIEW - VEHICLE MODELING .....	24
3.1 Vehicle Dynamics Terminology .....	24
3.1.1 Vehicle Terminology .....	24
3.1.2 Motion Variables .....	26
3.1.3 Suspension Terminology .....	27
3.1.4 Vibrating Systems Terminology .....	28

	Page
3.1.5 Tire Terminology.....	29
3.2 Vehicle Models.....	30
3.2.1 Handling Models.....	31
3.2.2 Computers In Vehicle Dynamics Modeling.....	32
3.2.3 Vehicle Handling Model Types.....	34
3.2.3.1 Steady State.....	34
3.2.3.1.1 Low Speed.....	35
3.2.3.1.2 High Speed.....	36
3.2.3.2 Transient Models.....	36
3.2.4 Vehicle Representations.....	38
3.2.4.1 Bicycle Model.....	38
3.2.4.2 Four Wheel Model.....	41
3.2.4.3 Suspension Modeling.....	42
3.3 Tire Models.....	44
3.3.1 Linear Tire Models.....	44
3.3.2 Empirical Models.....	46
3.3.3 Complex Models.....	47
3.4 Closure.....	49
CHAPTER 4 MODEL DEVELOPMENT.....	50
4.1 Purpose.....	50
4.2 Vehicle Model Assumptions and Limitations.....	50
4.2.1 Suspension.....	51
4.2.2 Mass Distribution.....	52
4.2.3 Inertia.....	53
4.2.4 Coordinate Axes.....	56
4.2.5 Degrees Of Freedom.....	57
4.2.6 Other Assumptions.....	60
4.3 Development of the Equations of Motion.....	61
4.3.1 Sprung Mass.....	62
4.3.2 Front and Rear Suspension.....	63
4.4 Tire Model.....	66
4.5 Slip Angle Development.....	69
4.6 Flywheel Development.....	71
4.7 Vehicle Baseline Configuration.....	73
4.8 Validation of Model.....	75
4.8.1 Steady State Model.....	76
4.8.2 Bicycle Model.....	78
4.9 Closure.....	83

CHAPTER 5 RESULTS AND ANALYSIS .....	84
5.1 Test Configuration .....	84
5.2 Flywheel Orientation .....	86
5.2.1 X-Axis Alignment .....	87
5.2.2 Z-Axis Alignment .....	89
5.2.3 Y-Axis Alignment .....	91
5.2.3.1 Y-Axis Alignment Effects - Sideslip Angle ( $\beta$ ) .....	92
5.2.3.2 Y-Axis Alignment Effects -Yaw Rate ( $r$ ) .....	94
5.2.3.3 Roll Yaw Coupling .....	96
5.2.3.4 Y-Axis Alignment-Roll Effects .....	97
5.2.3.4.1 Roll Rate( $p$ ) .....	97
5.2.3.4.2 Roll Angle( $\phi$ ) .....	99
5.2.3.4.3 Roll Over Tendency .....	101
5.2.3.5 Y-Axis Alignment - Lateral Acceleration Effects .....	102
5.2.4 Symmetry of Gyrodynamic Effect .....	104
5.3 Effect on Overall Damping Characteristics .....	108
5.3.1 Variation of Roll Damping .....	108
5.3.1.1 Sideslip Angle .....	110
5.3.1.2 Yaw Rate .....	112
5.3.1.3 Roll Angle .....	113
5.3.1.4 Lateral Acceleration .....	115
5.3.2 Roll Damping Removed .....	117
5.4 Effect on Understeer Coefficient .....	119
5.5 Closure .....	122
CHAPTER 6 SUMMARY AND CONCLUSIONS .....	124
6.1 Summary .....	124
6.2 Conclusions .....	126
6.3 Recommendations .....	128
6.4 Future Efforts .....	129
LIST OF REFERENCES .....	131

## LIST OF FIGURES

Figure	Page
Figure 3.1 SAE vehicle axis system.....	25
Figure 3.3 Change of steer angle with speed .....	27
Figure 3.4 Tire slip angle definition .....	29
Figure 3.5 Geometry of a turning vehicle .....	36
Figure 3.6 Step response of a system in the time domain.....	37
Figure 3.7 Cornering of a bicycle model .....	39
Figure 3.8 Roll Center Location.....	43
Figure 3.9 Roll axis orientation .....	43
Figure 3.10 Cornering stiffness .....	45
Figure 4.1 Vehicle masses and axis system .....	53
Figure 4.2 Small angle assumptions .....	57
Figure 4.3 Representation of one side of vehicle.....	59
Figure 4.4 Free body diagram of sprung mass.....	61
Figure 4.5 Free body diagram of typical suspension .....	64
Figure 4.6 Combined raw tire data and empirical model data .....	68
Figure 4.7 Interpolation results.....	68
Figure 4.8 Four wheeled vehicle negotiating a right turn .....	69
Figure 4.9 Determination of front slip angle, $\alpha_f$ .....	70
Figure 4.10 Determination of rear slip angle, $\alpha_r$ .....	71
Figure 4.11 Bicycle model with linear tire - response to 1° step steer input..	80
Figure 4.12 Sideslip angle response to 1° step steer input at 60 kph.....	81
Figure 4.13 Yaw rate response to 1° step steer input at 60 kph.....	81
Figure 4.14 Roll rate response to 1° step steer input at 60 kph.....	81
Figure 4.15 Roll angle response to 1° step steer input at 60 kph .....	82
Figure 4.16 Lateral acceleration response to 1° step steer input at 60 kph...	82
Figure 5.1 X-Axis flywheel alignment results.....	89
Figure 5.2 Z-Axis flywheel alignment results.....	91
Figure 5.3 Y-Axis alignment - sideslip response.....	93
Figure 5.4 Y-Axis alignment - yaw rate response .....	95
Figure 5.5 Y-Axis alignment - roll-yaw undamped response .....	96
Figure 5.6 Y-Axis alignment - roll rate response .....	98
Figure 5.7 Y-Axis alignment - roll angle response.....	100
Figure 5.8 Y-Axis alignment - lateral acceleration response .....	103

Figure	Page
Figure 5.9 Y-Axis alignment - sideslip angle response for $+1^\circ$ and $-1^\circ$ steer angles .....	106
Figure 5.10 Y-Axis alignment - yaw rate response for $+1^\circ$ and $-1^\circ$ steer angles .....	106
Figure 5.11 Y-Axis alignment - roll rate response for $+1^\circ$ and $-1^\circ$ steer angles .....	107
Figure 5.12 Y-Axis alignment - roll angle response for $+1^\circ$ and $-1^\circ$ steer angles .....	107
Figure 5.13 Y-Axis alignment - lateral acceleration response for $+1^\circ$ and $-1^\circ$ steer angles .....	108
Figure 5.14 Y-Axis alignment - variation of roll damping - sideslip angle response times .....	111
Figure 5.15 Variation of roll damping - sideslip angle illustration of in/out of deadband .....	112
Figure 5.16 Y-Axis alignment - variation of roll damping - yaw rate response times .....	113
Figure 5.17 Y-Axis alignment - variation of roll damping - roll angle response times .....	114
Figure 5.18 Y-Axis alignment - variation of roll damping - lateral acceleration response times .....	116
Figure 5.19 Y-Axis alignment - variation of flywheel orientation - roll rate damped response .....	118
Figure 5.20 Y-Axis alignment - transient understeer coefficient response ..	120
Figure 5.21 X-Axis alignment - transient understeer coefficient response ..	121
Figure 5.22 Z-Axis alignment - transient understeer coefficient response...	122

## LIST OF TABLES

Table	Page
Table 2.1 PNGV vehicle baseline and targets.....	19
Table 4.1 Reaction torque components produced by vehicle rotations .....	54
Table 4.2 Baseline configuration - validation .....	74
Table 4.3 Steady state model comparison .....	78
Table 5.1 Vehicle configuration - testing phase .....	85
Table 5.2 Reaction torque components produced by vehicle rotations .....	87
Table 5.3 Calculated roll rate damping due to flywheel.....	118
Table 6.1 Qualitative effects of y-axis flywheel alignment .....	128

## ABSTRACT

Greer, James LaMonte, M.S.M.E, Purdue University, December 1996.  
Gyrodynamic Effects of an Energy Storage Flywheel on the Handling  
Properties of a Hybrid-Electric Vehicle. Major Professor: John M. Starkey,  
School of Mechanical Engineering.

This research presents the results of numerical simulation of the handling characteristics of a hybrid-electric vehicle which uses a flywheel for temporary energy storage. The work is presented in an effort to understand the potential interaction of the flywheel and the vehicle, and to predict what positive and negative outcomes may result. The vehicle is modeled with four wheels, and the roll, yaw, and sideslip-angle degrees of freedom. The simulation uses an empirical model of the non-linear interface between the tire and the road. The results are presented graphically, and are analyzed on both quantitative and qualitative bases.

The vehicle parameters used to define the baseline vehicle are based on the broad guidelines set forth by the Partnership for a New Generation of Vehicles. The size and speed range of the flywheel is based on a compilation of results presented in the popular literature.

Analyses of the results are based on alignment of the angular momentum vector of the flywheel along the three axes of the vehicle. The speed of the flywheel is varied from -100,000 rpm to +100,000 rpm. Negative speeds represent orientation of the angular momentum vector of the flywheel along the negative axes, and positive speeds represent orientation along the positive axes. It is shown that the response of the vehicle to positive steer

angle input is symmetric with the response from a negative steer angle input. Symmetry shows that the vehicle will respond in a similar fashion whether turning left or right. The vehicle response data is plotted versus the flywheel speed for the full range of values used in the simulations, and interpretation of the results are given in each section. The concept of a transient understeer coefficient is investigated, and the effect of the flywheel on this parameter is shown.

Based on analysis of the results, conclusions are drawn about which orientations of the flywheel may be beneficial to vehicle handling, and which may lead to undesirable characteristics. Alignment of the flywheel spin axis along the x and z axes are found to be neutral in the analysis of handling, but show potential for affecting the ride response of the vehicle. Alignment of the flywheel spin axis along the positive y-axis shows potential to increase the likelihood of vehicle rollover during emergency maneuvers.

## CHAPTER 1

### INTRODUCTION AND ORGANIZATION

#### 1.1 Introduction

The number one concern of many new car buyers is now safety. However, more efficient cars provide broader benefits to society, and reduce the serious deterioration of urban air. In an effort to achieve cleaner air and less dependence on imported crude oil, the federal and state governments have begun anew in their efforts to encourage the development of increasingly more efficient vehicles for the motoring public. A leader in the effort to encourage clean air progress has been the California Air Resources Board (CARB). Analysis by the CARB shows that with the projected growth in vehicle miles traveled, recent improvements in air quality could soon be canceled out. The only apparent solution is to introduce and make available to consumers a large number of vehicles that produce virtually no emissions.

To speed the access to cleaner more efficient vehicles, regulations have been passed in California requiring the gradual reduction in emissions from new vehicles. These sets of related regulations are referred to as the Low Emission Vehicle (or LEV) Regulations, and consist of increasingly lower limits from the Transition Low Emission Vehicle (TLEV), to the Low Emission Vehicle (LEV), to the Ultra Low Emission Vehicle (ULEV), to the Zero Emission Vehicle (ZEV). Through this legislation, CARB has mandated

that the seven major automakers make available for sale as ZEVs, 2% and 5% of their new car sales in 1998 and 2001 respectively. Recently that mandate was delayed, as CARB Voted in March of 1996 to Delay the ZEV Requirements until the year 2003, when all automakers will be required to offer 10 percent of their cars and light-duty trucks as ZEV models (CARB, 1996). Regardless of this delay, the LEV Regulations provided a major impetus for the automotive industry and the Federal government to move in the direction of developing ZEV, and other related technologies.

As a result of this effort, two new vehicle classes have been created to move toward providing a step-wise improvement in emissions. These are the Electric Vehicle (EV) and the Hybrid Electric Vehicle (HEV). Unlike an EV, an HEV utilizes the intermittent operation of a small engine to assist a typically battery-powered electric propulsion system. The ultimate clean, efficient car is an EV, but there are questions about the mid-term viability of EVs. This is due to unresolved technical issues of on-board energy storage capacity, high vehicle cost, and infrastructure limitations (e.g., lack of public charging stations, repair/replacement facilities, battery-recycling centers). Hybrid Electric Vehicles are almost as clean as EVs and have vehicle performance characteristics comparable to that of today's standard internal combustion engine vehicles. More important, such performance appears to be available within the next 5 years, and therefore represents a practical, technically-achievable alternative approach. In fact, prudence suggests that both EVs and HEVs be developed in parallel, as many of the technical advancements can be shared and because either or both will be needed to achieve efficiency and clean air goals.

This is not to say that HEV are without their problems. Several obstacles exist to the introduction of HEV on a mass production basis. The primary problem is the fact that current technology is not able to support the energy storage demands of a HEV. Batteries, flywheels and ultracapacitors

are not at a point in their development that they can be built at a cost low enough to make the vehicles viable in the incredibly competitive and cost sensitive market place. Resistance to the vehicles' higher price and slightly reduced performance may be abated if HEVs are accepted as ULEVs under California's stringent definition of reduced emissions.

In a statement from the California Air Resources Board:

The primary question with regard to HEVs and other clean car technologies which have potential to emit fewer pollutants than ULEVs is whether these vehicles should receive credit as ZEVs. HEVs offer driving ranges similar to gasoline vehicles while using an electric drive system at least part of the time. This enhances their capability to serve a wider variety of functions than a pure EV. However, HEVs are not yet available for real-world testing of their emissions benefits, making it difficult to evaluate how much credit they should receive under the ZEV regulation. (CARB, 1996)

As can be seen in this statement, the recognition of HEVs as pollution-reducing vehicles is likely to attract the support of regulators and public interest groups. Such support could be reflected in purchase rebates, favorable tax treatment, preferred driving lanes and parking, and other financial incentives to prospective buyers and operators. In addition, consumers may be more likely to accept future HEVs since their operational differences are more likely to be "transparent" to the vehicle operator than those of an EV.

In addition to the cost factor, there are safety concerns regarding both EV, and HEV. Electric vehicles have questionable crashworthiness, due to the problem of containment of the chemical solutions in the batteries. A similar concern for HEV is the containment of a high energy flywheel, should it fail in a catastrophic manner. Another concern, although less spectacular, is the effect that an energy storage flywheel will have on the handling characteristics of a HEV. When a spinning flywheel is precessed, it will

exert a torque proportional to the rate of precession, that reaction torque is known as the gyrodynamic effect.

This thesis will address the gyrodynamic effect, and its physical meaning to the designer and user of HEV. The question will be addressed using a computer based dynamic model of a hybrid vehicle that uses an energy storage flywheel, and the results will indicate where possible problems exist and where possible windfall benefits may be found.

## 1.2 Organization of the Thesis

This thesis is organized into six chapters. Chapter-2, Literature Review - Hybrid Electric Vehicles, presents a review of HEVs, providing insight into the motivation behind development of HEVs. In addition, the merits and drawbacks of using a flywheel as an energy storage device are presented.

Chapter-3, Literature Review - Vehicle Modeling, contains a review of vehicle dynamics terminology that is pertinent to this thesis. Vehicle handling models and their use with digital computer simulation are presented. Steady-state and transient model types are discussed, focusing on their application to the bicycle and four-wheeled vehicle models used in this work. Finally, tire modeling is reviewed with an emphasis on defining the basic types of tire models in use, and their applicability to modeling vehicle handling.

Chapter-4, Model Development, details the overall development of the vehicle handling model used in this investigation. The assumptions relating to the model are presented, and the level of complexity of the model is discussed as it relates to the objectives of the investigation. Based on this discussion, the equations of motion and the tire model are developed. Next,

the baseline vehicle is defined using the goals set forth in the Partnership for a New Generation of Vehicles. The energy-storage flywheel is defined for this simulation. The target values for the energy storage capacity and rotational speed of the flywheel are determined from the popular literature. At this point, the model is fully developed and the method of validation and the results of the validation process are presented.

Chapter-5, Results and Analysis, details the results of exercising the model using the handling and tire models developed in the previous chapter. The results are presented for three alignments of the angular momentum vector. The three alignments of the flywheel are based upon the three axes of the vehicle, and the orientation and speed of the flywheel are varied within each of these alignments. In addition, the effect of the flywheel on the transient understeer coefficient is discussed. The results are analyzed on a quantitative as well as a qualitative basis focusing on the effects the flywheel has on the overall handling characteristics of the vehicle.

Chapter-6, Summary and Conclusions, recapitulates the primary areas of this thesis, and discusses the overall implications of including a flywheel in the energy system of a HEV. Ways of using the flywheel as a handling design element are discussed, as are ways of mitigating the negative effects of the flywheel. Finally, areas for future investigation are presented.

## CHAPTER 2

### LITERATURE REVIEW - HYBRID ELECTRIC VEHICLES

#### 2.1 Hybrid Vehicles

A Hybrid Electric Vehicle (HEV) is a vehicle that has two sources of motive energy. There are many hybrid system concepts using fuel cells, gas turbines, diesels, and lean burn gasoline engines as hybrid power units (HPU) in combination with flywheels, batteries, and ultracapacitors as energy storage devices. No matter which concept or combination is used, there are two fundamentally different ways to build the electric and fuel system of an HEV; using either a parallel configuration or a series configuration.

##### 2.1.1 Series and Parallel HEV

The Department of Energy's National Renewable Energy Laboratory (NREL) defines an HEV with a series configuration as one that uses the heat engine with a generator to supply electricity for the battery pack and electric motor. Series HEVs have no mechanical connection between the HPU and the wheels; therefore, all motive power is transferred electrically to an electric motor that drives the wheels. This class of HEV is known as a "Series Range-Extender," which means that the vehicle is series-configured

and uses a range-extender control strategy, meaning it operates like an electric vehicle until its stored electrical energy is depleted, at which time its HPU turns on to power the vehicle. This configuration is particularly well suited to HPUs such as gas turbines that do not mate well with the drive train of an automobile (Wipke, 1994).

The NREL defines an HEV with the parallel configuration as follows: an HEV with a parallel configuration has a direct mechanical connection between the HPU and the wheels as in a conventional vehicle, but has an electric motor which assists the HPU in driving the wheels as well. For example, a parallel vehicle could use the power created from an internal combustion engine for highway driving and the power from the electric motor for accelerating. This class of HEV is known as "Parallel Power-Assist," which means the vehicle is parallel-configured and uses a power-assist control strategy whereby the electric driveline provides extra power when called upon to do so (Wipke, 1994).

### 2.1.2 Merits of HEV Configurations

Each of the configurations has its benefits, for the series configuration these benefits include:

- The engine rarely idles, thus reducing vehicle emissions.
- The engine drives a generator, hence the engine can be run at its optimum performance level.
- The operation of the engine is independent of the road load conditions.
- A wide variety of packaging options are available to the designer when mounting the engine and vehicle components.
- A transmission may not be needed.

Some benefits of the parallel configuration HEV include:

- The vehicle has more peak power available because both the engine and the motor can supply power simultaneously (not a typical mode for the Range Extender control scheme).
- Most parallel vehicles have no need of a generator.
- The power of a fuel engine is directly coupled to the road, thus, it can be delivered more efficiently.

### 2.1.3 Disadvantages of HEV Configurations

Yamaguchi *et al* (1996) detailed several of the existing disadvantages of each of these configurations. The series configuration uses full electrical energy conversion of the output of the engine, which increases losses due to the inherent inefficiency of converting mechanical energy to electrical energy. In addition, the generator must be sized large enough to handle conversion of the maximum output of the engine. The parallel configuration requires the inclusion a transmission in the drivetrain to provide torque multiplication of the output of the engine. Additionally, because of the direct mechanical coupling of the engine to the drive train, the operation of the engine is necessarily tied to the road load through gear ratios and thus cannot be designed and sized to operate at a single optimum speed or load level.

### 2.1.4 Why HEV

Typical Internal Combustion Engine (ICE) vehicles convert fuel energy to shaft work, which is used to overcome the tractive energy required by the vehicle to drive forward. In addition, the energy is used to operate the vehicle accessories and overcome driveline losses. A traditional ICE vehicle only uses approximately 16% of its energy to accelerate the vehicle while the rest of the

energy either becomes waste heat from the thermodynamic cycle of the internal combustion engine or is used to overcome frictional losses (such as aerodynamic drag or rolling resistance). HEVs minimize losses to make as much energy available as possible to propel the vehicle. For example, HEVs use regenerative braking to minimize energy losses.

### 2.1.5 Regenerative Braking

Regenerative braking describes the ability of a vehicle to usefully convert some of the kinetic energy that would otherwise be lost into stored energy that is available for use at a later time. Regenerative braking takes advantage of the fact that a conductor that is moved through a magnetic field has current induced in it. Through high-power switching in the controller, the motor (which is a large wrapping of conductors) performs this function and acts as a generator to supply current in the reverse direction to the energy storage device. In addition to using the motor for braking, standard hydraulic disc and drum brakes are still used when the braking demands exceed the deceleration capabilities of the drive motor. One driver of an HEV noted that the need for the conventional brakes is even more dramatic in HEVs due to the lack of compression braking that results from letting up on the accelerator pedal of an ICE propelled vehicle (Lorentzen, 1996). The use of regenerative braking is based upon the ability of the energy storage device to accept energy in a relatively short period of time. Currently, the only device capable of "fast charging" is the flywheel, and this energy storage device will be of particular interest in this thesis.

## 2.2 Flywheels in HEV

Flywheels show technical promise as a potential load-leveling device for hybrid electric vehicles. However, they are still under development and are not yet commercially viable. Flywheels have the potential for being excellent high power density storage devices, with one optimistic estimate for specific power ranging between 2000 W/kg in the near-term, and 8000 W/kg in the long-term time horizon (Anerdi, et. al 1994). These estimates are countered by the Partnership for a New Generation of Vehicles (PNGV) program plan that mentions an installed prototype system in a bus with a much lower specific energy of 5 Wh/kg and a specific power of 375 W/kg. For reference, future lead-acid batteries are expected to range between 200 W/kg (current) and 450 W/kg (potential) (Mason, et. al 1994), and ultracapacitors have demonstrated a specific energy of 2-5 Wh/kg and power densities of 2000 to 4000 W/kg. The design challenges for commercial viability of flywheels include increasing specific energy, reducing material costs, designing lightweight containment, and developing a simplified system integration.

As an energy storage device, flywheels store energy mechanically in the form of kinetic energy. Flywheels of composite construction can store up to 80 Wh/kg with a long term storage (100,000 cycles to failure) capacity of 40 Wh/kg. This level of energy density is unparalleled in any other form of energy storage device (Flanagan & Keating, 1990). Post *et al* (1994) have proposed a flywheel based energy storage device known as an Electro Mechanical Battery (EMB) as a replacement for the electrochemical battery. In the EMB, a high speed flywheel is constructed of composite materials with a permanent magnet material (NdFeB) as an integral part of the flywheel disk. The entire disk assembly spins in a sealed evacuated chamber, thus eliminating the parasitic aerodynamic losses that plague other

high speed flywheel designs. The EMB is projected to produce energy density levels on order of 5-10 kW/kg, spin at speeds of up to 60,000 rpm, and achieve two way energy recovery efficiencies of 95% (kW-h out / kW-h in). In the EMB approach to energy storage, the flywheel will take an electrical input from the regenerative braking system or the ICE driven generator to accelerate the rotor up to speed. The EMB will return electrical energy as a high speed generator, supplying energy during periods of peak demand, thus leveling the load on an ICE driven generator or electrochemical battery bank. Testing of prototype EMBs have produced output levels of 100 kW with an energy storage capacity of 1 kW-h and a two way energy recovery of 92% (Post *et al*, 1994).

In a similar design developed specifically for hybrid vehicle drives, Flanagan *et al* (1990) propose a 500 W-h fiber composite flywheel coupled directly to a high speed 40 kW permanent magnet motor/alternator, all encased in the same hermetically sealed enclosure. This design is based upon existing technology, and represents a near term solution. Flanagan and Keating's (1990) research on the optimum configuration of this particular package shows that it could be incorporated into a HEV with impressive results. The inclusion of the flywheel motor/alternator combination yielded load leveling of the demands on the battery pack of their test flywheel/electric hybrid. In the end, battery charge life was doubled while maintaining driveability and acceleration levels that exceeded the standardized driving schedule under which the vehicle was tested.

In the design of flywheels, there exists a trade-off between size and rotational speed. The equation for the kinetic energy stored in a flywheel is:

$$KE = \frac{1}{2} I \omega^2, \quad (2-1)$$

where,

$I$  = the mass moment of inertia of the flywheel

$\omega$  = the rotational velocity of the flywheel

This equation leads to the conclusion that more kinetic energy can be stored by: 1) spinning the flywheel faster, or 2) using a flywheel with a larger moment of inertia. Each of the previous examples of flywheel based energy storage and retrieval systems is predicated on the ability of a flywheel to withstand the rigors of very high rotational speeds. An engineering challenge arises, however, because spinning the flywheel faster causes larger centrifugal forces and subsequent tensile stresses that the rim material must be able to withstand without flying apart. These centrifugal forces are also proportional to the mass of the rim and the square of the rotational speed:

$$F_{centrifugal} = M\omega^2 r, \quad (2-2)$$

where:

$M$  = mass of an element of the ring

$\omega$  = the rotational velocity of the flywheel

$r$  = the radius of the flywheel.

What this relationships tell us is that a high density rim stores more energy than a low density one, but also induces higher stresses. Therefore, a low density rim can spin faster than a high density rim before experiencing failure. Finally, since the kinetic energy stored rises with the square of the rotor speed, but only linearly with mass, the optimum flywheel will be made of a strong material with low density (high tensile strength to density ratio).

It follows from the above discussion that the most significant factor affecting flywheel design is the materials used to construct the flywheel rim. A flywheel rim needs to be made of a high tensile-strength-to-density-ratio

material to maximize the kinetic energy stored (through having a high rotational speed) while minimizing the chance of failure. This requirement for a high tensile-strength-to-density-ratio leads flywheel developers to composite materials that have a high tensile strength and a low density such as fiberglass/epoxy and Kevlar/epoxy as opposed to steel. For example, 4340-steel has a tensile strength of 1517 MPa, a density of  $7700 \text{ kg/m}^3$ , and a subsequent ratio of 54.7 Wh/kg. Kevlar/epoxy, on the other hand, has a tensile strength of 1930 MPa, a density of just  $1400 \text{ kg/m}^3$ , and a resultant ratio of 382.9 Wh/kg. Therefore, Kevlar/epoxy has a tensile-strength-to-density-ratio that is 7 times that of steel, indicating it is a much better candidate material for use in flywheels.

### 2.3 HEV Safety

In general, Hybrid Electric Vehicles are just as safe as today's gasoline powered vehicles because HEVs must adhere to the same strict federal motor vehicle safety standards as today's conventional vehicles. However, because there are some differences in the components that HEVs use, special designs must be considered and safety standards for HEVs. In addition to general vehicle safety issues, the existence of a battery system or flywheel in an HEV will impose an array of additional safety issues.

This section will briefly describe some of the existing flywheel safety issues. The HEVs and EVs of the future may contain flywheels. In general, the flywheel technology to be used in HEVs and EVs will be designed to be safe to the vehicle driver, passengers, other motorists, pedestrians, and the environment. The National Highway Traffic Safety Administration (NHTSA) has determined that HEVs and EVs should comply with all existing vehicle

safety standards. The agency recognizes the need to modify some existing regulations that do not apply to the unique requirements of HEVs and EVs.

### 2.3.1 Flywheel Burst Containment

Rotor fragments eject when the containment vessel fails, either during operation or an accident. The energy content of a high-speed flywheel that fails is tremendous. Therefore, the rotor must be contained during operation and during an accident. To avoid any hazardous situations associated with the failure of a high-speed rotor, the rotor must be contained in the surrounding housing and the housing structure must not separate from its mounting structure. Flywheels with composite rotors are expected to be used for automotive applications because of their high tensile-strength-to-density-ratio, and their containment vessel may also be made using composite materials in an effort to reduce total flywheel system weight.

When a spinning flywheel bursts, the total angular momentum is conserved, or converted to the linear momentum of the free particles. When the stress in the rotor material is too high and the rotor disintegrates into fragments as a result of internal stresses or collision with the containment vessel, this momentum is transferred to the containment structure by the impact of the burst fragments. This catastrophic failure could degrade the integrity of the containment vessel, allowing the rotor fragments to eject at very high speeds. One containment strategy mentioned in NREL(1) (1996) is the use a separate internal burst-containment cylinder that is not attached to the containment vessel, but is free to rotate under the effect of angular impulse of burst fragments. The impact of high-energy burst fragments against the soft inner liner would expand the liner radially, driving the entire volume of cushion outward against the vacuum chamber walls. The

compliance in the cushion liner would dissipate much of the flywheels kinetic energy during the expansion process, the remaining energy would be absorbed by deformation of the vacuum chamber walls. With steel rotors, relatively large fragments may collide with and penetrate through the containment vessel, so the vessel should be thick and strong enough to prevent the fragments from escaping. The aerospace industry has used composite wrappings around the periphery of turbine engines to contain fragments from burst compressor rings (Post *et al* 1994).

### 2.3.2 Gyrodynamic Effects

The use of flywheels as torque generating actuators on Earth orbiting satellites was first proposed in the 1950's (DeLisle *et al*, 1964), and have been used to generate gyrodynamic torques for stability and attitude control on spacecraft up through the present day. Hence, the gyrodynamic effects of flywheels on space vehicles are well known in the astronautical engineering community. The gyrodynamic effects of flywheels on some terrestrial vehicles have also been studied extensively. One such application of flywheels for stabilization of ground vehicles can be found in the work by Arnold (1963), where a large flywheel is studied as a stabilizer for a monorail train. The author discusses the possibility of mounting a flywheel with the spin axis horizontal and transverse to the direction of travel such that the gyrodynamic torque of the spinning flywheel resists the tendency of a monorail to tip to one side or the other during a turn. Flywheels have been studied as a means of stabilizing ships at sea as well (Scarborough, 1958). The approach used with ships is similar to that proposed for the monorail, and in fact predates the monorail application by about 20 years. In the ship stabilization application, the flywheel is used to reduce the period and

amplitude of roll oscillations of a ship under the influence of wave motion that is near the natural frequency for rolling of the ship without the flywheel.

Based on the discussion above, it is clear that the gyroscopic effects of the spinning flywheel have the potential to affect vehicle stability during a turn (the focus of this work). As with any other vehicle component, proper system design must be implemented to make the flywheel safe. In the case of flywheel orientation, McDonald (1980) presented a method for designers to reduce the gyrodynamic properties of the flywheel to parametric forms, and then used these forms to develop nomographs to be used in determining the gross effects of including a flywheel in the dynamic equations of motion of a motor vehicle. In this way, the designer can determine the torques that a flywheel will impose upon the vehicle chassis during various vehicle maneuvers. The work of Schilke *et al* (1986) details the integrated development of a flywheel/ICE hybrid vehicle. In this work, the gyrodynamic forces are predicted analytically, and deemed to be insignificant in this particular case, because the flywheel speed was low (12,000 rpm) as was its moment of inertia ( $0.3 \text{ kg-m}^2$ ). These were valid assumptions at the time, but in light of the current state of flywheel development they would not be valid today.

### 2.3.3 Road Impact Effects

Road shocks can affect flywheel operation. This is related to the previous problem, except in this case the vehicle imposes forces on the flywheel system. Road loads can come in many forms ranging from noise-vibration-harshness to torques imposed during vehicle maneuvers. In the work by Flanagan *et al* (1990), the peak loading of the bearing supports was found to be unacceptable at 2275 lb (10.1 kN) as a result of a low-speed turn

at the traction limit while dropping over a curb. The integration of magnetic bearings into the flywheel system is complicated by the existence of loads just such as these and have limited the scope of investigators such as Post *et al* (1994) to looking at non-vehicular applications. The dynamic inputs from the environment to the flywheel can have stability implications as well. Jayaraman *et al* (1991) have shown that for magnetic bearing systems using closed loop control, the forces and torques that a flywheel supported by magnetic bearings can withstand before contact between the bearing surfaces, or between the wheel and its enclosure, are low enough to be of concern.

#### 2.4 Competitions, Prototypes and Research

Much time and effort has been devoted to the research, design, and development of the hardware and software required to put prototype HEVs on the road. There are competitions sponsored by the US Department of Energy, that encourage universities to design and construct HEVs to compete, with the resulting innovations being made available to the public sector through technology transfer. In addition to these competitions, in 1993 the Partnership for a New Generation of Vehicles (PNGV) was announced. The PNGV represents a collaborative agreement between eight federal agencies and associated national laboratories, and the United States Council for Automotive Research (USCAR), which represents Chrysler, Ford, and General Motors. The PNGV is intended to bring to bear the considerable research and development capabilities of the national laboratories and the automakers in an effort to strengthen US competitiveness by developing a new generation of energy-efficient and environmentally-friendly vehicles. The three broad goals of PNGV are:

1. "Significantly improve national competitiveness in manufacturing."
2. "Implement commercially viable innovations from ongoing research on conventional vehicles."
3. "Develop a vehicle to achieve up to three times the fuel efficient of today's comparable vehicles." (Patil, 1996)

In pursuit of these goals, PNGV and USCAR have established three baseline vehicles: the Chrysler Concourse, the Ford Taurus, and the GM Lumina. The baseline performance parameters and the target levels are as listed in Table 2.1:

Table 2.1 PNGV vehicle baseline and targets  
(Patil, 1996)

PARAMETER	CURRENT	TARGET
Fuel Efficiency	average 26.6 miles per gallon of gas equivalent (114,132 BTU)	average 80 miles per gallon of gas equivalent (114,132 BTU )
Curb Weight	3200 lbs (1451 kg)	Variable
Acceleration	0-62 mph in 12 seconds	0-62 mph in 12 seconds
Operating Range	380 miles (minimum)	380 miles (minimum)
Total Life	100,000 miles (minimum)	100,000 miles (minimum)

The technological target of PNGV can be pared down to one simple yet difficult to attain goal, triple the energy efficiency of vehicles currently in production while maintaining or improving customer appeal in driveability, comfort, and convenience. This task will require unprecedented cooperation between industry and government, and significant technological advancements.

Several prototype flywheel/electric hybrid vehicles have been developed for proof-of-concept and research purposes. An early effort by Schilke *et al* (1986) at General Motors Research Labs was the inclusion of an energy storage flywheel and a Continuously Variable Transmission (CVT) in the drive train of a standard ICE powered vehicle. The intent of this project was to use regenerative braking to capture energy for storage in the flywheel for later use. The available energy in the flywheel is used to level the load on the ICE during periods of peak power demand. The CVT allowed the engine to be operated at near wide-open-throttle, hence it could be optimally sized for the demands of steady-state operation rather than for the peak power demand of acceleration. The goal of this project was to attain performance equivalent to that of the production version of the vehicle while improving the efficiency and environmental-friendliness of the vehicle. The flywheel used in this project was a low power unit capable of storing 65 W-h at 12,000 rpm ( $I = .30 \text{ kg-m}^2$ ).

In a study performed by Aceves and Smith (1995) at Lawrence Livermore National Lab using their "Hybrid Vehicle Evaluation Code", a engine/flywheel hybrid vehicle burning hydrogen fuel was modeled to determine the potential energy efficiency and performance capabilities of such a vehicle. The HEV was tested using the Federal Urban Driving Schedule as input to the model. The vehicle used a flywheel with 2 kW-h of energy storage capacity, and based upon assumptions about the maximum rated speed of the flywheel ranging from 40k rpm to 60k rpm, the moments of inertia ranged from  $0.87 \text{ kg-m}^2$  to  $0.36 \text{ kg-m}^2$  respectively. The results were encouraging for such a vehicle, as performance was within the goals of PNGV, while meeting the clean-air standards of California's LEV regulations. An interesting result noted in this study was, that the urban fuel efficiency was slightly higher than highway fuel efficiency due to the contribution of regenerative braking and flywheel energy storage.

The GM Impact is currently being tested in 12 regional markets through the PrEView Program to educate the public, allow utilities to learn about infrastructure requirements for EVs, and to learn more about customer expectations. With a 137 horsepower AC induction motor, the Impact EV produces an impressive 0-60 mph acceleration time of 8.5 sec. Everything about this vehicle has been carefully designed to maximize efficiency giving it the largest possible range on electric power. GM has not indicated that they would offer a hybrid version of the Impact, but it is probable that many of the energy efficient ideas from the Impact could be applied to hybrids.

One of the most ambitious projects to be carried out is the Patriot Hybrid Race Car built by Chrysler, SatCon Technology Corporation, Reynard Ltd., and Westinghouse Electronic Systems Group. The vehicle is a test bed for future HEV technologies, and has garnered much attention from the automotive media (Brooke, 1994; Jost, 1994; Scott, 1995). The 2000 lb. car is capable of 200+ mph speeds, and was built in the span of 6 months. Patriot has integrated several leading edge technologies into one extremely high performance powertrain package. The HPU in this vehicle is a hybrid gas turbine engine and electrical alternator, called a "turboalternator," designed to convert mechanical energy into electrical energy. The turboalternator combines a liquid natural gas burning turbine engine with an integral three phase alternator to produce 500 horsepower while weighing less than 200 pounds. A "flywheel battery" designed by SatCon is capable of storing 4.35 kW-h of energy at 58,600 rpm ( $I = 0.84 \text{ kg-m}^2$ ). The flywheel battery consists of a carbon-fiber wheel and integral permanent magnet three-phase motor enclosed in a liquid cooled and vacuum sealed enclosure. According to SatCon, this 135 lb. flywheel battery package is capable of storing 50 times the energy of a lead-acid battery of equal weight. To put all this power to the racetrack, Patriot uses a 24,000 rpm alternating current induction motor weighing 145 lbs that is capable of generating in excess of 500 horsepower.

In addition to putting power to the track, the motor is also capable of 15-20% regenerative braking.

The body styling for hybrid electric vehicles (HEVs) need not be different from that of conventional vehicles, because the unique aspect of HEVs are their propulsion systems. However, since energy efficiency is one of the reasons to use an alternate propulsion system, such as a hybrid electric propulsion system, an aerodynamic body style and light-weight chassis will complement the system and increase vehicle efficiency. The hybrid propulsion system of a vehicle will have little if any effect on the vehicle's aerodynamic drag, but it can have a dramatic effect of the vehicle chassis and the overall vehicle weight and its subsequent rolling resistance. For every reduction in the mass of a vehicle, a corresponding improvement in fuel economy may be expected. Reduction in mass could be accomplished through careful selection of materials, but the most significant reductions in weight can be the use of flywheels over electrochemical cells. As has been shown in the previous sections, electromechanical batteries offer a viable alternative to the use of electrochemical batteries in the drivetrains of hybrid electric vehicles.

## 2.5 Closure

In this chapter, the foundation of Hybrid-Electric vehicle technology has been discussed. The future of HEV development will include some form of short term energy storage system in which the energy recovered by regenerative braking will be stored. One form of energy storage device that shows considerable promise is the flywheel, but its use is not without technical challenges. The future of flywheels in HEVs will depend upon the solution of three safety problems, gyrodynamic effects of the flywheel on the

vehicle, flywheel burst containment, and the effects of road inputs on the flywheel system.

Increases in flywheel energy storage capacity come as a result of higher rotational speeds or larger mass moments of inertia, or both. These variables of flywheel design directly affect the first of the safety concerns mentioned above. The question becomes, will the gyrodynamic force of the flywheel effect handling, especially in high-g emergency maneuvers. This is the subject of this investigation.

## CHAPTER 3

### LITERATURE REVIEW - VEHICLE MODELING

#### 3.1 Vehicle Dynamics Terminology

The terminology used in the field of vehicle dynamics has been standardized by the Society of Automotive Engineers (SAE). The standards developed by SAE will be used as much as possible in this work, and any deviations will be noted as such. The following paragraphs detail the standards that are of importance in this work. The following definitions are taken from SAE standard J670e, *Vehicle Dynamics Terminology*, (Society of Automotive Engineers, 1994).

##### 3.1.1 Vehicle Terminology

**Vehicle Axis System:** The axis system developed by the SAE is as shown in Figure 3.1. "This system is a right-hand orthogonal axis system fixed in a vehicle such that with the vehicle moving steadily in a straight line on a level road, the  $x'$ -axis is substantially horizontal, points forward, and is in the longitudinal plane of symmetry. The  $y'$ -axis points to the driver's right and

the  $z'$ -axis points downward." In this work, the origin of the vehicle axis system is fixed in the vehicle center of gravity with the above orientations.

**Angular Orientation:** "The orientation of the vehicle axis system ( $x',y',z'$ ) with respect to the Earth-fixed axis system ( $X,Y,Z$ ) is given by a sequence of three angular rotations. The following sequence of rotations, starting from a condition in which the two sets of axes are initially aligned, is defined to be the standard:

- (1) A yaw rotation,  $\Psi$ , about the aligned  $z'$ - and  $Z$ -axis.
- (2) A pitch rotation,  $\Theta$ , about the vehicle  $y'$ -axis.
- (3) A roll rotation,  $\phi$ , about the vehicle  $x'$ -axis."

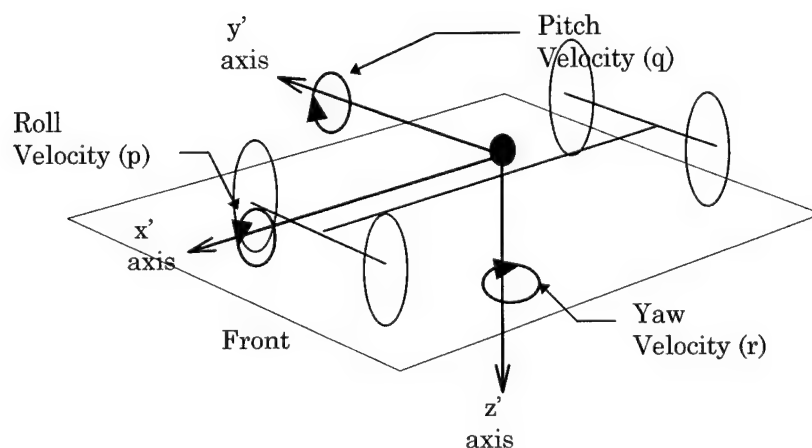


Figure 3.1 SAE vehicle axis system

**Sprung Weight ( $W_s$ ):** "All weight that is supported by the suspension of the vehicle, including portions of the weight of the suspension members."

Unsprung Weight ( $m_{uf/r}g$ ): "All weight that is not supported by the suspension system, but is supported directly by the tire or wheel, and is considered to move with it."

### 3.1.2 Motion Variables

Lateral Acceleration ( $a_y$ ): "The component of the vector acceleration of a point in the vehicle perpendicular to the vehicle  $x'$ -axis and parallel to the road plane." Generally, the point of interest for this work will be either the center of gravity or the point of intersection of the  $z'$ -axis and the roll-axis.

Longitudinal Velocity ( $U_x$ ): "...of a point in the vehicle is the component of the vector velocity in the body fixed  $x'$ -direction."

Lateral Velocity ( $U_y$ ): "...of a point in the vehicle is the component of the vector velocity perpendicular to the  $x'$ -axis and parallel to the road plane."

Roll Velocity ( $p$ ): "The angular velocity about the  $x'$ -axis."

Pitch Velocity ( $q$ ): "The angular velocity about the  $y'$ -axis."

Yaw Velocity ( $r$ ): "The angular velocity about the  $z'$ -axis."

Side Slip Angle ( $\beta$ ): "The angle between the traces on the X-Y plane of the vehicle  $x'$ -axis and the vehicle velocity vector at some specified point in the vehicle." In this study, the point of interest will typically be the intersection of the roll axis with the  $z'$ -axis.

### 3.1.3 Suspension Terminology

Steer Angle ( $\delta$ ): "The angle between the projection of a longitudinal axis of the vehicle and the line of intersection of the wheel plane and the road surface."

Understeer Gradient ( $K_{us}$ ): (See Figure 3.2)

Neutral Steer ( $K_{us}=0$ ): A vehicle is neutral steer if no steer angle change is needed to maintain a circular path on a constant-radius turn, when speed is varied.

Understeer ( $K_{us}>0$ ): A vehicle is understeer if additional steer angle is needed to maintain a circular path on a constant-radius turn when speed is increased.

Oversteer ( $K_{us}<0$ ): A vehicle is oversteer if less steer angle is needed to maintain a circular path on a constant-radius turn when speed is increased.

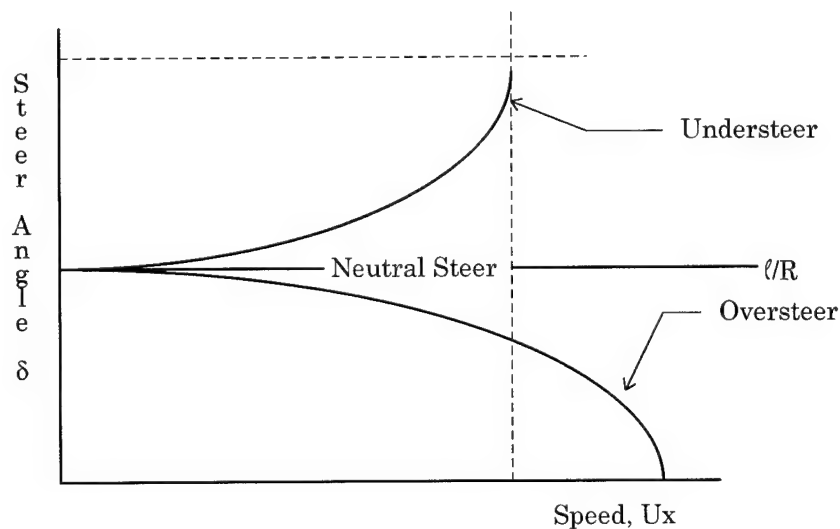


Figure 3.2 Change of steer angle with speed

Suspension Rate (**K**): “The change of wheel load, at the center of tire contact, per unit vertical displacement of the sprung mass relative to the wheel at a specified load.”

Roll Center: “The point in the transverse vertical plane through any pair of wheel centers at which lateral forces may be applied to the sprung mass without producing suspension roll. The roll center constitutes an idealized concept and does not necessarily represent a true instantaneous center of rotation of the sprung mass.”

Roll Axis: “The line joining the front and rear roll centers.”

Suspension Roll Angle ( $\phi$ ): “The angular displacement produced by the rotation of the vehicle sprung mass about the  $x'$ -axis with respect to a transverse axis joining a pair of wheel centers.”

Suspension Roll Stiffness (**K**): “The rate of change in the restoring couple exerted by the suspension of a pair of wheels on the sprung mass of the vehicle with respect to change in suspension roll angle.”

### 3.1.4 Vibrating Systems Terminology

Degrees Of Freedom (DOF) : “The number of degrees of freedom of a vibrating system is the sum total of all ways in which the masses of the system can be independently displaced from their respective equilibrium positions.”

**Linear Systems:** “Linear vibrating systems are those in which all the variable forces are directly proportional to the displacement, or the derivatives of the displacement, with respect to time.”

**Damped Systems:**

**Viscous Damping ( $\frac{\partial L}{\partial p}$ ):** “Damping in which the force opposing the motion is proportional and opposite in direction to the velocity.”

**Critical Damping:** “The minimum amount of viscous damping required in a linear system to prevent the displacement of the system from passing the equilibrium position upon returning from an initial displacement.”

### 3.1.5 Tire Terminology

**Slip Angle ( $\alpha$ ):** “The angle between the direction of wheel heading and the direction of travel of the center of tire contact,” see Figure 3.3. The sign on the slip angle in this figure is a deviation from the SAE standard that is required in the tire model to be defined later.

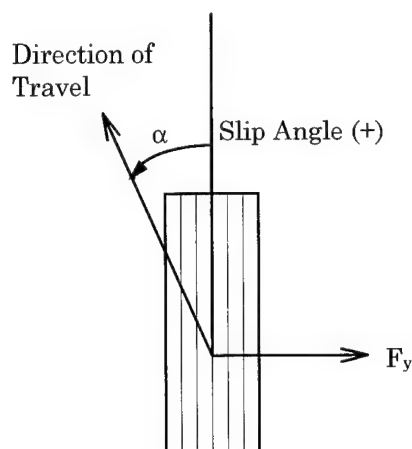


Figure 3.3 Tire slip angle definition

Cornering Stiffness ( $C_\alpha$ ) : "The rate of change of lateral force with respect to change in slip angle, usually evaluated at zero slip angle." In this work, a non-standard definition for cornering stiffness will be used. The SAE standard calls for  $C_\alpha$  to be the negative of what is defined here.

### 3.2 Vehicle Models

Dynamic models are used to mathematically represent the response of wheeled vehicles to various types of perturbations. Mathematical models are a simplified representation of the real vehicle, and simplification requires that the modeler choose carefully which parameters are important and which can be neglected. Attempts have been made to develop models to simulate the effects of nearly all known phenomena affecting a motor vehicle, both on and off the road. Models vary widely in their complexity based upon the degree of accuracy required of the simulation, and the amount of input data required is directly related to the level of detail of the model.

In general, vehicle dynamic modeling can be divided into three broad areas: performance, ride, and handling. Performance modeling focuses on predicting the longitudinal acceleration and braking behavior of a motor vehicle. Performance modeling combines information about the engine torque, engine power and braking capabilities of a vehicle with its inertial properties and a tire model to make predictions about longitudinal dynamic reactions to those braking and engine torque inputs. Ride modeling is primarily concerned with the parameters of bounce and pitch which arise as a result of inputs from the road profile. Ride modeling is associated with predicting occupant comfort. Modeling of vehicle handling is the study of a vehicles reaction to lateral forces. Lateral forces may be generated by

steering inputs from the driver, or by perturbing forces from outside agents such as winds.

### 3.2.1 Handling Models

In this thesis, the handling area of vehicle dynamics will be the primary topic of research. More specifically, this thesis deals with the open-loop "directional response" of a HEV with an energy-storage-flywheel to a small step input of the steer angle. The model is open-loop because the intent of the work is to quantify the handling characteristics of the vehicle. The driver is not included in the model. Inclusion of the driver in the model introduces uncertainty to the problem. The driver observes the position or direction of the vehicle, and introduces control strategies in reaction to the directional response of the vehicle. The driver's response obscures the data, making it difficult to discern between the drivers behavior and the behavior of the vehicle.

According to Alstead and Whitehead (1994), there are two open-loop tests that give a good general description of vehicle handling behavior. These are the steady state circular test, and the pseudo random steer input test, with a variation of the random steer scheme being a step steer input. These two tests produce information about the steady state and transient handling vehicle response properties of the vehicle. The steady state circular test involves driving a vehicle around a circular path at constant speed and recording data such as lateral acceleration, steering wheel position, and steering wheel torque. One of the most useful results of this test is the determination of the understeer or oversteer response of the vehicle. The step steer test provides insight to the transient response characteristics of the vehicle. Transient response data consists of rise and settling times for the

response variables, as well as the damping characteristics of the vehicle system.

These tests can be carried out on the test track with prototype and production vehicles, but as a design tool, they should first be carried out on a computer through the use of a vehicle dynamics handling model. The advantage of the computer model is that vehicle parameters can be changed readily and objective data can be collected without actually having to build the vehicle in that configuration.

### 3.2.2 Computers In Vehicle Dynamics Modeling

Alstead and Whitehead (1994) point out that suspension development is often carried out, not as a preliminary step, but after body styling, power train, chassis and floorpan designs have been laid down thus dictating many aspects of the suspension system before hand. The suspension is then developed based upon what has worked in the past, requiring considerable amounts of development time to refine the ride and handling characteristics to meet the demands of the market place. In an increasingly competitive automotive market, this time intensive development period must be reduced in order to meet the goal of reducing the product development cycle. One approach to shortening the development time is to use as much objective data as possible in the development of prototype vehicles. Objective data is obtained as a result of modeling the vehicle on the computer prior to building it, thus allowing some iteration of the suspension design and integration with the rest of the vehicle packaging before building it.

Each of the model types discussed in this work lend themselves to computer solution. The engineer or designer has several choices regarding the method of computer solution to be utilized. The model can be developed

in-house through computer code developed by the engineer, or one of the excellent commercial off-the-shelf software packages such as ADAMS ('Automatic Dynamic Analysis of Mechanical Systems', Mechanical Dynamics Inc., Ann Arbor, Michigan), and DADS ('Dynamic Analysis and Design Systems software', Computer Aided Design Software Inc., Oakdale, Michigan) can be used to develop the model. Each approach has advantages; the in-house approach has the advantage of flexibility and an intimate understanding of the model and is useful when the degree of complexity required to achieve the desired results is low enough to allow a simple model to be built. The draw back of the in-house approach is that it requires considerable skill in developing the code, and the complexity grows considerably with the inclusion of detailed kinematics of the suspension. The commercial packages have the capability of solving models having many degrees of freedom and have considerable capacity for expansion. In addition, they are modular in their treatment of the system, and they are effective at handling models with large numbers of kinematically constrained members. The drawbacks of the multibody programs are that they require a considerable amount of time to become proficient in their use and they are expensive to purchase and maintain.

For major model development, the commercial packages have the advantage, and are in widespread use in the automotive industry. ADAMS and DADS are three-dimensional multibody dynamics programs that have the ability to model certain vehicle characteristics in the non-linear range. These programs are capable of formulating and solving the dynamical equations of motion for a wide range of dynamic systems. Schröder and Chung (1995) describe the use of 80 to 100 degree-of-freedom ADAMS models to predict the influence of tire properties on vehicle lateral response. The use of ADAMS allowed relatively small differences in tire properties to be discerned by removing the uncertainty associated with track testing the

vehicles. Trom *et al* (1986) developed a multi-degree-of-freedom model of a midsized passenger car using DADS. The work is an exercise in the use of multi-body simulation programs to model bushed revolute suspension joints as spherical joints without bushing models. Bushing models increase the computational burden by increasing the degrees of freedom of the model. The results from the linear range of the model are compared to those obtained using the bicycle model, and the results from the non-linear range are checked against test data. The model produced acceptable results in both the linear and non-linear ranges.

Independent of the approach taken to model the vehicle, at some point in time a vehicle must be built and tested to ensure that the computer model and reality are indeed consistent with one another.

### 3.2.3 Vehicle Handling Model Types

Vehicle handling models are commonly divided into two types, steady state and transient, each of which are described in the following sections.

#### 3.2.3.1 Steady State

Steady-state handling models simulate the response of a wheeled vehicle to sustained lateral forces. Two types of lateral forces can be imposed on a vehicle, those due to a turn, and those due to external forces applied to the body of the vehicle. Steady state models focus on the dynamic reaction of the vehicle after sufficient time has passed for the transient effects to settle out. Steady state handling is conveniently broken into low-speed and high-speed regimes, with the importance of non-linear tire models becoming evident only in the high speed regime.

### 3.2.3.1.1 Low Speed

In the low speed regime, the tires of the vehicle do not need to generate lateral forces, hence they roll without slipping. This means that the tire must turn without a slip angle, and vehicle must behave as illustrated in Figure 3.4. Low speed implies that lateral forces are small, hence slip is negligible compared to the steer angle,  $\delta$ , and the ratio of the wheelbase to the turn radius,  $l/R$ . If the rear wheels have no slip angle, the center of the turn must lie on the line extended from the rear axle. In addition, the lines perpendicular to the front wheels should also intersect this line at the same point if they are to negotiate the turn without experiencing slip. In the course material presented by Gillespie (1991), this idealized situation is known as "Ackerman Geometry," where the geometry of the turn dictates the required front steer angles. These angles are defined as follows:

$$\delta_o \cong \frac{L}{(R + t/2)} \quad (3-1)$$

$$\delta_i \cong \frac{L}{(R - t/2)} \quad (3-2)$$

The average angle of the front wheels (assuming small angles) is defined as the "Ackerman Angle."

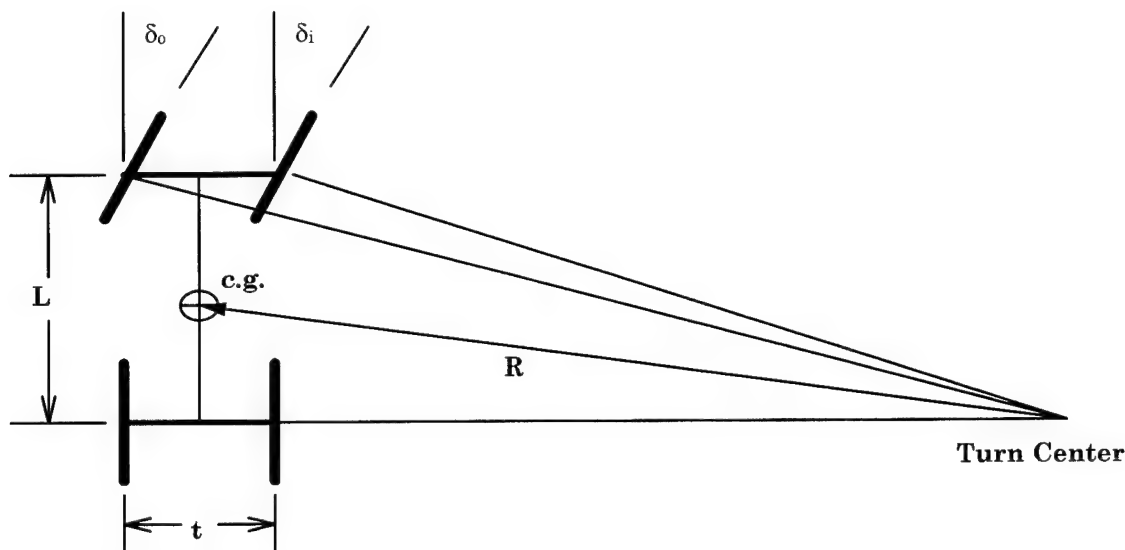


Figure 3.4 Geometry of a turning vehicle

#### 3.2.3.1.2 High Speed

The high speed regime is defined by the presence of high levels of lateral acceleration. At high speeds, the tires no longer roll without lateral slip and the equations of motion differ due to the presence of significant lateral acceleration. To put the vehicle in a state of equilibrium, the tires must generate lateral forces resulting in slip angles at each of the wheels. The presence of lateral slip introduces a considerable amount of complexity in the modeling process, and creates the requirement for modeling the tire and its interaction with the road surface. As will be shown in a later section, this is a broad area of research in and of itself.

#### 3.2.3.2 Transient Models

Between the initiation of steering input and the time the vehicle reaches a steady state motion, the vehicle is in a transient state. The characteristics exhibited by a vehicle during this period of transition from

one steady state motion to another are known as the transient response characteristics of a vehicle. The overall handling properties of the vehicle depend greatly on the transient response characteristics. According to Wong (1978), the optimum transient response is one that minimizes the time required to reach a desired deadband about the steady state value, with the least amount of oscillations along the way.

Control theory provides some standard measures of transient performance in the time-domain (Dorf, 1989). These standard measures are concerned with the swiftness of the response and the time required to reach steady state. Measures of response swiftness are rise time, ( $T_{\text{rise}}$ ), and peak time, ( $T_{\text{peak}}$ ), and the measure of time to steady state is the settling time, ( $T_{\text{settle}}$ ). The rise time is defined as the amount of time required for the parameter of interest to reach a particular level for the first time, the level of interest in this work will be 90% of the steady state value. Settling time is the amount of time required to enter the deadband for the last time, see Figure 3.5, the deadband will be  $\pm 5\%$  for this investigation.

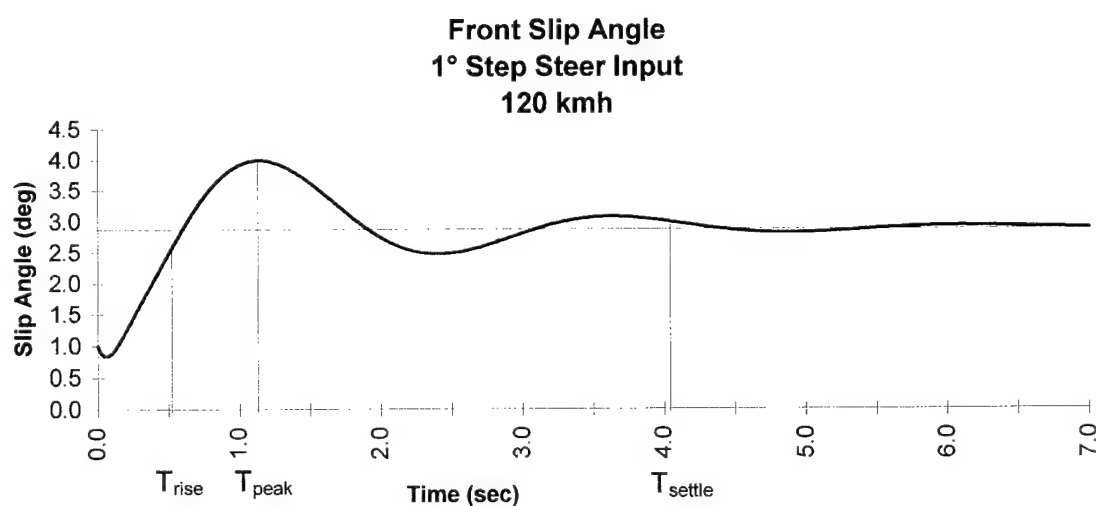


Figure 3.5 Step response of a system in the time domain

### 3.2.4 Vehicle Representations

The handling characteristics of a vehicle may be modeled in several ways. The level of complexity of the model depends upon the desired output of the model. For models concerned with gross motion of the vehicle, simple models with few degrees of freedom are sufficient. As the complexity of the model increases, the number of degrees of freedom rises. The following sections describe two types of vehicle representations that are appropriate for modeling low degree-of-freedom vehicle systems.

#### 3.2.4.1 Bicycle Model

The simplest form of vehicle handling model is the bicycle model. The bicycle model, Figure 3.6, was developed in Segel's (1956) fundamental work describing a mathematical model to simulate the responses of a vehicle to steering control. In Segel's model, three output variables are of particular interest, sideslip angle of the center of gravity of the sprung mass, the suspension roll angle, and the yaw rate of the vehicle fixed axis system. These three variables are solved for simultaneously as a result of a single input variable, the steer angle. The great simplification of the bicycle model is the representation of the two front and two rear wheels as single wheels at the front and rear of the vehicle, collecting the tire force properties of the two wheels into one single tire with equivalent properties. This simplification is made possible by assuming that the differences in steer angles between the left and right front tires due to Ackerman angle do not exist. The advantage of using the bicycle model is the simplicity of developing the equations of motion. An inherent disadvantage of the bicycle model is its inability to

account for lateral weight transfer during maneuvering, thus ignoring the effects of the suspension in generating lateral tire forces. For this reason, linear tire models are generally used with the bicycle handling model.

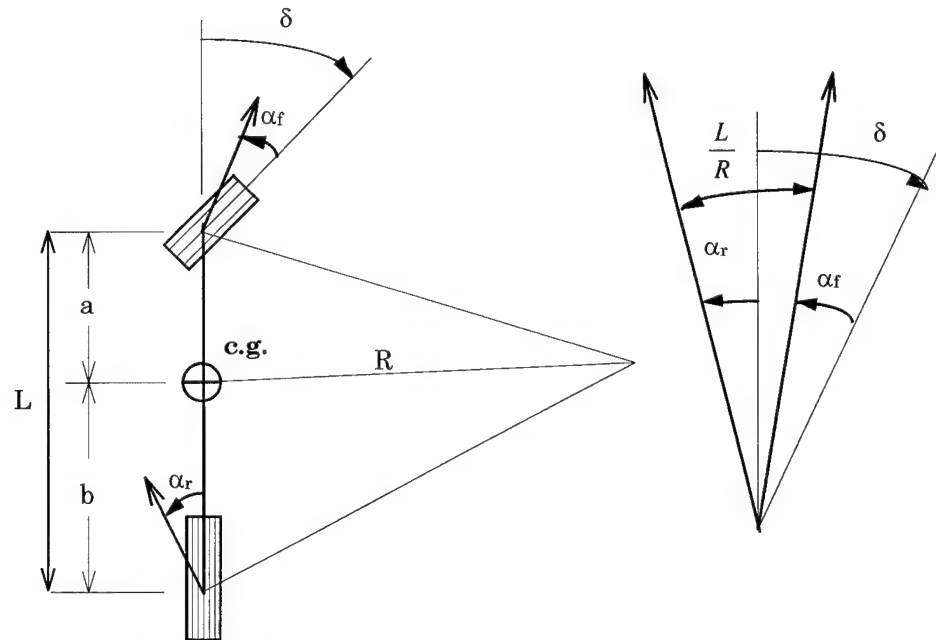


Figure 3.6 Cornering of a bicycle model

Segel's bicycle model continues to be used today in current research such as Chen and Guenther's (1991) work on the effects of suspension roll stiffness on handling responses, where they find that increased roll stiffness results in decreased steady state roll angle and roll damping, and increased roll natural frequencies and steady state yaw rate and sideslip angle at high speed. In this work, the limitation of lateral weight transfer is overcome by the use of coefficients in the derivation of the model for non-linear suspension effects such as roll steer and roll camber. In addition, the bicycle model has

been used as a benchmark for comparison of the linear range performance of the model in this work and those of others such as Trom *et al* (1986).

The bicycle model is also widely taught in classrooms around the country. Wong (1978) uses the bicycle model in the development of a simplified transient response model that addresses yaw rate and sideslip angle, but neglects roll angle. Gillespie (1992) uses the bicycle model as an instructional tool to used present the concepts of the steady state model for understeer and oversteer, and the transient handling model as well.

An example of the usefulness of the bicycle model is the development of the understeer gradient of a vehicle, which is a measure of open-loop handling performance under steady state conditions. The equation for understeer gradient is:

$$\delta = \ell / R + K_{us} a_y \quad (3-3)$$

where:

$\delta$  = Steer Angle

$\ell$  = Wheel Base of Vehicle

$R$  = Radius of Turn

$K_{us}$  = Understeer Coefficient (deg/g)

$a_y$  = Lateral Acceleration.

Equation 3.3 describes how the steer angle of the vehicle must be changed with the radius of turn,  $R$ , or the lateral acceleration,  $V^2/(g R)$ . Conversely, with a fixed steer angle, equation 3.3 can be used to determine the understeer coefficient using the relationship:

$$K_{us} = \frac{\alpha_f - \alpha_r}{a_y / g} \quad (3-4)$$

developed from the geometry of the bicycle model in a turn, Figure 3.6. We will see later that this has implications for the transient response of a vehicle where the transient understeer coefficient may differ considerably from the steady state value.

#### 3.2.4.2 Four Wheel Model

In all modern production motor vehicles, the suspension consists of parts which move independently of the chassis. To accurately model the dynamics of a vehicle, the model must include the effects of this relative motion to some degree. Most detailed treatments of vehicle handling models invariably include the effects of all four wheels and some of the suspension components of a vehicle. The level of detail depends upon the desired results. For models designed to predict gross deflections of the sprung mass, simple models of the spring and damper system are all that is required. For models designed to predict the actual deflection of suspension members under road load conditions, the model must account for far more of the suspensions components and linkages and their specific dimensions and orientations. The work by Morse (1995) describes a method whereby Force-Based Roll Centers (FBRC) are used to produce a solution for the loading of a vehicle chassis during a steady-state handling maneuver. This work is presented as an evolution of traditional Kinematic Roll Center (KRC) modeling, which assumes that the vehicle rolls about a fixed roll-axis neglecting the heave effects that occur as a result of the products of inertia and suspension geometry. The FBRC approach relaxes some of the assumptions of the KRC approach, most significantly, FBRC no longer assumes that the roll center of

the suspension is fixed in the chassis, and it includes nonlinear tire models and suspension deflections to define lateral load shifts.

#### 3.2.4.3 Suspension Modeling

The KRC modeling approach has been in use for quite some time, and is the standard approach to date. KRC is popular for its relative simplicity, and the fact that it lends itself to intuitive understanding of the vehicle reaction to lateral forces. Fundamental to the KRC approach is the understanding of a kinematic instant center of rotation based upon the geometry of the vehicle under static loading. Figure 3.7 depicts a vehicle with an independent suspension under static load conditions. The extension lines from the suspension arms intersect one another at the instant center of rotation for that wheel and its suspension components forming a four-bar linkage. The lines connecting the instant centers with the centers of the tire contact patches form another four-bar linkage with the ground and the line between instant centers acting as the other two members. The extension lines connecting the instant center with the center of the tire contact intersect to locate the instant center of rotation for the whole suspension system at that end of the vehicle. This point is known as the roll-center for the front or rear suspension, and the line connecting the front and rear roll-centers is known as the roll-axis.

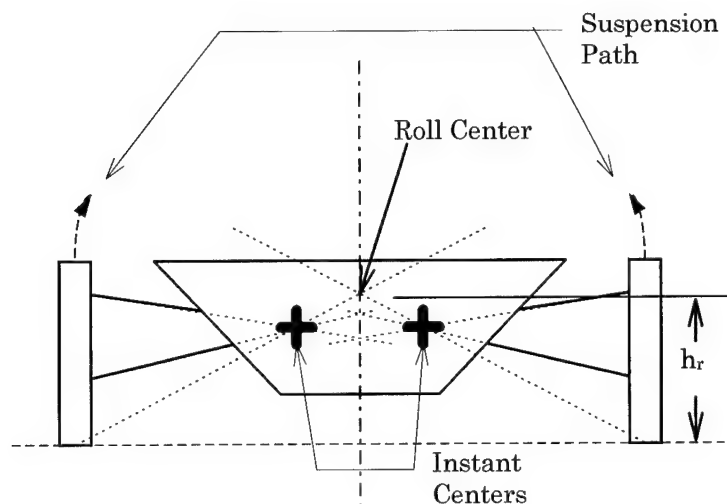


Figure 3.7 Roll Center Location

In the KRC approach to suspension modeling, the location of the roll-axis is fixed in the vehicle, where  $h_{rf/r}$  is the height of the front or rear roll axis. The value of  $h_{rf/r}$  will, in general, be different for the front and rear suspensions as shown in Figure 3.8. This development of the roll center assumes that the suspension is symmetric about the x-z plane of the vehicle whereby dictating that the roll-center will fall in that plane.

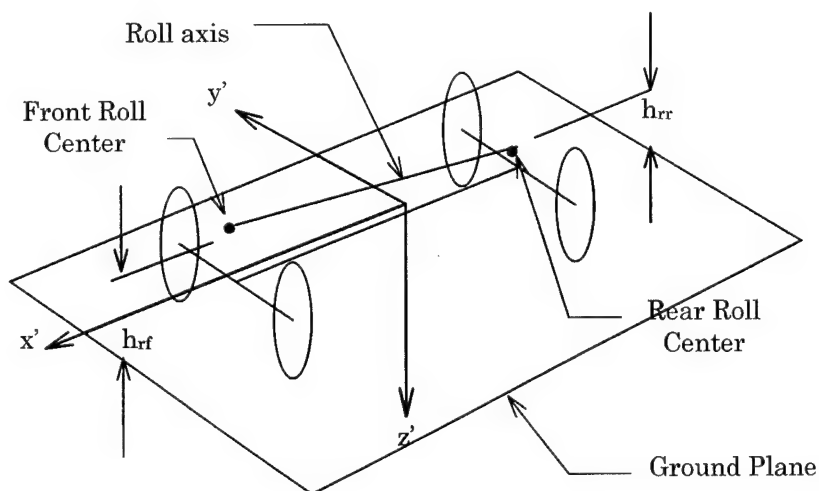


Figure 3.8 Roll axis orientation

### 3.3 Tire Models

The development of accurate tire performance models has been an area of active research for the past 40 years. The importance of accurately predicting the reaction forces generated at the tire-road interface is central to the success of most vehicle dynamics models. The level of complexity of the tire model may be correlated to the complexity of the vehicle model being developed. Tire models can be classified based upon complexity and will fall into one of three categories: linear, empirical, and complex.

#### 3.3.1 Linear Tire Models

The linear tire model assumes that a linear relationship exists between lateral tire force (cornering force) and slip angle,  $\alpha$ . This assumption is valid for a limited range of slip angles, and should only be used in situations where the slip angles are expected to be 6° or less (Bernard *et al*, 1977). In the linear model, the cornering force grows with slip angle by the relationship:

$$F_y = C_\alpha \alpha, \quad (3-5)$$

where:

$$C_\alpha = \left. \frac{\partial F_y}{\partial \alpha} \right|_{\alpha=0}$$

This relationship, shown in Figure 3.9, is often assumed to be true for any value of the vertical load on the tire, and thus limits the usefulness of the linear model.

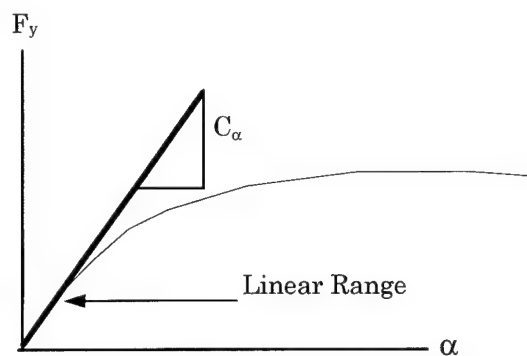


Figure 3.9 Cornering stiffness

The linear tire model is widely used in the development of simple vehicle models for academic purposes as in Gillespie (1992), Starkey (1995), and Wong (1978), because it introduces the concept of a simple and understandable model of the interaction between the tire and the road through the slip angle, without introducing the complexities of the other types of tire models. In vehicle modeling research, such as that done by Segel (1956), Starkey (1993), the linear tire model is most often used with bicycle-model based simulations that do not take into account the transfer of weight from the inside wheels to the outside wheels. Trom (1986), on the other hand, used the linear tire model in the development of a multibody model of a midsized passenger car in which tire models for longitudinal and vertical tire forces were also included.

In situations where differences between the vertical loads exerted on the tires at the four wheel locations of the vehicle are generated, it is of benefit to be able to model the lateral force generated as a function of the vertical load and the slip angle. The limitation of the linear tire model regarding the assumed independence of lateral force from vertical load has led researchers to search for more satisfactory models for vehicle dynamics investigations where lateral weight transfer occurs.

### 3.3.2 Empirical Models

Empirical tire models are sets of equations that represent various tire characteristics and the effect of these characteristics on the interaction of the tire with the road. These equations can be representations of particular tire characteristics based on a body of data collected over years of testing, or they may be the result of extensive tire testing carried out on a specific tire or class of tires. Tire testing requires the use of a test apparatus capable of varying input parameters and recording the reaction of the tire to those inputs. van Oosten and Bakker (1993) describe a test rig that is capable of applying various combinations of input parameters such as slip angle ( $\pm 20^\circ$ ), vertical load (1 - 10 kN), braking torque (free rotation to full locked), and camber angle to a tire moving at constant speed (up to 110 km/h). The rig is capable of measuring such tire parameters as self aligning torque, overturning moment, brake force, wheel load, and lateral force under a wide range of environmental conditions. In general, this data is generated based upon discrete values of vertical load, speed, camber angle, and torque while varying the slip angle.

Once the test data is collected and tabulated, polynomials are typically fit to the data for each of the fixed conditions used in the test. These polynomials are generated to represent the characteristics of the tire in computer modeling.

Empirical tire models have the distinct advantage of being computationally simple, and empirical tire models reflect real tire data measured in a strictly controlled environment that can be varied to represent a wide variety of anticipated conditions. The disadvantage of empirical models is that they lack the flexibility to extrapolate the data obtained from

the testing to various tire characteristics that were not within the realm of the initial test configuration.

### 3.3.3 Complex Models

In situations where different types of tires and tire construction methods are to be evaluated in a vehicle dynamics simulation, the tire model must be flexible. Flexibility implies that tire characteristics may be varied without redeveloping the entire model, or testing a full range of tire constructions. The most flexible types of tire models are complex tire models. Complex tire models are of two types, analytical and semi-empirical.

As the name implies, analytical models are based on purely analytical treatments of the physics of the tire and its construction. The spokes model developed by El-Nasher (1994) is representative of this class of tire model. In the spokes model, a series of spokes in a planar arrangement are attached to the hub of the wheel through a complex arrangement of radial, lateral, and circumferential springs. The spokes model follows the deformation of the springs as they pass through the contact region of the tire, and brings to equilibrium the forces generated by deforming the spokes with the available adhesion of the road surface. The spokes model, as presented by El-Nasher, is developed especially for use in modeling tire moments and lateral forces in transient situations where step inputs of angular velocity, lateral slip angle and vertical load are the possible input variables. The model has shown good agreement with data obtained through tire testing.

Semi-empirical models combine aspects of empirical modeling with purely analytical treatments of the physics of the tire and its construction. Semi-empirical models vary in complexity from the simple Linear Tire Model discussed earlier, which uses the empirical stiffness coefficient, to the more

complex 'Magic Formula' Tyre Model developed by Pacejka and Bakker (1993).

An early semi-empirical model developed by Dugoff *et al* (1970), is used in the 7-DOF vehicle model developed by El-Gindy (1986). The Dugoff model uses the concept of a stiffness coefficient in concert with modifying factors to calculate the longitudinal and lateral force components acting on a tire. This approach is limited to the linear range of the tire's lateral force response to vertical load and slip angle. Bernard *et al* (1977) built upon the work of Dugoff and others to develop a semi-empirical model capable of predicting shear forces at the tire-road interface under combined lateral and longitudinal slip conditions. The model is based upon measurement of free rolling lateral force versus slip angle characteristics, and longitudinal forces generated by a skidding tire. This data, in combination with knowledge of the sliding friction coefficient for the surface in question and some empirically determined factors for tire construction, allows the model to predict combined force response for a wide range of lateral and longitudinal slip conditions. The Magic Formula mentioned above has become a popular tire model, finding use in multi-body simulation programs, such as ADAMS, as a packaged tool for use in vehicle modeling. Prior to development of the Magic Formula tire model, tire models were limited to treating lateral and longitudinal slip conditions, but most neglected the effects of camber angle, rolling resistance, ply steer, conicity, and the asymmetry of the longitudinal shear force response to braking and driving. The magic model is capable of treating each of these effects in the process of modeling tires under combined lateral and longitudinal slip conditions. The benefit of such a model is that it allows a wider range of vehicle input combinations to be addressed. In any case, data must be collected from tire testing in order to develop the coefficients used in the models, the difference being the level of data that must be collected.

### 3.4 Closure

In this chapter we have seen the elements that must come together to develop a comprehensive vehicle dynamics model. First of all, a common language must be used based on widely understood standards for representing the vehicle. The representation of the vehicle must be developed as a series of equations which describe the kinematic and dynamic relationships that exist between the components that make up the vehicle. Finally, the connection of the vehicle with its environment must be developed. In the case of handling, this means the development of a tire model to simulate the interface of the vehicle with the road. In the development of all these relationships, assumptions must be made. These assumptions and their assembly into the model of this thesis are the subject of the next chapter.

## CHAPTER 4

### MODEL DEVELOPMENT

#### 4.1 Purpose

The purpose of this model is to simulate the directional response of a four wheeled HEV to a step input of the steer angle,  $\delta$ , looking specifically at the interaction of the gyroscopic properties of the flywheel and the handling characteristics of the vehicle in which the flywheel is mounted. The model is to produce output which gives insight into the gross handling effects that result from the inclusion of an energy storage flywheel in the HEV power train. In order to achieve this insight, the model will produce output of the following degrees of freedom: sideslip angle, roll rate, and the yaw rate. The results are obtained by developing the set of first order non-linear differential equations of motion, then solving them numerically through the implementation of a fourth order Runge-Kutta numerical integration algorithm (Hoffman, 1992).

#### 4.2 Vehicle Model Assumptions and Limitations

Because of the uncertainties of knowing the precise configuration of a physical system, simplifying assumptions must be made. These simplifying

assumptions allow the model to represent, in some limited way, the actions of the physical system. The following sections will detail the assumptions and limitations of this model.

#### 4.2.1 Suspension

The suspension model for this work is based on the KRC model discussed in the previous chapter. The KRC model will be used because the model is intended to simulate the gross handling of the vehicle, and not to provide detailed data on the kinematic reactions of independent suspension members. The simplicity of the KRC model coupled with the insight that it provides will compliment the goals of this work.

The front and rear axles are modeled as solid axles which couple the motions of the left and right wheels to one another. There is no fore-aft degree-of-freedom in the motion of the suspension relative to the body of the vehicle. The motion of the body relative to the front and rear axles is constrained to be purely rotational about the roll-axis. In addition, the wheels are assumed to remain in contact with the road surface at all times. This road contact constraint is implemented in the computer code rather than in the equations of motion. The following assumptions are inherent in the KRC model of the suspension:

1. The tires are pinned to the road. The tires are assumed to maintain a fixed distance between the centers of the contact patches, both fore-and-aft and side-to-side. This assumption neglects any lateral deflection of the tire carcass under the influence of lateral acceleration.
2. The roll axis position within the chassis does not change with suspension deflection. The roll axis will be assumed to remain fixed in the space of

the vehicle coordinate frame for all time and all orientations of the body and suspension.

3. The motion of the body with respect to the axles is purely planar rotation about the roll axis. Modeling of the suspensions as solid axles with a pivot joint at the attachment to the chassis allows this assumption to be made.
4. The roll stiffness is the result of linear springs and linear relationships in the actuation of those springs with suspension deflection. Roll stiffness is treated as two linear torsional springs located at the intersection of the roll-axis and the transverse vertical plane formed by the wheel centers of the front and rear suspensions respectively.
5. The roll damping is the result of viscous damping. Roll damping is implemented in the same manner as roll stiffness through the use of viscous dampers located coincident with the torsional springs.

#### 4.2.2 Mass Distribution

Masses in the model are distributed across three locations, the sprung mass of the chassis, the unsprung mass of the front suspension, and the unsprung mass of the rear suspension, see Figure 4.1.

1. The sprung mass is assumed to be located at the *c.g.* for the sprung mass at a height  $h$  above the roll axis and lying on the  $-z'$ -axis.
2. The location of the *c.g.* for the sprung mass is fixed in the chassis of the vehicle, and is assumed to be located at the same  $x$ - $y$  plane position as the *c.g.* for the entire vehicle. This assumption introduces some error in calculating the reaction of the vehicle to steering input, but alleviates the need for product of inertia calculation. According to Durisek *et al* (1994), determination of the products of inertia requires detailed design

measurements, or tilt table measurements from the vehicle being modeled. This data is not widely available for HEV, in fact it may not exist at all at this stage of HEV development.

3. The unsprung masses are assumed to be located in the center of the axles at a height  $r_w$  above the road. The variable,  $r_w$ , is the radius of the wheel under static load conditions. The unsprung masses are constrained to move only in the Earth fixed X-Y plane, they do not move in roll.

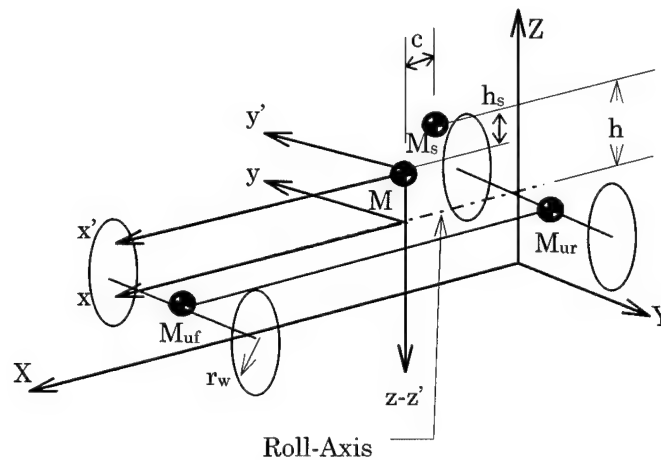


Figure 4.1 Vehicle masses and axis system

#### 4.2.3 Inertia

The gyrodynamic effect of the rotational inertia of an energy-storage flywheel system is the primary focus of this investigation, hence special consideration must be given to this aspect of the model. A spinning flywheel will resist changes in orientation of the spin axis with a gyrodynamic torque, also known as the gyroscopic reaction moment. The gyrodynamic torque that results from precessing a rotating flywheel is the vector product of the angular momentum of the flywheel and the imposed rotation. The angular momentum of a rotating body is given by the equation:

$$\bar{H} = I\bar{\omega} \quad (4-1)$$

where:

$I$  = Moment of Inertia (kg-m<sup>2</sup>)

$\bar{\omega}$  = Angular velocity vector of the flywheel (rad/sec)

The flywheel is assumed to be rigidly mounted to the chassis of the vehicle, therefore, some or all of the rotation of the vehicle may be imposed upon the flywheel during vehicle maneuvers. As discussed in the previous chapter, there are three degrees of freedom for rotation of a vehicle, these are roll, pitch and yaw. The gyrodynamic reaction of a flywheel to imposed rotations can be determined using Table 4.1:

Table 4.1 Reaction torque components produced by vehicle rotations  
Source: McDonald, 1982 (Updated to SAE axis convention)

Orientation of Flywheel Spin Axis (Positive SAE convention)	Imposed Vehicle Rotation (Positive direction assumed)		
	Roll	Pitch	Yaw
Lateral	-YAW	0	+ROLL
Vertical	+PITCH	-ROLL	0
Longitudinal	0	+YAW	-PITCH

The results in the table may be determined analytically using the equation:

$$\bar{T} = \frac{\partial \bar{H}}{\partial t} = \bar{H} = \bar{H} \times \bar{\Omega} \quad (4-2)$$

where:

$T$  = the reaction torque exerted by the flywheel against its supports,

and

$\bar{\Omega}$  = the precession rate.

The sense of the resultant torque is determined by the right hand rule, and its magnitude can be calculated as:

$$T = H\Omega \sin(\Theta_{H\Omega}) \quad (4-3)$$

where:

$\Theta_{H\Omega}$  = the smallest angle from  $\bar{H}$  to  $\bar{\Omega}$ .

In addition to the angular momentum of the flywheel, there are also contributions due to the other rotating bodies on the vehicle. Other rotating bodies include such components as the wheel and tire assemblies and certain components of the power train. In the realm of HEVs, the powertrain may include such high speed equipment as a gas turbine engine coupled to an alternator rotating at speeds near 100,000 rpm, but with small moments of inertia. In this model, the only additional angular momentum contribution that will be accounted for is that of the wheel and tire assembly, but provision has been made for inclusion of other rotating bodies and their associated moments of inertia at various stations on the vehicle. The additional angular momentum contribution of the wheel is calculated in exactly the same manner as it is for the flywheel. The angular momentum of all four wheels are directed parallel to the negative y-axis. Rotation of the wheels in the opposite direction is not allowed in the model. The angular momentum of the front wheels is assumed to remain parallel to the y-axis and steer angles are assumed to be small. In practice, this would be reasonable under most driving conditions. Steer angles up to  $10^\circ$  result in three place accuracy of the assumption, where  $10^\circ$  represents the approximate steer angle for emergency maneuvers (El-Gindy and Ilosvai, 1983).

#### 4.2.4 Coordinate Axes

The coordinate axes used in the development of the equations of motion for this model are of special interest, and are shown in Figure 4.1. The  $x,y,z$  axis system is fixed in the sprung mass of the vehicle and will move with the sprung mass as it is displaced due to vehicle maneuvers. Segel (1956) has shown that utilizing this orientation has several implications, but does not adversely affect the results of the model. The assumptions associated with the axis system used in this model are as follows:

1. The roll axis is assumed to be parallel with the  $x'$ -axis of the vehicle. The assumption of parallelism is reasonable based on the similarity of the front and rear suspensions, resulting in the roll centers at the front and rear having the same heights relative to the ground plane.
2. The  $x$ -axis is defined to be coincident with the roll axis, and all dynamic equations derived about the  $x',y',z'$  axis system will be translated to the  $x,y,z$  axis system.
3. For small roll angle,  $\phi$ , the lateral velocity,  $U_y$ , along the inclined  $y$ -axis will be equivalent to a lateral velocity in the ground plane, Figure 4.2.
4. For small  $\phi$ , the yawing velocity,  $r$ , about the tilted  $z$ -axis will be equivalent to a yawing velocity about an axis perpendicular to the ground plane, Figure 4.2.

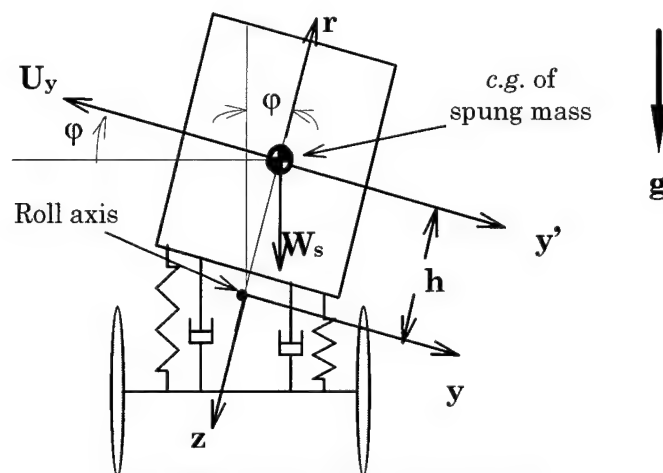


Figure 4.2 Small angle assumptions

#### 4.2.5 Degrees Of Freedom

The usefulness of a vehicle handling model is determined by the ability of the model to produce data that accurately describes the reaction of the vehicle to steering inputs. The factor that determines the ability of a model to describe the motion is the number of degrees of freedom of the model. In this work, the number of DOF needed to sufficiently describe the vehicle while satisfying the need to highlight the effects of including an energy storage flywheel in a HEV were determined to be three. The degrees of freedom used in this development are: Sideslip Angle, Roll Angle, and Yaw Rate. Intermediate to determining the roll angle is determination of the roll rate.

Sideslip angle ( $\beta$ ), has been developed in many different books and papers by authors such as Gillespie (1992), Wong (1978), and Segel(1956), and the development is generally carried out through the use of the bicycle model. Sideslip angle is a means of characterizing the relationship between the lateral and longitudinal velocities. In general, the sideslip angle

describes the angle between the longitudinal axis of the vehicle and the local direction of travel. In this model,  $\beta$  describes the angle between the positive x-axis and the velocity vector of the c.g. of the entire vehicle. During low speed maneuvers, each rear tire will track to the inside of the corresponding front wheel, but as lateral acceleration increases, the rear of the vehicle must drift outward in order to generate the necessary slip angles. As this outward drift increases,  $\beta$  changes magnitude and sign. By SAE convention,  $\beta$  is positive when measured clockwise from the x-axis to the velocity vector as shown in Figure 4.3. The speed of the vehicle at which the sign of  $\beta$  changes is known as the transition speed (Starkey, 1995), this speed is independent of the radius of the turn. Sideslip angle is defined as:

$$\beta = \tan^{-1} \left( \frac{U_y}{U_x} \right). \quad (4-4)$$

For small angles,

$$\beta = \left( \frac{U_y}{U_x} \right) \Rightarrow \beta U_x = U_y. \quad (4-5)$$

Roll angle, ( $\phi$ ), is simply the angle that the y-axis, fixed in the sprung mass, makes with the local horizontal plane. The Roll rate, ( $p$ ), is the variable solved for in the model, then that value is integrated to determine  $\phi$ . The roll angle is positive if it satisfies the right hand rule about the x-axis,  $\phi$  is shown in a positive sense in Figure 4.2.

Yaw rate, ( $r$ ), is the rate at which the x-y plane of the vehicle rotates in the earth fixed X-Y-Z reference frame. In steady state analysis,  $r$  is simply the radius of the turn divided by the forward speed, but the relationship can

not be defined that simply in analysis of the transient response. The yaw rate is positive for rotations that satisfy the right hand rule about the z-axis as shown in Figure 4.3.

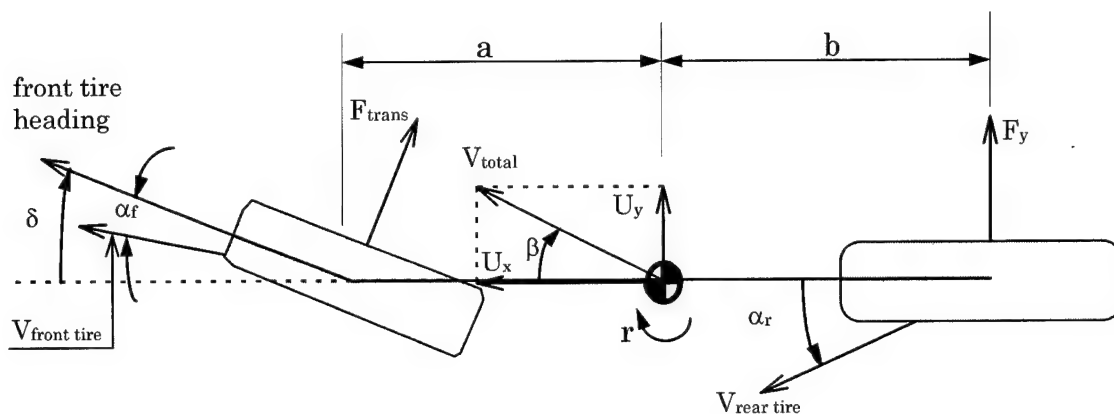


Figure 4.3 Representation of one side of vehicle

In order to maintain only three degrees of freedom, the forward velocity of the vehicle is assumed to be constant during all maneuvers of the vehicle. This assumption necessarily leads to the result that longitudinal acceleration of the vehicle is zero (Gillespie, 1992). From the relationship in equation 4-5 and the assumption of constant forward velocity, we can express the lateral acceleration as:

$$\dot{U}_y = \dot{\beta} U_x + \beta \dot{U}_x \Rightarrow \dot{U}_y = \dot{\beta} U_x \quad (4-6)$$

These last two relationships are fundamental to the development of the equations of motion.

Other DOF are possible in the development of vehicle handling models. The pitch rate is one possibility, but pitch is more commonly associated with the study of braking and ride, and it is assumed that the variables of pitch and

bounce have little effect on the handling characteristics of the vehicle. This assumption has been shown to be accurate in the work by Segel(1956).

#### 4.2.6 Other Assumptions

In addition to the assumptions stated above, several other simplifying assumptions were made.

1. The tractive force at the rear wheels is assumed to be constant and equal to any aerodynamic loads and rolling resistance imposed on the vehicle from the external environment (Segel, 1956).
2. Several minor suspension and tire effects have been neglected. Those effects include, camber thrust, roll steer, pneumatic trail, and rolling resistance. These assumptions have been made in an effort to focus the data to that which result from inclusion of the flywheel into the vehicle system.
3. The slip angle is the same for both front wheels, that is, the effects of Ackerman angle are ignored. To do otherwise would require knowledge of the specific suspension geometry of the vehicle (Morse, 1995).
4. The slip angle at the rear wheels is the same. This is a reasonable assumption as long as the rear axle is of the solid type. Independently suspended rear axles would not necessarily have such a relationship nor would those employing four wheel steer techniques (Gillespie, 1992).
5. The tractive force is equally divided between the two wheels, and does not affect the mechanical properties of the tires (Segel, 1956). This is an idealized differential in which the power is evenly distributed between the driven wheels under all maneuver conditions. Introducing different values of tractive force at the two driven wheels would lead to combined lateral and longitudinal slip in the tire model, thus increasing the



### 4.3.1 Sprung Mass

A summation of forces in the y-direction and a summation of moments about the x and y axes results in the following three equations:

$$\sum F_y: F_{yf} + F_{yr} = M_s a_y \quad (4-7)$$

$$\sum M_x: W_s h \sin \varphi + M_f + M_r + r H_y = I_{xx} \dot{p} + I_{xz} \dot{r} + h F_y \quad (4-8)$$

$$\sum M_z: a F_{yf} - b F_{yr} - p H_y = I_{zz} \dot{r} + I_{xy} \dot{p} \quad (4-9)$$

where:

$$a_y = (\dot{\beta} + r) U_x + h \dot{p} \quad (4-10)$$

$$M_f = -K_{rf} \varphi - \left. \frac{\partial \mathcal{L}}{\partial p} \right|_f p \quad (4-11)$$

$$M_r = -K_{rr} \varphi - \left. \frac{\partial \mathcal{L}}{\partial p} \right|_r p \quad (4-12)$$

$$K = K_{rf} + K_{rr} \quad (4-13)$$

Equation 4-8 now becomes:

$$\sum M_x: W_s h \sin \varphi - K \varphi - \left( \left. \frac{\partial \mathcal{L}}{\partial p} \right|_f + \left. \frac{\partial \mathcal{L}}{\partial p} \right|_r \right) p + r H_y = I_{xx} \dot{p} + I_{xz} \dot{r} + h F_y \quad (4-14)$$

Summing moments at the front and rear roll centers results in the following equations:

$$\sum M_{zf}: -l F_{yr} + a F_y - p H_y = (I_{zz} + m_z a^2) \dot{r} + I_{xz} \dot{p} \quad (4-15)$$

$$\sum M_{zr}: l F_{yf} + b F_y - p H_y = (I_{zz} + m_z b^2) \dot{r} + I_{xz} \dot{p} \quad (4-16)$$

$$\sum M_{yf}: a W_s - l W_r + p H_z - r H_x = 0 \quad (4-17)$$

$$\sum M_{yr}: -bW_s + lW_f + pH_z - rH_x = 0 \quad (4-18)$$

Equations 4-15 and 4-16 provide the relationship between the front and rear suspensions, and the sprung mass. Equations 4-17 and 4-18 provide the relationship between the flywheel angular momentum, and fore/aft weight transfer. This is the only place in the model where pitch effects will be considered. To resolve the static indeterminacy of equation 4-18, the FBD for the suspension of the vehicle shown in Figure 4.5 must be analyzed.

### 4.3.2 Front and Rear Suspension

The FBD of Figure 4.5 is typical of the front and rear suspensions. The subscripts indicate which variables are specific to the front or rear of the vehicle. In the diagram, subscripts 1 and 2 represent the right and left front tires respectively, and subscripts 3 and 4 represent the right and left rear tires respectively. The angular momentum vector  $H_{yf/r}$  is the angular momentum of both tire and wheel assemblies of the front or rear, and could be varied to include other effects such as the placement of electric drive motors at the wheels as well. The two moments seen acting about the roll axis are the moments due to roll stiffness and roll damping, and they act opposite to the roll angle and roll rate respectively. They are shown acting together, and are combined in the equations as  $M_{f/r}$  from equations 4-11 and 4-12. Summing forces in the y and z directions, and summing moments about the contact patches of all four tires results in the following sets of equations:

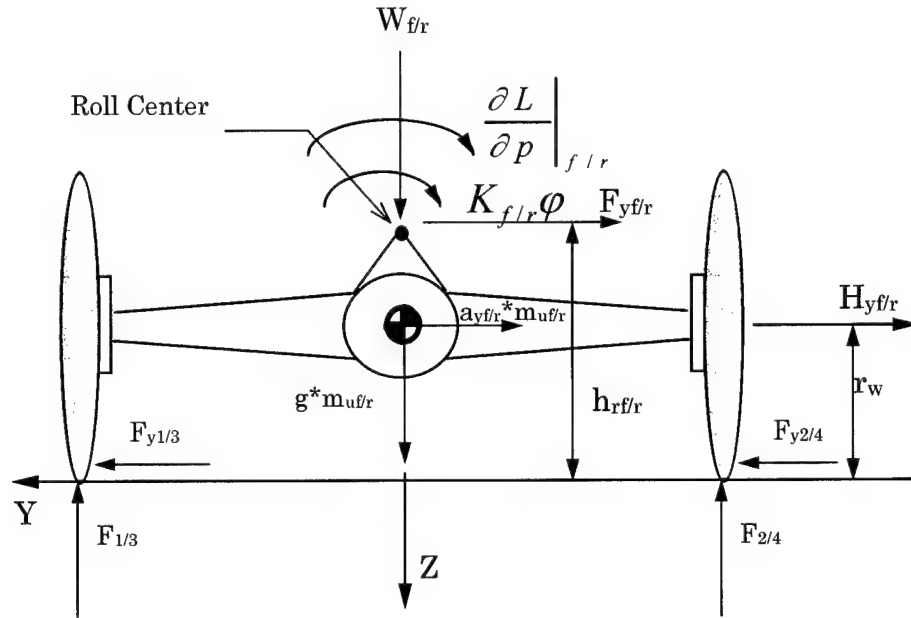


Figure 4.5 Free body diagram of typical suspension

Front Suspension:

$$\sum F_y: F_{y1} + F_{y2} - m_{uf} a_{yf} = F_{yf} \quad (4-19)$$

$$\sum F_z: W_f + g m_{uf} = F_1 + F_2 \quad (4-20)$$

$$\sum M_1: B_f F_2 = r H_{yf} + (g m_{uf} + W_f) t_1 + M_f + h_{rf} F_{yf} + m_{uf} a_{yf} r_w \quad (4-21)$$

$$\sum M_2: B_f F_1 = -r H_{yf} + (g m_{uf} + W_f) t_2 - M_f - h_{rf} F_{yf} - m_{uf} a_{yf} r_w \quad (4-22)$$

Rear Suspension:

$$\sum F_y: F_{y3} + F_{y4} - m_{ur} a_{yr} = F_{yr} \quad (4-23)$$

$$\sum F_z: W_r + g m_{ur} = F_3 + F_4 \quad (4-24)$$

$$\sum M_3: B_r F_4 = r H_{yr} + (g m_{ur} + W_r) t_3 + M_r + h_{rr} F_{yr} + m_{ur} a_{yr} r_w \quad (4-25)$$

$$\sum M_4: B_r F_3 = -r H_{yr} + (g m_{ur} + W_r) t_4 - M_r - h_{rr} F_{yr} - m_{ur} a_{yr} r_w \quad (4-26)$$

Where  $M_f$  and  $M_r$  are given in equations 4-11 and 4-12. Looking at the total acceleration of the front and rear unsprung masses due to motion of the vehicle in yaw results in the following equations for the total acceleration of those masses:

$$a_{yf} = (\dot{\beta} + r)U_x + a\dot{r} \quad (4-27)$$

$$a_{yr} = (\dot{\beta} + r)U_x - b\dot{r} \quad (4-28)$$

The vertical force exerted by the chassis on the suspension is the result of the weight of the sprung mass as well as the gyrodynamic effects of the flywheel. From equations 4-17 and 4-18, the relationship is as follows:

$$W_f = \frac{(bW_s - pH_z + rH_x)}{l} \quad (4-29)$$

$$W_r = \frac{(aW_s + pH_z - rH_x)}{l} \quad (4-30)$$

Taking the results for  $F_{yr}$  and  $F_{yf}$  from equations 4-19, and 4-23, which are derived from the front and rear suspension equations, and combining them with the equations derived for the sprung mass results in the combined equations of motion. After much simplification, the differential equations of motion can be written in matrix form as follows:

$$\begin{bmatrix} MU_x & (am_{uf} - bm_{ur}) & M_s h \\ (am_{uf} - bm_{ur})U_x & (I_{zz} + a^2 m_{uf} + b^2 m_{ur}) & I_{xz} \\ hM_s U_x & I_{xz} & I_{xx} \end{bmatrix} \begin{Bmatrix} \dot{\beta} \\ \dot{r} \\ \dot{p} \end{Bmatrix} =
 \begin{bmatrix} 0 & -MU_x & 0 \\ 0 & (bm_{ur} - am_{uf})U_x & -H_y \\ 0 & H_y - hM_s U_x & -\frac{\partial L}{\partial p} \Big|_{f+r} \end{bmatrix} \begin{Bmatrix} \beta \\ r \\ p \end{Bmatrix} + \begin{bmatrix} 1 & 1 & 0 \\ a & -b & 0 \\ 0 & 0 & W_s h - K \end{bmatrix} \begin{Bmatrix} F_{y1} + F_{y2} \\ F_{y3} + F_{y4} \\ \phi \end{Bmatrix} \quad (4-31)$$

where:

$$M = m_{uf} + m_{ur} + M_s \quad (4-32)$$

This is the final form of the equations of motion, but a closed form solution is not possible because of the empirical tire model, which produces the lateral tire forces,  $F_{y1}, F_{y2}, F_{y3}$ , and  $F_{y4}$ . The lateral tire forces depend on vehicle motion,  $(\beta, r, \phi)$ , as well as the vertical loads on the tires,  $F_1$  through  $F_4$ . This relationship is nonlinear, and for this model is represented by a set of 10th order polynomials that have been fit to empirical tire data.

#### 4.4 Tire Model

The tire model is developed based on test data for P215/70R14 tires made by the *Firestone Tire and Rubber Co.* The tires were tested while mounted on 14" X 5.5" wheels and inflated to 35 psi. The testing was carried out over a range of camber angles, slip angles and vertical loads. The data from the 0° camber angle test was the only data set used in this work, as camber angle was not variable in the vehicle model presented. This tire data has been shown to be accurate in experimental and analytical use by Morse (1995).

MATLAB (MATLAB, 1991) was used in developing the polynomials to describe the relationship between lateral force and slip angle. The tire data used in this model was limited to that which was obtained using slip angles from  $-11^\circ$  to  $+11^\circ$ . The data outside this range did not lend itself to an accurate polynomial fit. After the equations for the empirical tire model were developed, the model was built as a stand-alone computer program. The program was then used to test the output of the model against the original raw data. The results of the polynomial fit are shown in Figure 4.6, the figure shows the raw data plotted along with the data generated by the polynomial fit. The error bars represent  $\pm 2\%$  from the test data. It is evident from the plot that the polynomial fit is very good.

For the test configuration of this investigation, the available slip angle data was sufficient to analyze speeds over 130 km/h without exceeding the  $\pm 11^\circ$  bounds of the tire model. In addition to the slip angle limitations, the tire test data was limited to vertical wheel loads of 2800 LB (1270 kg) or less. Checks were placed in the computer code to ensure that neither of these limitations on the tire model were exceeded during solution of the equations of motion.

Interpolation is required to determine the value of the lateral force at a given slip angle and vertical load. The interpolation scheme in this tire model utilizes Lagrange Polynomials. An  $n^{\text{th}}$  order Lagrange polynomial is an equation that passes directly through the  $n+1$  data points used to generate the polynomial. The spacing between successive curves of increasing vertical tire load at fixed slip angle was analyzed. The relationship is very nearly quadratic in form. Figure 4.7 shows, as solid bars, the discrete values of lateral force for the five vertical loads provided by the raw data. Figure 4.7 also shows, as hollow bars, interpolated values of lateral force for a range of vertical loads. The trend line across the top of the data bars illustrates the fit of the quadratic assumption. Based upon this

result, the Lagrange Polynomials in the interpolation scheme used in the tire model are of second order.

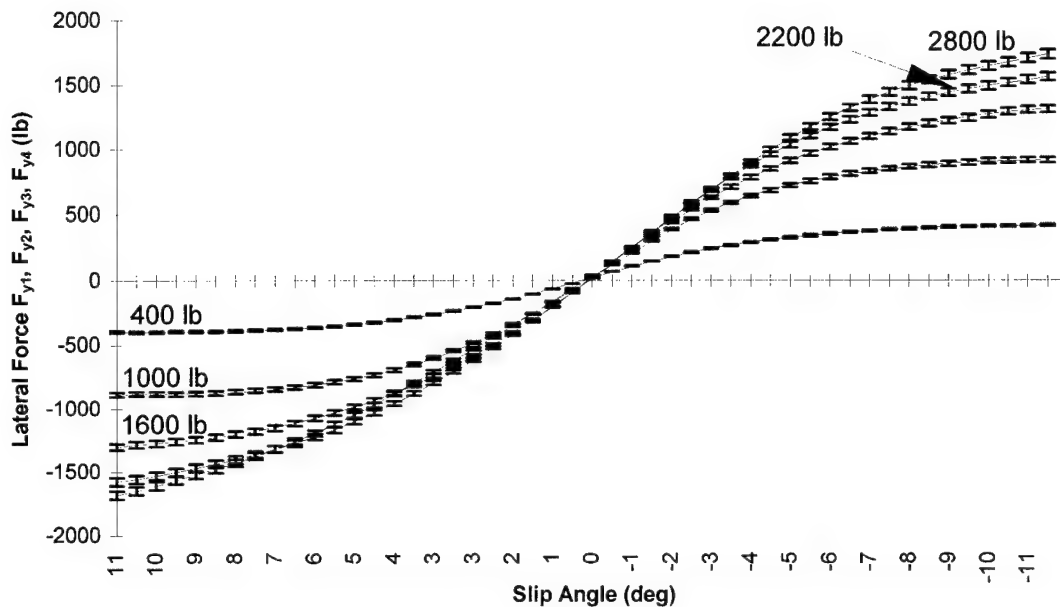


Figure 4.6 Combined raw tire data and empirical model data

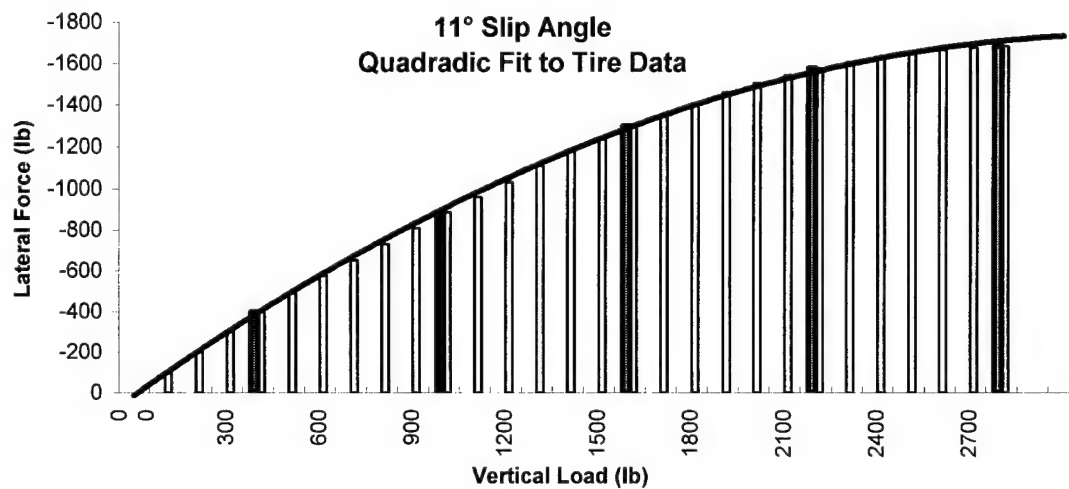


Figure 4.7 Interpolation results

#### 4.5 Slip Angle Development

Looking back at Figure 4.6, or back at Figure 4.3, it is evident that negative slip angles were chosen to produce positive lateral forces on the tire, in accord with SAE convention. When dealing with the linear tire model, this seeming inconsistency is dealt with by defining the cornering stiffness coefficient to be the negative of the slope of lateral force versus slip angle. In the empirical model of this thesis, this problem is dealt with by using a non-standard definition of positive slip angle. A slip angle is positive as shown in Figure 4.8, where counter clockwise measurement of the angle is defined to be positive. In this way, a positive slip angle produces a positive force of the road on the tire.

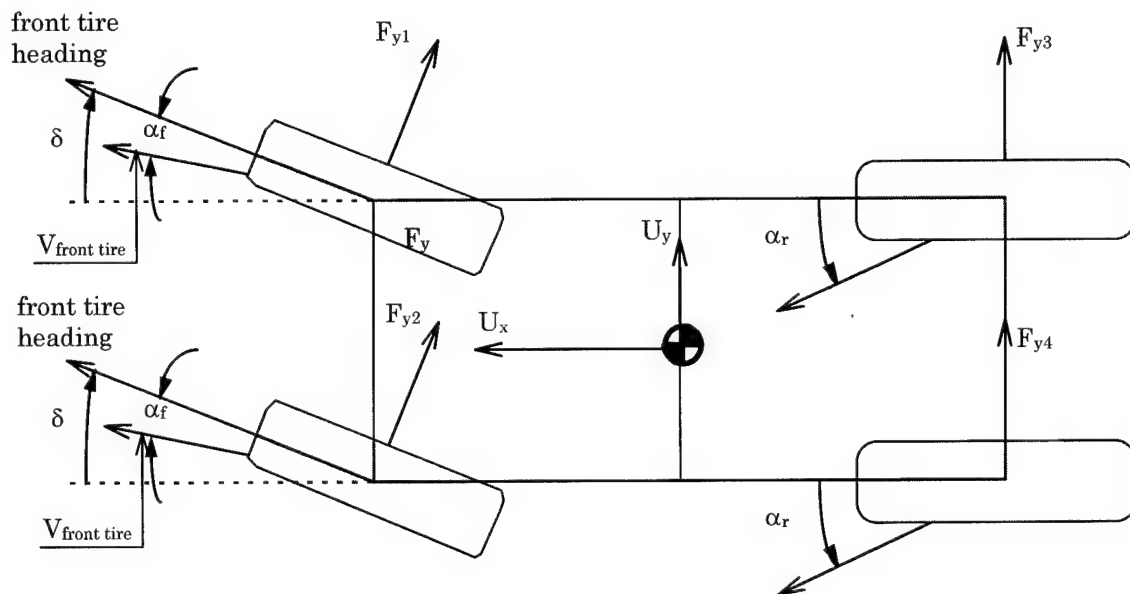


Figure 4.8 Four wheeled vehicle negotiating a right turn

Based on the assumption that both front tires and both rear tires experience the same slip angle, we can determine the relationships for the front and rear slip angles using the bicycle model. Once condensed to this

representation as previously shown in Figure 4.3, we can isolate the front and rear wheels. The front wheel and the associated rotation, heading, and slip angle are shown in Figure 4.9.

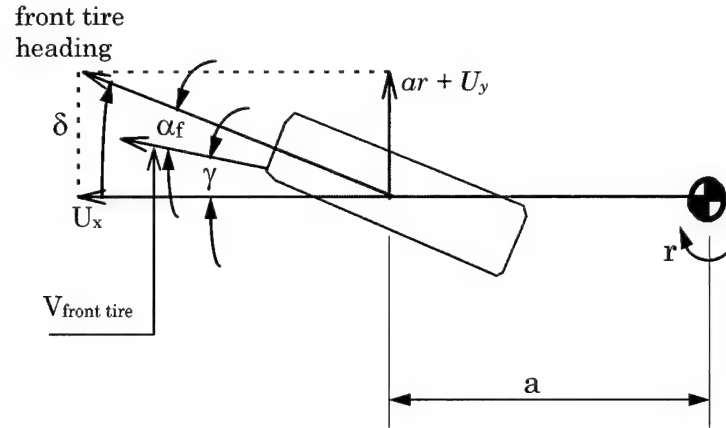


Figure 4.9 Determination of front slip angle,  $\alpha_f$

Determination of the slip angle can be accomplished by noting that, for small angles of  $\delta$ ,  $\alpha_f$ , and  $\gamma$ .

$$\gamma = \delta - \alpha_f = \tan^{-1} \left( \frac{ar + U_y}{U_x} \right), \quad (4-33)$$

but,

$$\frac{U_y}{U_x} = \beta \quad (4-34)$$

hence,

$$\alpha_f = \delta - \beta - \frac{ar}{U_x}. \quad (4-35)$$

Using Figure 4.10 and a similar approach to that used for the front wheel, the slip angle of the rear tire is determined to be:

$$\alpha_r = \frac{br}{U_x} - \beta \quad (4-36)$$

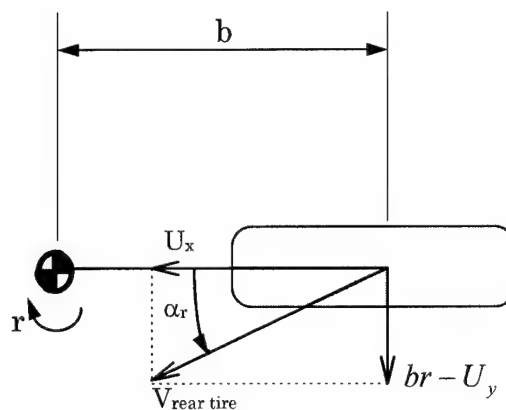


Figure 4.10 Determination of rear slip angle,  $\alpha_r$

#### 4.6 Flywheel Development

In developing the vehicle model for this investigation, it became necessary to design a flywheel as an energy storage device. The design is based on the need to store a particular amount of energy at a maximum rotational rate.

The first target is to determine the energy storage requirement of the vehicle system into which the flywheel will be integrated. In this case, a target energy level of 1 kW-hr has been chosen based on data presented in the works by Aceves and Smith (1995), Flanagan and Keating (1990), Brooke (1994), and Schreiber *et al* (1995), and an inclination toward acceleration performance.

The second target is to set a reasonable limit on the rotational speed that the flywheel must maintain during operation. The works by Post *et al*

(1994), Brooke (1994), Flanagan *et al* (1990), and Jayaraman (1991) indicate that flywheel speeds may range anywhere from 20,000 rpm up to 100,000 rpm. With such a wide range of values to consider, a compromise value of 40,000 rpm was chosen. The compromise is based on the desire to use a flywheel that would be buildable at this time, without reliance on exotic materials and processes (Flanagan *et al*).

Based on the knowledge of the two previously mentioned targets, the mass moment of the flywheel can be determined by the following relationships:

The kinetic energy of a flywheel is given by:

$$KE = \frac{1}{2} I \omega^2. \quad (4-37)$$

The energy storage capacity of a flywheel,  $E_{fw}$ , in W-hr is:

$$W \cdot hr = \frac{(\text{joules})}{3600 \text{ sec/hr}} = \frac{KE}{3600} \Rightarrow E_{fw} W \cdot hr \cdot 3600 \frac{\text{sec}}{\text{hr}} = KE. \quad (4-38)$$

Solving equations 4-37 and 4-38 for  $I$ , the moment of inertia of the flywheel is found to be:

$$I = \frac{7200 E_{fw}}{\omega^2}, \quad (4-39)$$

where  $\omega$  is in radians per second.

The end result is a flywheel with a mass moment of inertia of  $0.410 \text{ kg} \cdot \text{m}^2$ .

This value will be used in all further modeling calculations that require the moment of inertia of the flywheel.

#### 4.7 Vehicle Baseline Configuration

The parameter values used in the baseline configuration reflect the need to verify results on some level, hence certain vehicle parameter measurements from the work of Chen and Guenther (1991) were used to facilitate checking the results of the model against those obtained in that work. In particular, the magnitude of the steady state yaw rate and sideslip angle were verified between this work and that of Chen and Guenther. In light of these specifications and considerations from other works by El-Gindy (1986), and Scott (1995), the baseline vehicle of this thesis has been defined in Table 4.2, where sources of the values are shown in parenthesis.

Table 4.2 Baseline configuration - validation

Parameter	Value	Units
Ms - Sprung Mass (Chen & Guenther, 1991)	1000.00	kg
Muf - Front Unsprung Mass	0.00	kg
Mur - Rear Unsprung Mass	0.00	kg
Ixx - Moment of Inertia about x-axis (Chen & Guenther, 1991)	300.00	$kg \cdot m^2$
Izz - Moment of Inertia about z-axis(Chen & Guenther, 1991)	1610.00	$kg \cdot m^2$
Ixz - Product of Inertia about x-z plane (Chen & Guenther, 1991)	11.00	$kg \cdot m^2$
Krf - Front Roll Stiffness - (Chen & Guenther, 1991)	6000.00	$\frac{N \cdot m}{rad}$
Krr - Rear Roll Stiffness - (Chen & Guenther, 1991)	10250.00	$\frac{N \cdot m}{rad}$
dLdPf - Front Roll Damping (Chen & Guenther, 1991)	800.00	$\frac{N \cdot m \cdot sec}{rad}$
dLdPr - Rear Roll Damping (Chen & Guenther, 1991)	900.00	$\frac{N \cdot m \cdot sec}{rad}$
a - Distance from c.g. to Front Axle Centerline (Chen & Guenther, 1991)	1.20	m
l - Wheelbase (Chen & Guenther, 1991)	2.50	m
h - Height Of c.g. Above Roll Axis - (est)	0.25	m
rw - wheel & tire radius - (measured on midsized vehicle under static loading at 35 psi inflation pressure)	0.33	m
hrf - Height of Front Roll Center - (est)	0.33	m
hrr - Height of Rear Roll Center - (est)	0.33	m
Bf - Front Track Width - (est)	2.00	m
Br - Rear Track Width - (est)	2.00	m
Ifw - Flywheel Moment of Inertia - (Scott, 1995)	0.82	$kg \cdot m^2$
Iwheel - Tire & Wheel Moment of Inertia - (El-Gindy, 1986)	0.20	$kg \cdot m^2$

#### 4.8 Validation of Model

In order to ensure that the results produced by a model are accurate, a means of validation must be established. Past works by Segel (1956) El-Gindy and Ilosvai (1983), and Morse (1995) have utilized vehicle testing to compliment the analytical work. Vehicles with adjustable suspension geometry, and extensive instrumentation have been designed to measure the lateral and longitudinal accelerations, rotation rates, and angles of the reaction of the vehicle to steering input. Experimentation is the ultimate form of validation, as it compares the results derived from the model with the actual system being modeled. Once correlation between the model and the real world is established, the model can be exercised over an expanded range of input parameters under varying configurations of the vehicle. The results of these extended tests are held out to be valid based on the performance of the model under a limited set of conditions corresponding to those conditions under which testing was carried out.

In works by Chen and Guenther (1991), Trom *et al* (1986), and Schröder and Chung (1995); the validation approach has been used whereby a model that has been validated through experimentation and peer review is used as the basis for validation of a new model. The existing model validation method will be employed in a two phase approach in this work. The data produced by the vehicle model will be validated by comparison to two proven models of less complexity. The first comparison will be against the theoretical steady state response, and the second comparison will be made against the transient response of the bicycle model.

#### 4.8.1 Steady State Model

The steady state model for a vehicle is presented in texts by Gillespie (1992) and Wong (1978). The basis of the steady state solution to the turning behavior of a vehicle is the summation of forces in the lateral direction:

$$\sum F_y: F_{yf} + F_{yr} = \frac{MU_x^2}{R}, \quad (4-40)$$

where the lateral forces generated by the tires have come to equilibrium with the centripetal acceleration of the c.g. due to the turn. In the steady state, moments about the c.g. must be at equilibrium as well, hence:

$$\sum M_z: aF_{yf} - bF_{yr} = 0. \quad (4-41)$$

It can be shown that the slip angles at the front and rear wheels that result from these equations are:

$$\alpha_f = \frac{W_f U_x^2}{C_{af} g R}, \quad (4-42)$$

and

$$\alpha_r = \frac{W_r V^2}{C_{ar} g R}. \quad (4-43)$$

Based on equations 4-41, 4-42, and 4-43, it is possible to explicitly solve for the steady state values of the independent variables that define the degrees of freedom for this model. The following equations were derived and used to validate the steady state results of the vehicle handling model of this thesis:

$$\beta = \frac{b}{R} - \frac{aMU_x^2}{lRC_{ar}} \quad (4-44)$$

$$r = \frac{U_x}{r} \quad (4-45)$$

$$\varphi = \frac{\frac{M_s h U_x^2}{R}}{K_{rf} + K_{rr} - M_s h g} \quad (4-46)$$

$$a_y = \frac{U_x^2}{Rg} \quad (4-47)$$

where:

$$R = \frac{\left[ l + \frac{MU_x^2}{l} \left( \frac{b}{C_{af}} - \frac{a}{C_{ar}} \right) \right]}{\delta}, \quad (4-48)$$

$M = \text{total mass}$

Noting that these relationships were developed with a linear tire model, and that these equations will not reproduce the results that would come from using the empirical tire model, hence it will be necessary to substitute the linear tire model for the empirical tire model for the purpose of generating comparison data. The results of this comparison are summarized in Table 4.3.

Table 4.3 Steady state model comparison

Parameter	Steady State Value	Modeled Value with Linear Tire	Units
Lateral Acceleration, $a_y$	0.2081	0.2081	g
Sideslip Angle, $\beta$	-0.4549	-0.4549	deg
Yaw Rate, $r$	7.0146	7.0146	deg/sec
Roll Rate, $p$	0	0	deg/sec
Roll Angle, $\phi$	2.9646	-2.9646	deg
Front Slip Angle, $\alpha_f$	0.9499	0.9499	deg
Rear Slip Angle, $\alpha_r$	1.0021	1.0021	deg

Note that the signs on the values of  $\phi$  are not the same because the steady state equation 4-46 returns only the magnitude of the roll angle, consequently, knowledge of the direction of the steer angle is required to determine the sign on  $\phi$ . The results in Table 4.3 indicate that the model proposed in this thesis agrees exactly with the results obtained using the closed form steady-state solution of the vehicle motion.

#### 4.8.2 Bicycle Model

As described in an earlier chapter, the equations of motion for the bicycle model were developed by Segel (1956), and were validated in that work using vehicle testing. Since that time, the bicycle model has been used and validated repeatedly to the point where it is accepted as a valid model of the directional response of a vehicle to steering input at low levels of lateral acceleration. The bicycle model is valid for both transient and steady state regimes. For this reason, the bicycle model was used as the basic check of the

transient response results for the model of this thesis. Unfortunately, the bicycle model does have limitations. The bicycle model can be used to test the tire model, but it cannot be used to gain insight into the effects of weight transfer. The tire model was validated separately, so, in an effort to distill the comparative results down to their essence, the linear tire model will be used once again.

The equations of motion for the three degree of freedom bicycle model are as follows:

$$\begin{bmatrix} MU_x & 0 & M_s h \\ 0 & I_{zz} & I_{xz} \\ M_s h U_x & 0 & I_x \end{bmatrix} \begin{Bmatrix} \dot{\beta} \\ \dot{r} \\ \dot{p} \end{Bmatrix} =
 \begin{bmatrix} (C_{\alpha f} + C_{\alpha r}) & (aC_{\alpha f} - bC_{\alpha r} - MU_x^2)/U_x & 0 \\ (aC_{\alpha f} - bC_{\alpha r}) & (a^2C_{\alpha f} + b^2C_{\alpha r})/U_x & 0 \\ 0 & -M_s h U_x & \frac{\partial L}{\partial p} \Big|_{f+r} \end{bmatrix} \begin{Bmatrix} \beta \\ r \\ p \end{Bmatrix} +
 \begin{bmatrix} 0 & -C_{\alpha f} \\ 0 & -aC_{\alpha f} \\ W_s h + K_{rf} + K_{rr} & 0 \end{bmatrix} \begin{Bmatrix} \varphi \\ \delta \end{Bmatrix} \quad (4-49)$$

When solved numerically, this equation produces a response to a one degree step input that has the form shown in Figure 4.11.

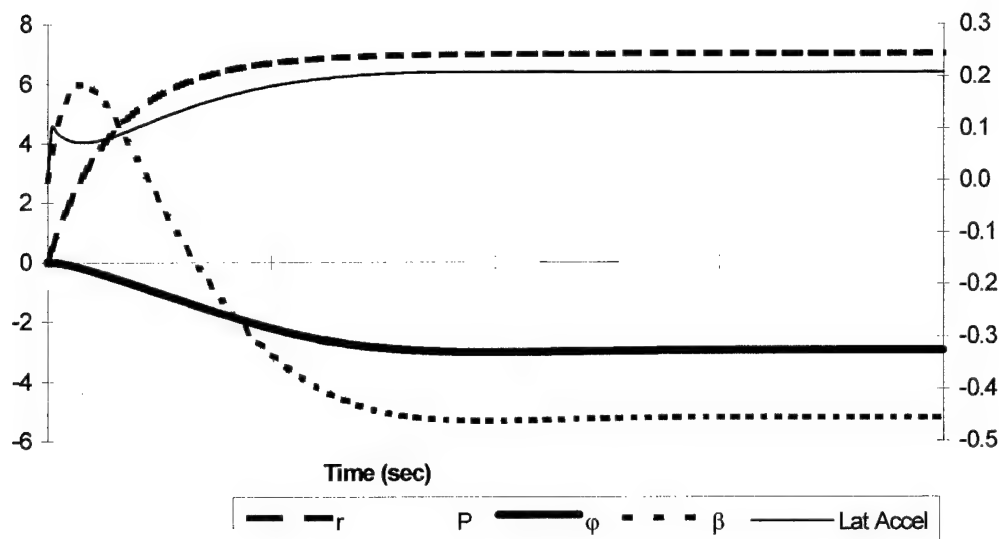


Figure 4.11 Bicycle model with linear tire - response to 1° step steer input

The bicycle model data depicted above will be expanded upon, and used to validate the results from the four-wheeled model of this thesis. The method of comparison will be to graphically evaluate the data produced from three separate computer runs. The first run will be for the bicycle model, the second for the four-wheeled model with the linear tire model, and the third run for the four-wheeled model with the empirical tire model. The two runs with the four-wheeled model will be performed without the angular momentum effects of the flywheel and the wheel and tire assemblies. After the model is validated, and the angular momentum the flywheel and the wheel and tire assemblies will be added, and their effects will become evident. The following figures graphically represent the three computer runs just described, where the label, "carpet," refers to the empirical tire model.

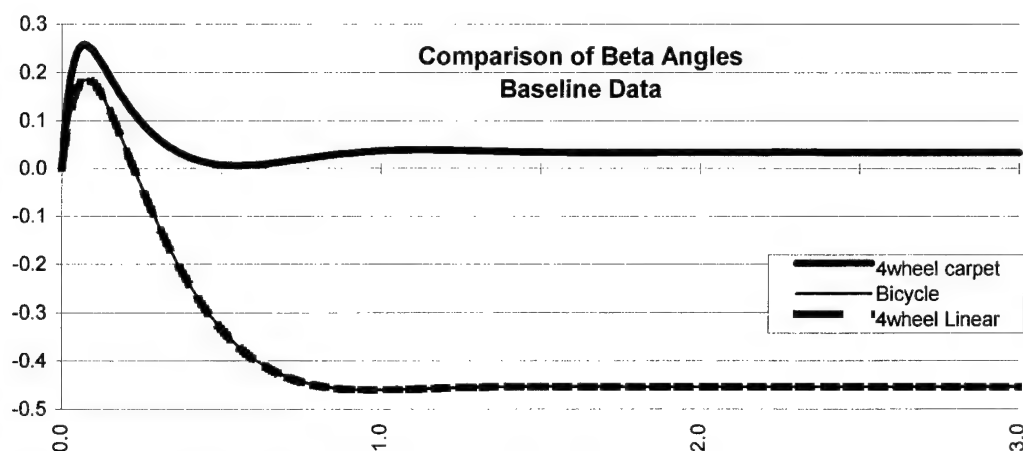


Figure 4.12 Sideslip angle response to  $1^\circ$  step steer input at 60 kph

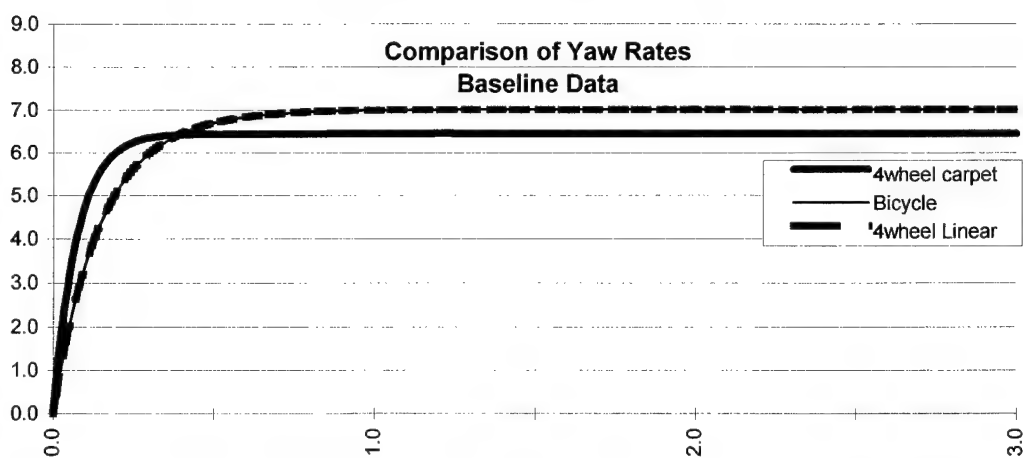


Figure 4.13 Yaw rate response to  $1^\circ$  step steer input at 60 kph

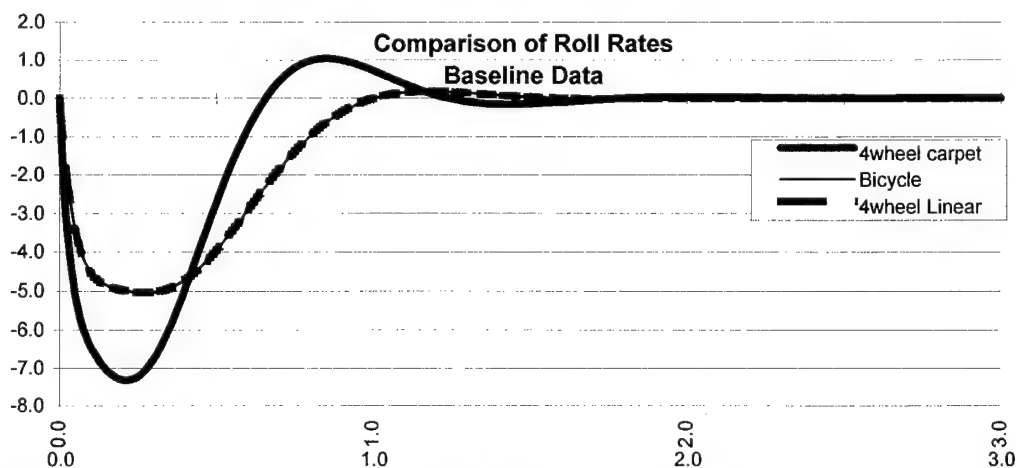


Figure 4.14 Roll rate response to  $1^\circ$  step steer input at 60 kph

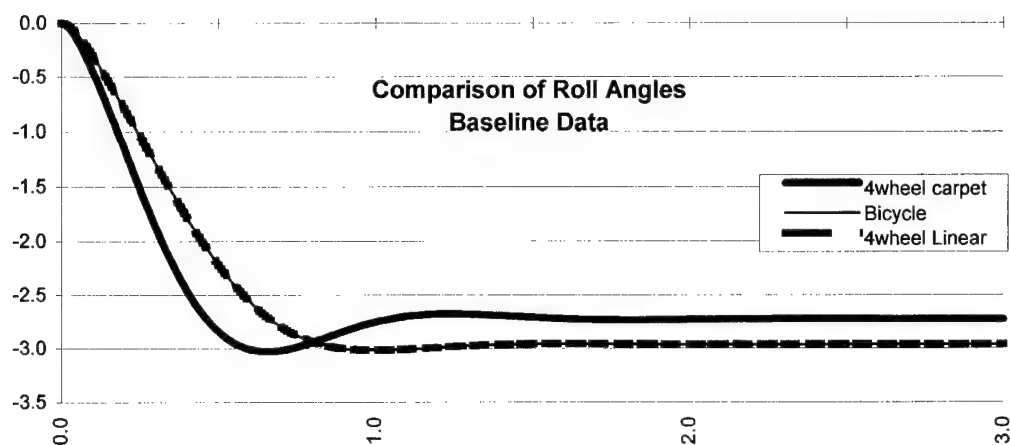


Figure 4.15 Roll angle response to 1° step steer input at 60 kph

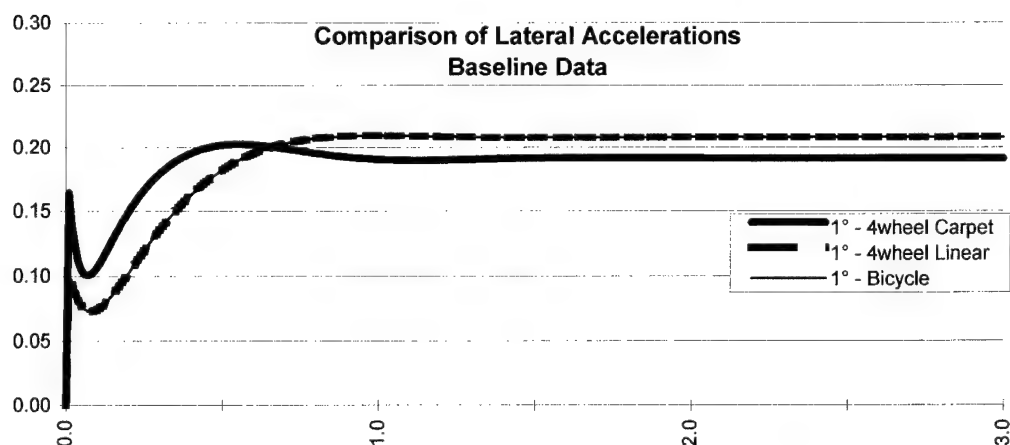


Figure 4.16 Lateral acceleration response to 1° step steer input at 60 kph

In looking at the results shown in the preceding figures, it is evident that the four-wheeled model produces exactly the same results as the bicycle model when the same cornering stiffness coefficient is used in each. The traces of the data for each of the two runs overwrite one another at every point. This indicates that the model is capable of producing the transient and steady state response results that are consistent with those produced by the bicycle model using the linear tire model in both cases.

The differences between the reaction of the vehicle with the linear tire model and with the empirical tire model are quite significant. These differences can be attributed to two interrelated items, the combination of

lateral weight transfer with the non-linear behavior of the tire, and the fact that the cornering stiffness values for the linear tire and the empirical model are not the same, nor are they expected to be. In the first item, lateral weight transfer forces the load dependency of the of the tire model to influence the reaction of the vehicle, and in the second item, the value of the cornering stiffness coefficient used in the linear tire model is not the same as the value that would be derived from determining the slope of the curve near the origin in Figure 4.6.

#### 4.9 Closure

In this chapter we have seen the development of the equations of motion for a four wheeled HEV that uses a flywheel energy storage device. The assumptions required to develop the equations involve simplification of the suspension and the mode of operation of the vehicle. Additionally, the equations are based on a vehicle system with distributed masses and an idealized axis system centered at the intersection of the roll axis and the z-axis of the sprung mass. The resulting equations are first order, non-linear differential equations. The non-linearity arises because of the presence of an empirical tire model that treats the weight dependent relationship between lateral force and slip angle as a set of five 10<sup>th</sup> order polynomials. The model is validated using two separate approaches: first, the steady-state results are compared to the analytical solution for the steady state-response; second, the transient and steady-state responses of the four wheeled model are compared to those attained using the bicycle model with a similar configuration of masses and a linear tire model. As a final check, the results obtained from the four-wheeled model are generated using the empirical tire model, and the shape of the response is compared to that obtained during the bicycle model testing.

## CHAPTER 5

### RESULTS AND ANALYSIS

This chapter presents the results of testing the model under a clearly defined set of circumstances. The model is exercised using various orientations of the flywheel over a wide range of flywheel rotation rates. The results are then analyzed to determine the handling effects that arise from including the flywheel in the vehicle system. Trends are noted and characteristics that are unique to the flywheel are identified. Metrics include the rise and settling times as well as interpretation of the damping characteristics of the vehicle response.

#### 5.1 Test Configuration

All tests are performed at a constant forward speed ( $U_x$ ) of 60 km/h. A step steering angle of  $+1^\circ$  is input to the vehicle, and the response of the system is calculated numerically. The results of the calculations for each of the degrees of freedom are plotted against time for various values of the angular speed of the flywheel. The model was exercised in 10,000 rpm increments of flywheel speed over a range from -100,000 to +100,000 rpm. To avoid overcrowding in the plots of the data, in some cases, not all of the data is plotted. The configuration of the vehicle for the simulation of the HEV is as shown in Table 5.1.

Table 5.1 Vehicle configuration - testing phase

Parameter	Value	Units
Front Roll Stiffness -	17189.00	$\frac{N \cdot m}{rad}$
Rear Roll Stiffness -	10313.00	$\frac{N \cdot m}{rad}$
Front Roll Damping	900.00	$\frac{N \cdot m \cdot sec}{rad}$
Rear Roll Damping	800.00	$\frac{N \cdot m \cdot sec}{rad}$
Longitudinal Velocity	60.00	$km/hr$
Distance from c.g. to the Front Contact Patch	1.20	$m$
Wheelbase	2.50	$m$
Height of c.g. above roll axis	0.25	$m$
Height of Front Roll Center	0.33	$m$
Height of Rear Roll Center	0.33	$m$
Front Trackwidth	1.56	$m$
Rear Trackwidth	1.56	$m$
Tire Rolling Radius	0.33	$m$
Mass Moment of Inertia about the X-Axis	435.00	$kg \cdot m^2$
Mass Moment of Inertia about the Z-Axis	2334.00	$kg \cdot m^2$
Mass Product of Inertia the Z-Axis	11.00	$kg \cdot m^2$
Steer Angle	1.00	$degrees$
Sprung Mass	1250.00	$kg$
Front Unsprung Mass	110.00	$kg$
Rear Unsprung Mass	90.00	$kg$
Flywheel Moment of Inertia	0.41	$kg \cdot m^2$
Tire & Wheel Moment of Inertia (each)	0.20	$kg \cdot m^2$

The vehicle total mass, wheelbase and trackwidth are based on the specifications for the 1997 Ford Taurus (Ford, 1996). The unsprung masses at the front and rear of the vehicle are estimated based upon an empirical relationship relating the unsprung mass of the suspension to the total mass of the vehicle as presented in the work by Barak (1991). The roll stiffness at the front and rear of the vehicle are also estimated based on data from the work by Barak. The moments of inertia for the vehicle were estimated based upon data from the work by Chen and Guenther (1991), and the moment of inertia for the tire and wheel assembly were based on data used in the work by El-Gindy and Ilosvai (1983). The heights of the front and rear roll centers, the tire rolling height, and the roll damping are unchanged from those presented in the baseline version of the vehicle used for validation of the model, (see Chapter 4).

The design of the flywheel is based on the description given in chapter 4. The energy capacity of the flywheel is 1 kw-hr, at a maximum expected speed of 50,000 rpm. Several of the simulations detailed in the following sections will use rotational speeds far in excess of this value to show the effects future high energy flywheels might have on a vehicle. An example of a high energy storage capacity flywheel is given in the articles relating to the Patriot Race Car (Jost, 1994, Brooke, 1994, Scott, 1995), in which a HEV drivetrain is discussed that uses a flywheel with a 2 kw-h energy storage capacity at 50,000 rpm. The simulations run at 100,000 rpm represent the potential effects that this flywheel might have on a vehicle.

## 5.2 Flywheel Orientation

Orientation of the flywheel will be investigated to determine the effect that various alignments might have on the handling performance of the

HEV. Possible effects include changes to the transient and steady state response characteristics of the model: understeer coefficient, sideslip angle, roll rate and angle, and lateral acceleration. Three possible orientations are investigated, including alignment along the x-axis, the z-axis, the y-axis. Off axis orientations could be investigated by decomposing the angular momentum vector of the flywheel into three components but the possible orientations are endless, and are not investigated in this work. Positive and negative axis alignments are carried out in the model by changing the sign of the angular momentum vector. This sign change is implemented by changing the direction of rotation of the flywheel.

Table 5.2 Reaction torque components produced by vehicle rotations

Source: McDonald, 1982 (Updated to SAE axis convention)

Orientation of Flywheel Spin Axis (Positive SAE convention)	Imposed Vehicle Rotation (Positive direction assumed)		
	Roll	Pitch	Yaw
Lateral	-YAW	0	+ROLL
Vertical	+PITCH	-ROLL	0
Longitudinal	0	+YAW	-PITCH

### 5.2.1 X-Axis Alignment

The spin axis of the flywheel, and thus the angular momentum vector, will be aligned with the longitudinal x-axis of the vehicle. Alignment of the spin axis with the x-axis results in coupling of the pitch and yaw degrees of freedom, as can be seen in Table 5.2. The pitch degree of freedom is not treated in this work, thus only a yaw precession can be imposed on the flywheel. The effect of positive yaw precession is to load the front wheels and

unload the rear wheels, with the opposite effect resulting from a negative yaw precession rate. This loading will effect the lateral forces generated by the front and rear wheels to some degree resulting in possible alteration of the handling performance of the vehicle.

Figure 5.1 depicts the effect of aligning the spin axis of the flywheel with the x-axis. The angular rates of the flywheel for this figure are +100,000 rpm, -100,000 rpm, and 0 rpm. The extreme values are chosen in order to clearly illustrate the effect that this alignment has on vehicle handling characteristics. The plots of the three values for the spin rate of the flywheel are virtually indistinguishable from one another, even for this very high spin rate. The conclusion that must be drawn for the x-axis alignment is that there is little effect on the handling characteristics of the vehicle due to alignment of the spin axis of the flywheel with the vehicle x-axis. Further study may indicate that this alignment will affect the ride properties of the vehicle.

These results are partly expected because the pitch degree of freedom is not treated in this work. The only pitch effect is the pitch moment generated by the flywheel when the vehicle rolls or yaws. This coupling shows up as changes in vertical loading at the tires.

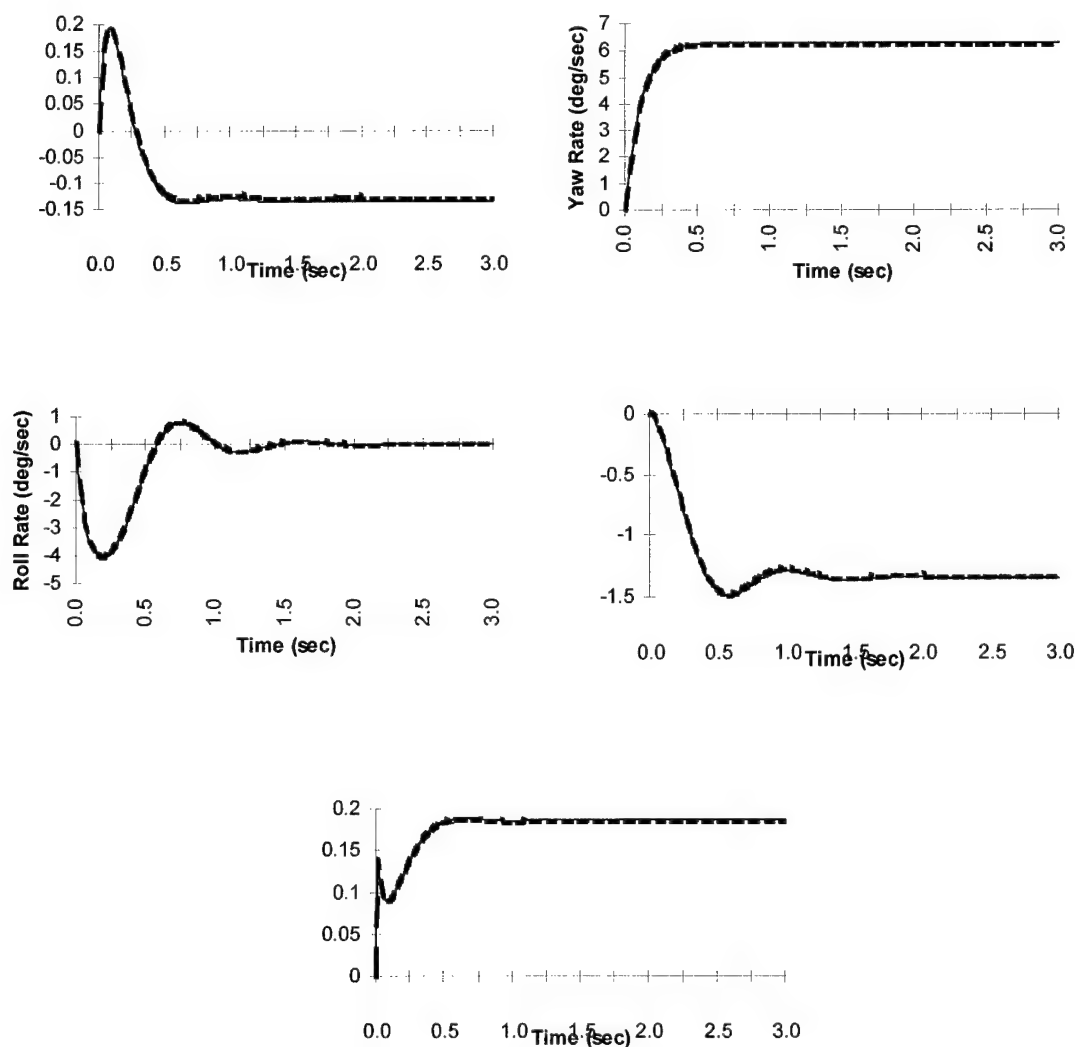


Figure 5.1 X-Axis flywheel alignment results

### 5.2.2 Z-Axis Alignment

Aligning the spin axis of the flywheel with the z-axis implies that the angular momentum vector will be directed into or out of the ground plane. This alignment couples the roll and pitch degrees of freedom. Again, the pitch degree of freedom is not treated in this work. Consequently, the only

effect that may result from this alignment is that a positive roll precession rate will tend to load the front tires and unload the rear, and negative roll precession rate will have the opposite effect. This orientation is similar to the case for the x-axis alignment, where the potential exists for the reaction torque of the flywheel to load the wheels and effect the handling of the vehicle.

Figure 5.2 shows the effects of the z-axis alignment. Once again, the angular rates of the flywheel for this figure are +100,000 rpm, -100,000 rpm, and 0 rpm in an effort to highlight the potential effects of this orientation of the flywheel. Analysis of the results show that aligning the flywheel with the z-axis has little effect on the handling properties of the vehicle. Similar to the x-axis orientation, the z-axis orientation may have ride implications due to the roll-pitch coupling.

The reasons for the minimal effect of aligning the flywheel with the z-axis is the same as that given in the previous discussion for the x-axis.

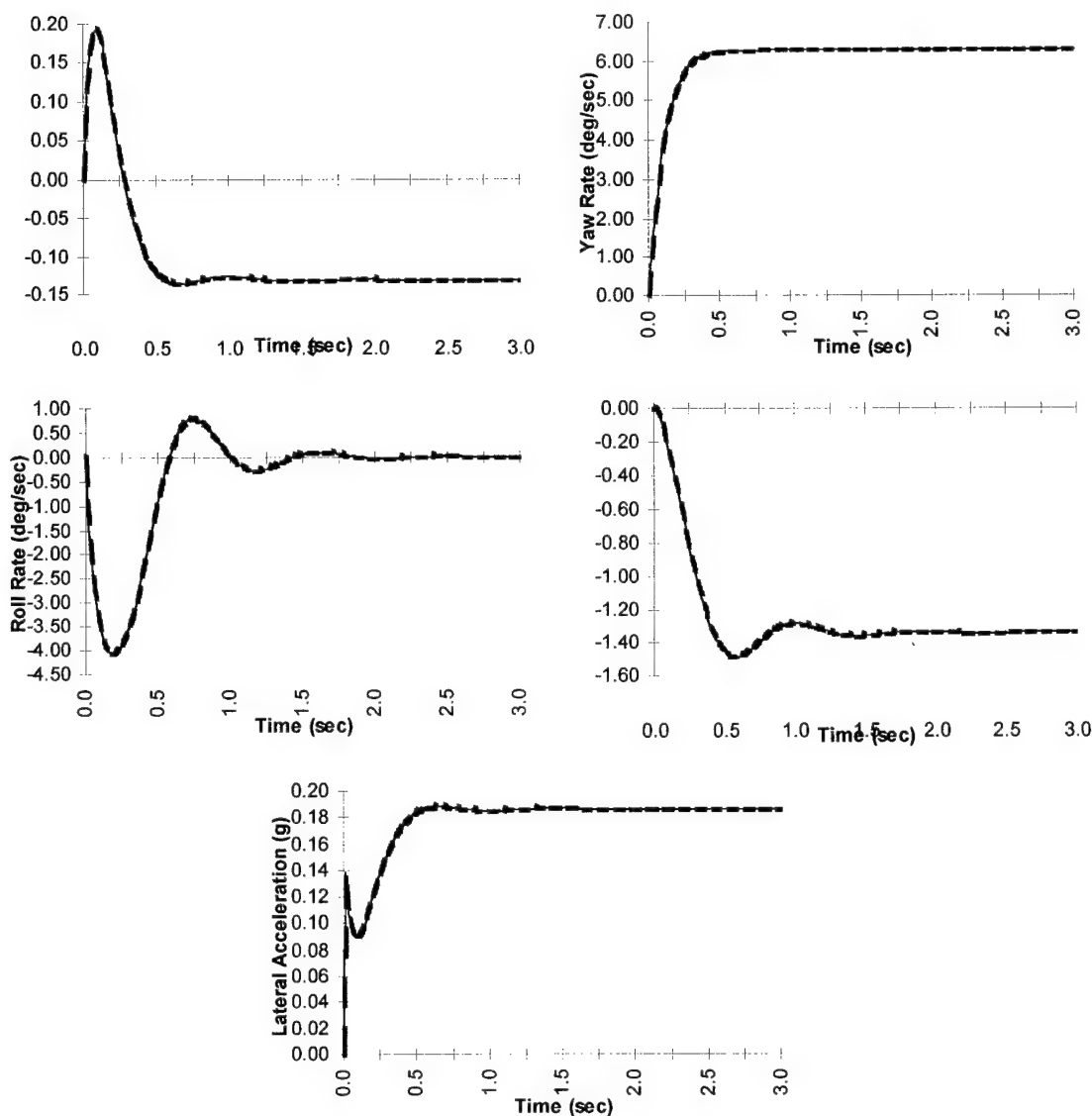


Figure 5.2 Z-Axis flywheel alignment results

### 5.2.3 Y-Axis Alignment

Aligning the spin axis of the flywheel with the y-axis puts the angular momentum vector transverse to the long axis of the vehicle. This alignment couples the roll and yaw degrees of freedom to one another. In the analysis of vehicle handling performance, these are the two degrees of freedom that are

of most interest. Because of this fact, the alignment of the spin axis of the flywheel with the y-axis has the most potential to significantly affect the handling properties of the vehicle in which the flywheel is mounted.

In analyzing the effects of the y-axis orientation, each of the degrees of freedom developed in this model will be studied individually. The various alignments of the flywheel will be referred to as "positive orientation" when the angular momentum vector of the flywheel is aligned with the positive y-axis, represented by the 0→100,000 rpm portion of the graph, and "negative orientation" when the angular momentum vector of the flywheel is aligned with the negative y-axis, shown by the 0 →-100,000 rpm range of the graph.

#### 5.2.3.1 Y-Axis Alignment Effects - Sideslip Angle ( $\beta$ )

Sideslip angle describes the motion of the vehicle in the transverse direction. It provides insight into the lateral velocity response of the vehicle. The relationship for sideslip angle is given by the equation:

$$\tan \beta = \frac{U_y}{U_x}, \quad (5-1)$$

but for small angles, this relationship becomes:

$$\beta = \frac{U_y}{U_x}, \quad (5-2)$$

where the velocities are in the vehicle frame. The effect on sideslip angle should come as a result of the changes in weight balance across the four tires as a result of the other degrees of freedom in the model, because no direct

coupling of sideslip angle and flywheel angular momentum is present in the model. The effect of flywheel orientation on transient and steady state response is depicted in Figure 5.3.

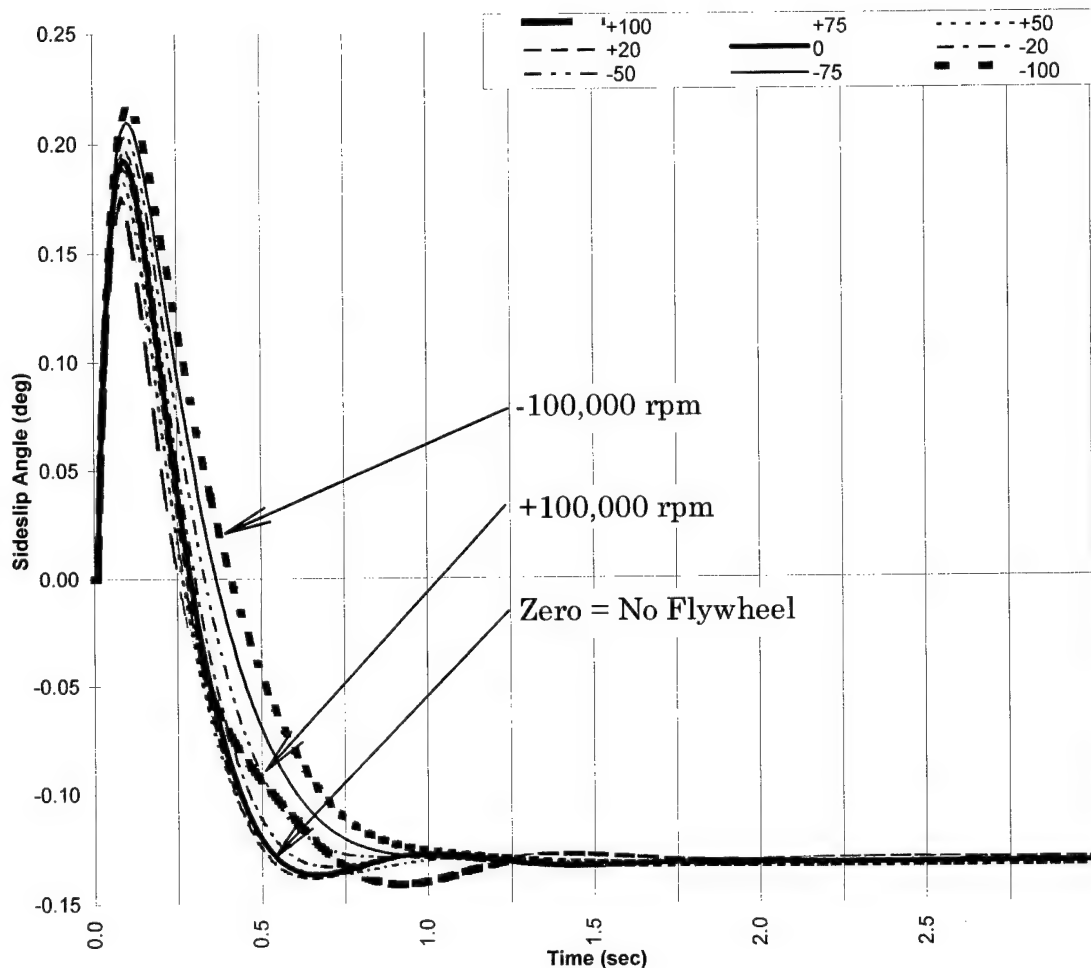


Figure 5.3 Y-Axis alignment - sideslip response

Orientation of the flywheel spin axis has minimal effect on the steady state value of sideslip angle, with the negative orientation slightly reducing the value, and the positive orientation slightly increasing it.

The transient response of the sideslip angle with the positive orientation of the flywheel moves the response toward that of a critically

damped system as the flywheel speed is made more positive, with the optimum value falling near 50,000 rpm. The no flywheel response is underdamped to begin with, and the positive orientation of the spin axis pushes the response of the system further in the underdamped direction, introducing more oscillation into the response and delaying the settling of the system. Reduction of the rise time in the sideslip parameter implies quicker handling of the vehicle. After the steer input, the vehicle begins to move laterally in less time for the positive orientation than for the negative. The longer settling time will result in a vehicle that feels unsettled. Fortunately, the differences in the results that have been generated in this simulation are very small, on the order of  $0.05^\circ$ , and are not significant for most practical purposes.

#### 5.2.3.2 Y-Axis Alignment Effects -Yaw Rate (r)

The yaw rate response of the system is gyroodynamically coupled with the roll rate response, and changing the orientation of the flywheel along the y-axis affects the yaw rate as shown in the Figure 5.4. The vehicle exhibits a near optimum yaw rate response without the inclusion of the flywheel. Any coupling that exists in the no-flywheel configuration must be due to coupling through the products of inertia, which are relatively small in this model.

Up to a speed of approximately 75,000 rpm, the effect of the positive orientation is to speed up the transient response, but overshoot of the steady state value occurs. At positive rotational speeds greater in magnitude than 75,000 rpm, the response curve dips back under that of the no-flywheel case resulting in a slower response and longer time until the steady state value is achieved.

The response with the negative orientation of the flywheel is slower for all values of flywheel speed. Addition of the flywheel to the vehicle system can only degrade the yaw rate response characteristics, resulting in reduced performance levels from the vehicle. In general, the effect of orienting the angular momentum vector along the negative y-axis would be to make the vehicle less responsive in yaw.

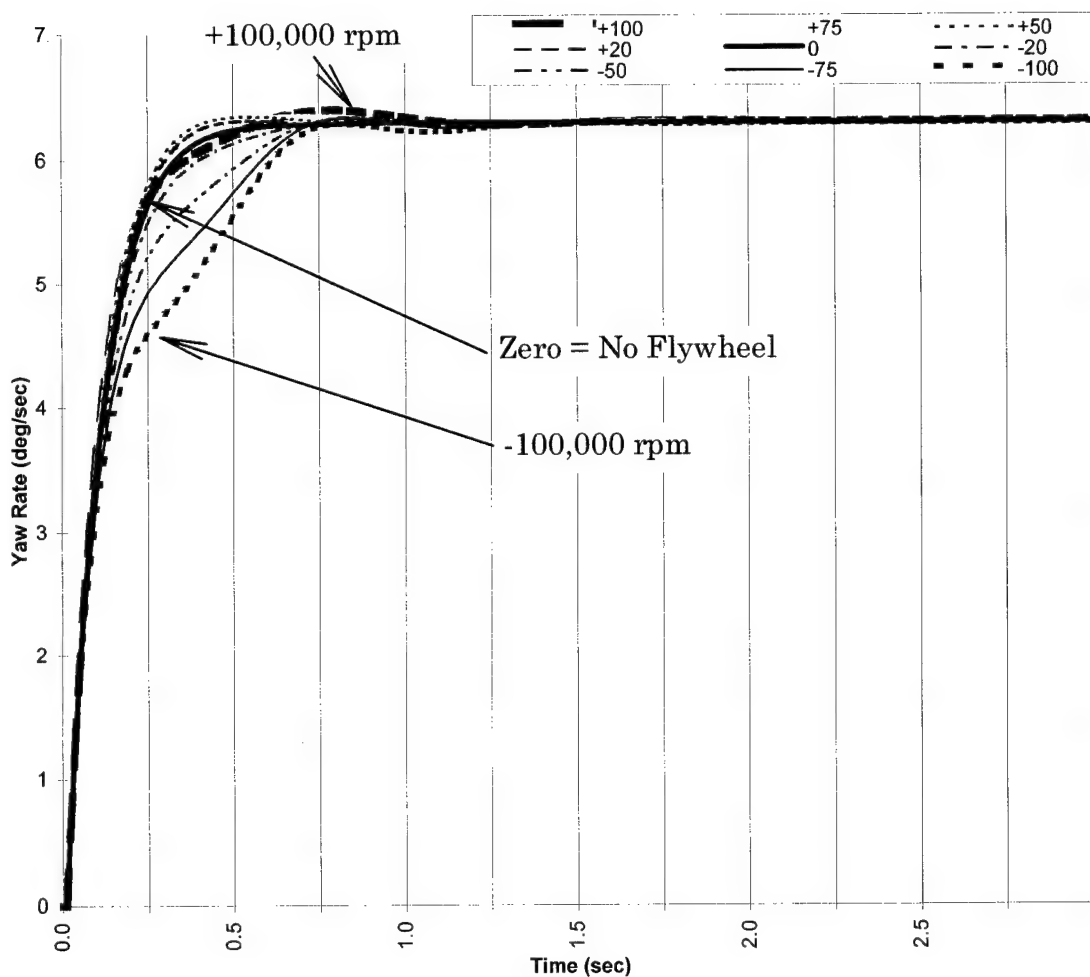


Figure 5.4 Y-Axis alignment - yaw rate response

### 5.2.3.3 Roll Yaw Coupling

The addition of the strong coupling of roll and yaw will result in changes in the response characteristics of both parameters. Figure 5.5 was generated without roll damping in the system to show the effects of the flywheel alone. The plot clearly shows that the oscillations in yaw rate are due completely to the presence of the flywheel, as there are no yaw rate oscillations in the no-flywheel case. In addition, this plot also shows that for a negative flywheel orientation, the roll and yaw rates are nearly in phase with one another, and for the positive orientation they are nearly 180° out of phase with one another.

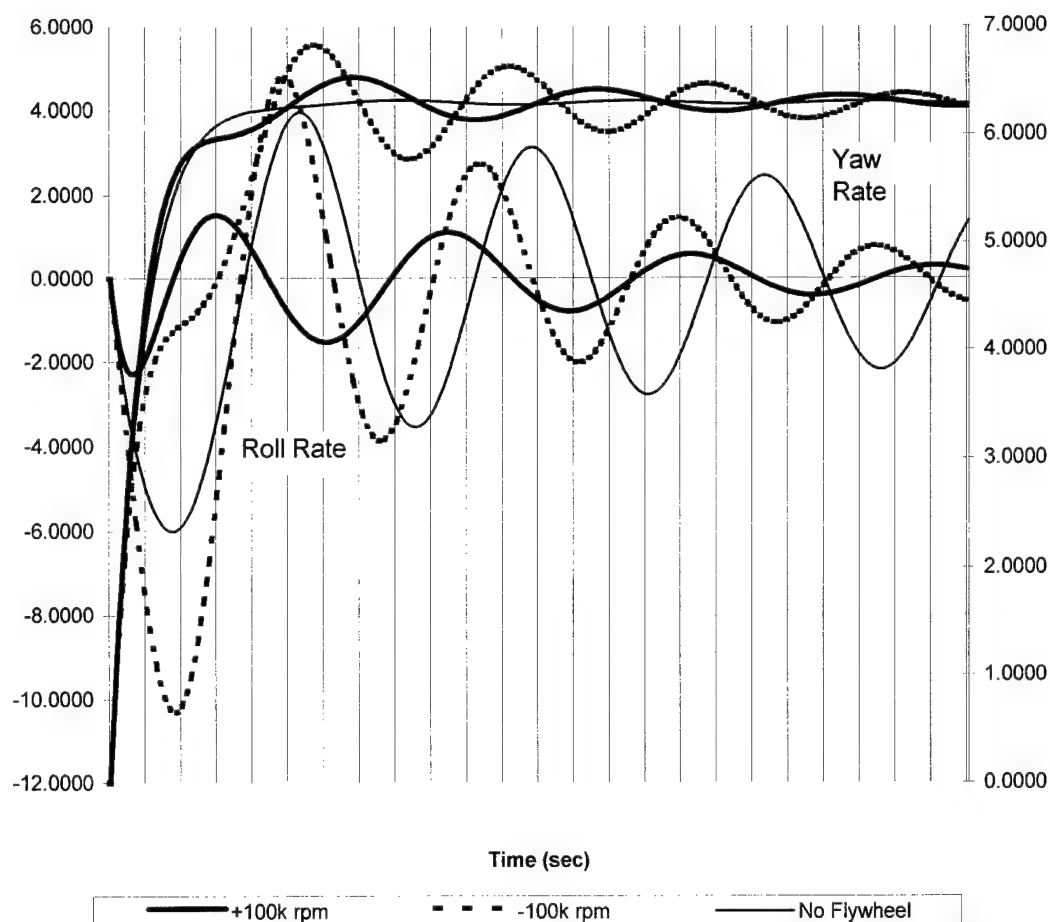


Figure 5.5 Y-Axis alignment - roll-yaw undamped response

These phase relationships can be understood by noting that yaw rate is a forcing function in this relationship, it is dictated by the direction of the turn. Positive steer angles result in positive yaw rates, this will couple with the negatively oriented flywheel to force the roll rate response in a negative sense based on the right hand rule and the axis orientation used in Table 5.2. This adds to the initial tendency of the sprung mass to roll in a negative sense resulting in an exaggerated roll rate amplitude and longer settling time. The positively oriented flywheel will couple with the yaw rate and tend to reduce the amplitude of oscillation and also appears to increase the frequency of oscillation. In the positively oriented case, the flywheel will oppose each roll oscillation thus damping the system more quickly.

#### 5.2.3.4 Y-Axis Alignment-Roll Effects

The effect of orienting the flywheel along the y-axis certainly has implications for the roll degree of freedom due to the direct gyrodynamic coupling between roll and yaw as discussed in the previous section. In the following sections, the individual effects on roll rate and the roll angle will be analyzed as well as the implications for the potential of the vehicle to rollover.

##### 5.2.3.4.1 Roll Rate(p)

One of the most dramatic effects of aligning the angular momentum vector of the flywheel with the y-axis became evident in the analysis of roll rate response. Figure 5.6 shows the effect induced by varying the rotational speed from -100,000 rpm to +100,000 rpm.

The data in Figure 5.6 shows that inclusion of the flywheel significantly affects the roll rate response of the vehicle. The vehicle without a flywheel exhibits a period of oscillation of 1.0 Hz, this is a commonly accepted target value for vehicle ride oscillations that is based on experimental data for driver comfort (Barak, 1991). The positive flywheel orientation maintains this target value, while the negative orientation reduces the period of oscillation by nearly 20%.

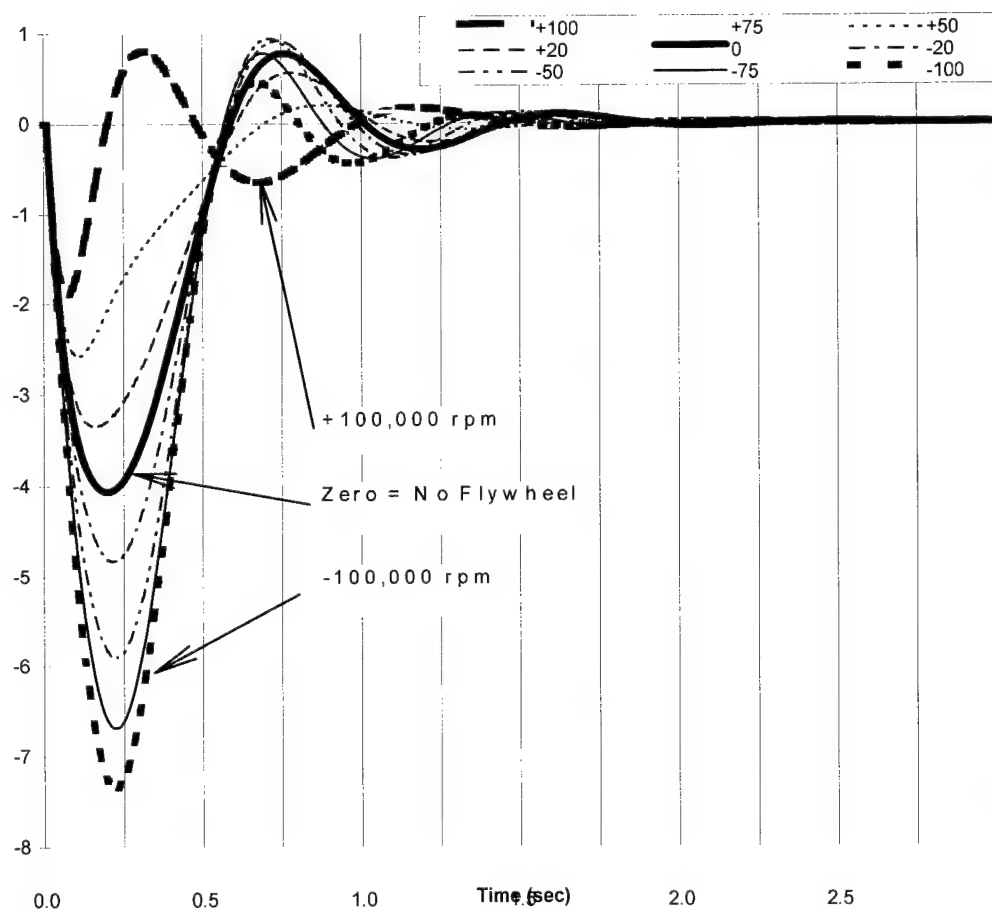


Figure 5.6 Y-Axis alignment - roll rate response

Looking at the response of the system, we can see the effect that the positive orientation has on decreasing both rise and settling times. The

positive orientation reduces the amplitude of the oscillations as well, resulting in lower peak roll rates. Lower rates translate to a more even loading of the tires, as the higher roll rates lead to inertial loading as the rotating mass must be slowed by the moments generated at the forces at the ground-tire interface.

Orienting the flywheel in the negative direction results in significantly larger roll rates and corresponding roll angles. The tire forces generated for such a configuration will show periodic behavior as a result of the roll oscillations, which will, in turn, affect the lateral acceleration and sideslip angles.

The roll rate response shows interesting possibilities from a design point of view. According to Gillespie (1992), roll control can be achieved through increased roll damping or through increased roll stiffness. By analyzing the portion of the graph corresponding to alignment along the positive y-axis, it can be seen that the flywheel has the effect of damping the suspension in roll. Conversely, by looking at the response to aligning the flywheel along the negative y-axis, it can be seen that the flywheel has the effect of reducing the roll stiffness of the suspension system. It is apparent that the flywheel adds to the overall roll damping and roll stiffness. For the suspension designer of future HEVs, this adds a new variable which may or may not be welcomed.

#### 5.2.3.4.2 Roll Angle( $\phi$ )

Figure 5.7 shows that varying the rotational speed of the flywheel from -100,000 rpm to 100,000 rpm has a significant effect on roll angle, both in the transient, and the steady state. The zero flywheel speed line on the graph

indicates the reaction of the vehicle if the flywheel were not present, and the reaction is underdamped.

Looking at the results in Figure 5.7, it is clear that the positive orientation of the flywheel reduces the transient and steady state roll angles. The steady state roll angle for the +100k rpm case is reduced to one fourth of the steady state value for the no-flywheel case. This reduction of the roll angle is equivalent to increasing the overall roll stiffness of the vehicle, leading to the potential to nearly eliminate roll all together if the roll stiffness of the vehicle and the operational speed range of the flywheel are designed properly.

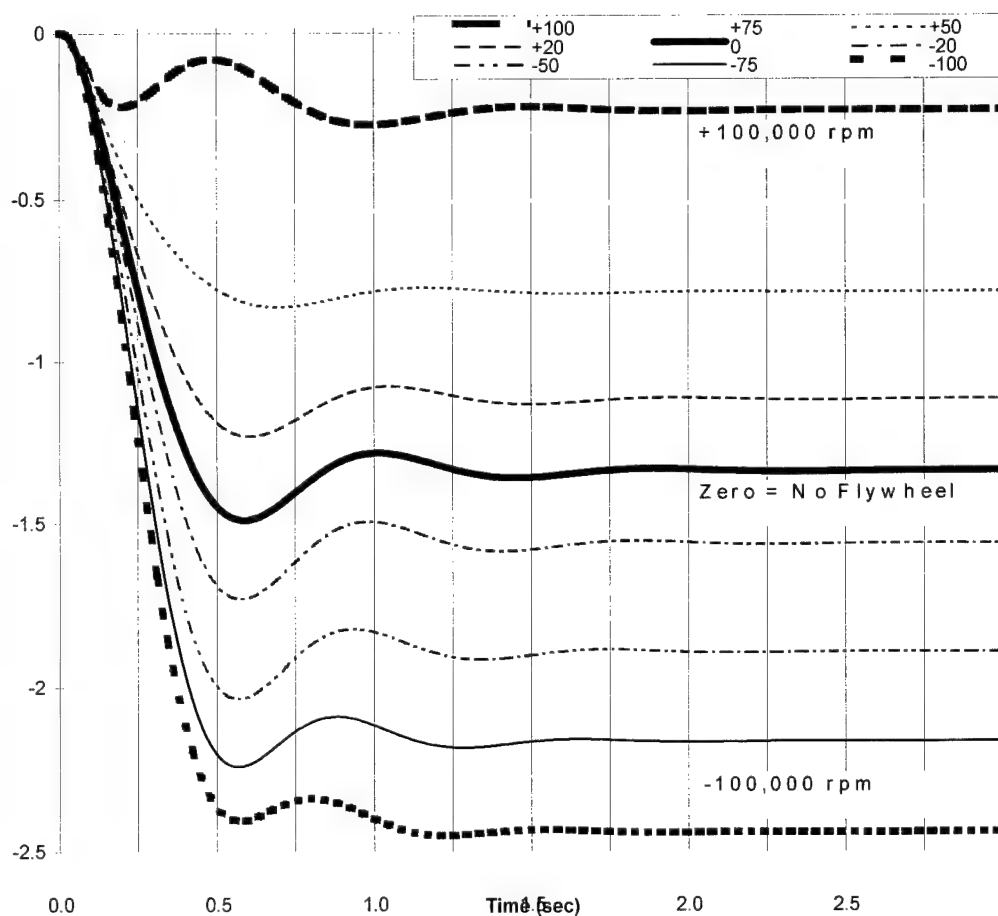


Figure 5.7 Y-Axis alignment - roll angle response

Orienting the flywheel in the negative direction has the opposite effect on the steady state roll angle, the effective roll stiffness of the vehicle suspension is reduced. The steady state roll angle is 50% greater than for the -100k rpm case, and would require increased roll stiffness to maintain the level of performance shown by the baseline vehicle without the flywheel.

#### 5.2.3.4.3 Roll Over Tendency

An additional consideration of including a flywheel in the energy system of a HEV is the possibility of vehicle rollover. Certain orientations of the flywheel exacerbate this situation. The x-axis and z-axis orientations have been shown to have no appreciable effect on handling, but the y-axis orientation is proving to have considerable impact on the handling characteristics of the vehicle, and rollover is should be addressed. If one looks at the Figure 5.7, it becomes apparent that as the flywheel speed is increased for the negative orientation, the vehicle rolls further and further for a given steer angle. Taken to the extreme, this relationship would roll the car over even at reasonable steer angle input levels. On the opposite side of the relationship, as the flywheel speed is increased in the positive direction, the roll angle for a given steer angle input is decreased. Taking this situation to the extreme results in a vehicle that leans "into" the corner in much the same manner as a motorcycle would.

From a tire performance perspective, having the vehicle remain flatter in a turn represents a desirable situation. The tires on either side of the vehicle see a more even distribution of vertical load, and respond with a more equal distribution of lateral forces as a result. The driver also benefits from

this situation, as the vehicle "feels" flatter without the exaggerated roll angle induced attitude experienced in a vehicle of lesser handling performance.

From a design standpoint, the roll response of the positive orientation of the flywheel has significant benefits over that of the negative orientation. The benefits include smaller roll rates and roll angles, flatter turns, and quicker response times, not to mention the rollover safety margin introduced. In the context of a racing or high performance environment, like that of the Patriot Race Car discussed earlier, the positive orientation of the flywheel would be preferred for roll control and handling.

#### 5.2.3.5 Y-Axis Alignment - Lateral Acceleration Effects

The effect of orienting the flywheel along the y-axis has implications for the steady state lateral acceleration, the results are shown in Figure 5.8. The lateral acceleration of the vehicle c.g. is given by the equation:

$$a_y = (\dot{\beta} + r)U_x + h\dot{p} \quad (5-3)$$

where the dotted terms are zero in the steady state, and the value of steady state yaw rate is given by:

$$r = \frac{U_x}{R} \quad (5-4)$$

leading to the familiar equation for centripetal acceleration given by:

$$a_y = \frac{U_x^2}{R} \quad (5-5)$$

This relationship implies the steady state lateral acceleration will be dependent on the steady state yaw rate, and any reduction in yaw rate will be seen in lateral acceleration.

The effect of the flywheel on lateral acceleration is similar to the effect noted for the yaw rate response. The transient response in lateral acceleration is coupled to all of the degrees of freedom of the model. Figure 5.8 shows that the response curve for the no-flywheel case has superior characteristics over the other two flywheel orientation cases.

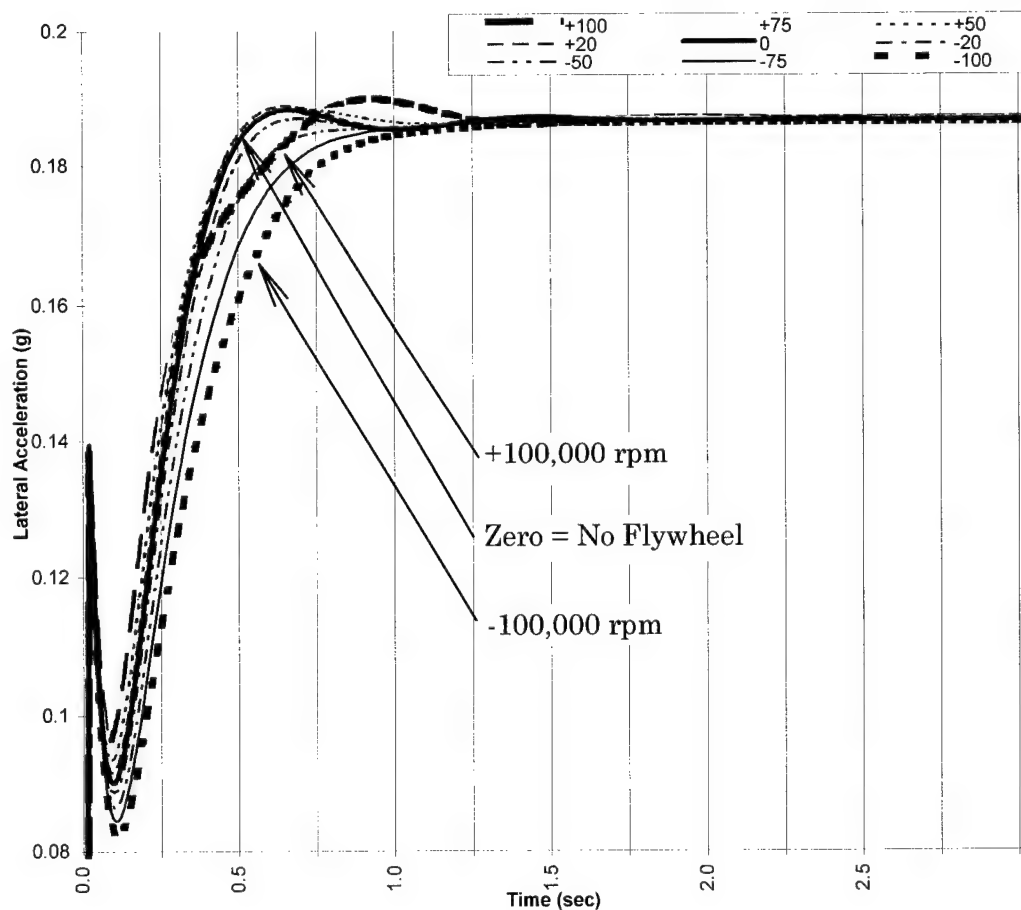


Figure 5.8 Y-Axis alignment - lateral acceleration response

The positive orientation produces a critically damped response near a flywheel speed of 75,000 rpm resulting in the quickest rise time, with no overshoot of the steady state value. The implication of this result is that the vehicle will respond more quickly and settle into its steady state lateral acceleration sooner resulting in a vehicle that is responsive and stable. The negative flywheel orientation has the effect of moving the damping of the system toward an over damped response. The rise time is increased, as is the settling time, resulting in a vehicle that feels less responsive but stable.

From a lateral acceleration performance perspective, the flywheel improves the responsiveness of the vehicle without the changing ride stiffness and damping rates.

#### 5.2.4 Symmetry of Gyrodynamic Effect

It must be noted that there is symmetry in the gyrodynamic effects of the flywheel on the measures of handling performance. For a given flywheel orientation, the response of the vehicle will be the same for both positive and negative steer angles. The reason for this relationship goes back to equation 4-2, shown here:

$$\bar{T} = \frac{\partial \bar{H}}{\partial t} = \bar{\dot{H}} = \bar{H} \times \bar{\Omega} \quad (5-6)$$

This equation represents the reaction torque that results when the angular momentum vector of the flywheel is precessed at the angular rate of  $\Omega$ . The sign of the reaction torque changes with the change in sign of the precession rate.

As an example, consider the results in Figure 5.12, where the imposed precession rate is the yaw rate of the vehicle. The torque that results from precessing a flywheel that has a positive y-axis orientation with a positive yaw rate,  $\Omega = r$ , is a positive roll torque. For the axis system in use, a positive yaw rate corresponds to a right hand turn, which naturally induces a negative roll angle. For this orientation of the flywheel, the roll angle of the vehicle will be reduced. The torque that results from precessing a flywheel that has a negative y-axis orientation with a negative yaw rate,  $\Omega = r$ , is a negative roll torque. A negative yaw rate corresponds to a left hand turn, which induces a positive roll angle, and the flywheel will once again reduce the roll angle of the vehicle. This result is consistent with the results produced in Scarborough's (1958) analysis of the monorail train in a curve.

The results shown in Figure 5.9 through Figure 5.13 illustrate the symmetry of response produced by the flywheel. The response for a given flywheel orientation will produce the same type of response whether turning left or right. Because of the symmetry of the response shown in the figures, it has only been necessary to investigate one step steer input to the vehicle, as the opposite steer input will produce the same form and magnitude of response as those shown in the previous section.

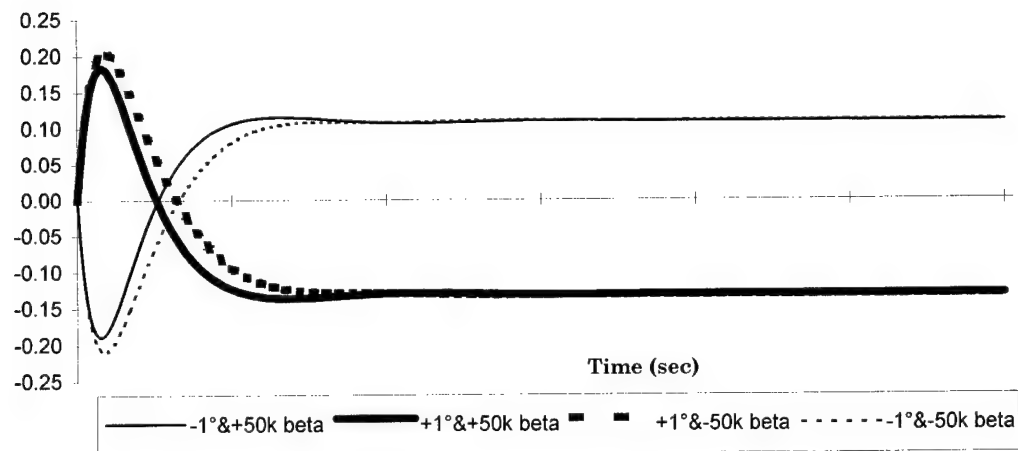


Figure 5.9 Y-Axis alignment - sideslip angle response for  $+1^\circ$  and  $-1^\circ$  steer angles

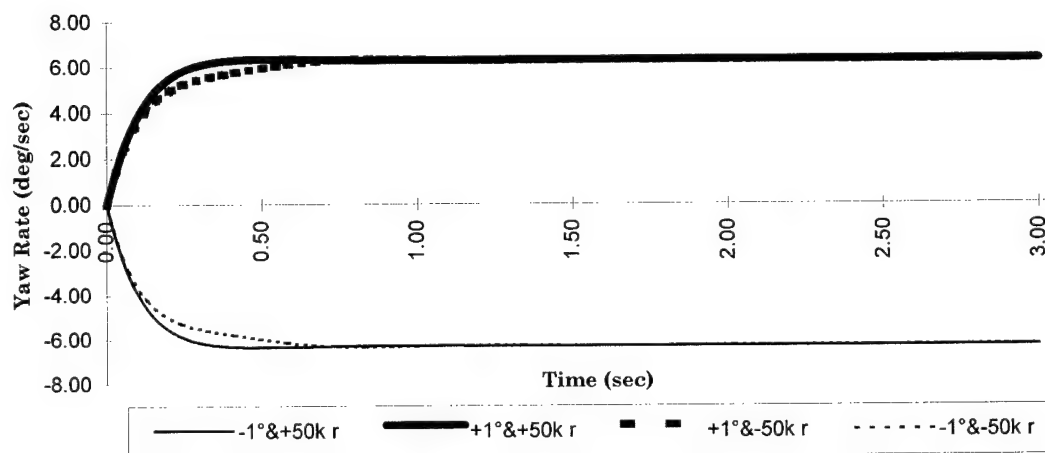


Figure 5.10 Y-Axis alignment - yaw rate response for  $+1^\circ$  and  $-1^\circ$  steer angles

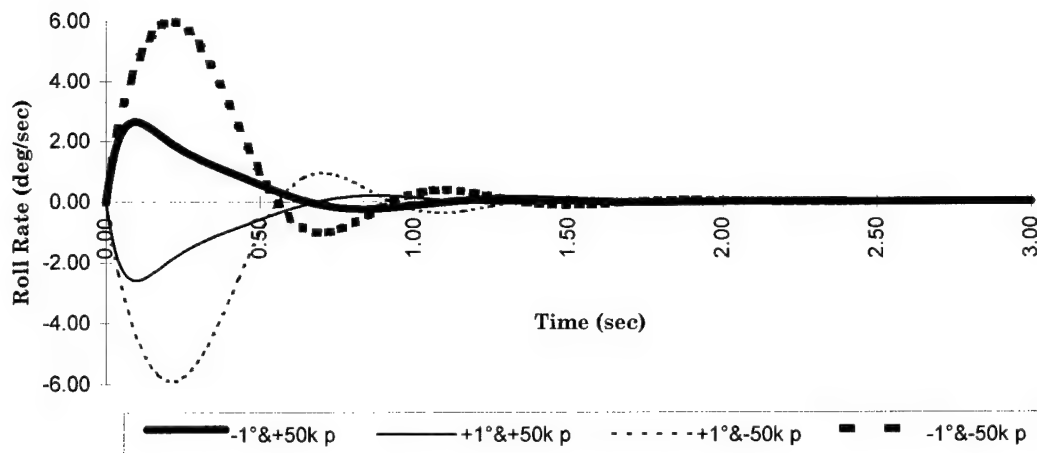


Figure 5.11 Y-Axis alignment - roll rate response for  $+1^\circ$  and  $-1^\circ$  steer angles

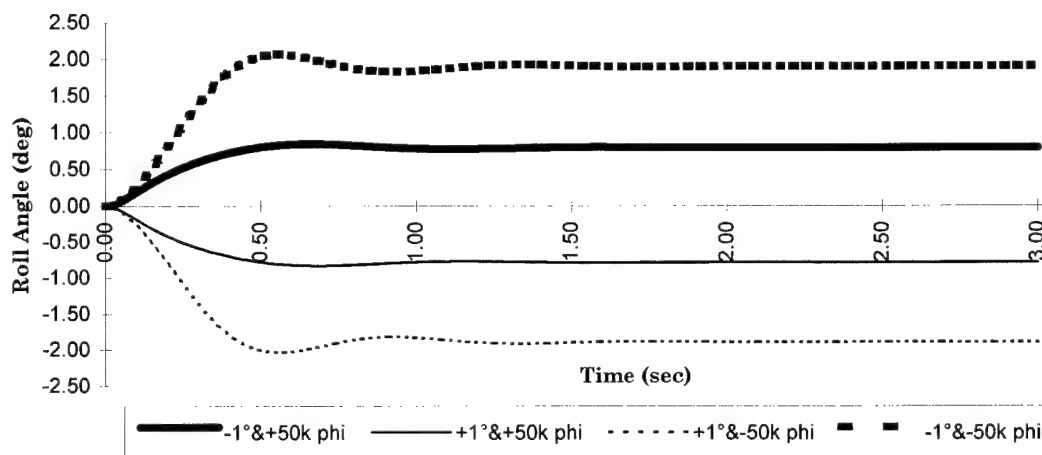


Figure 5.12 Y-Axis alignment - roll angle response for  $+1^\circ$  and  $-1^\circ$  steer angles

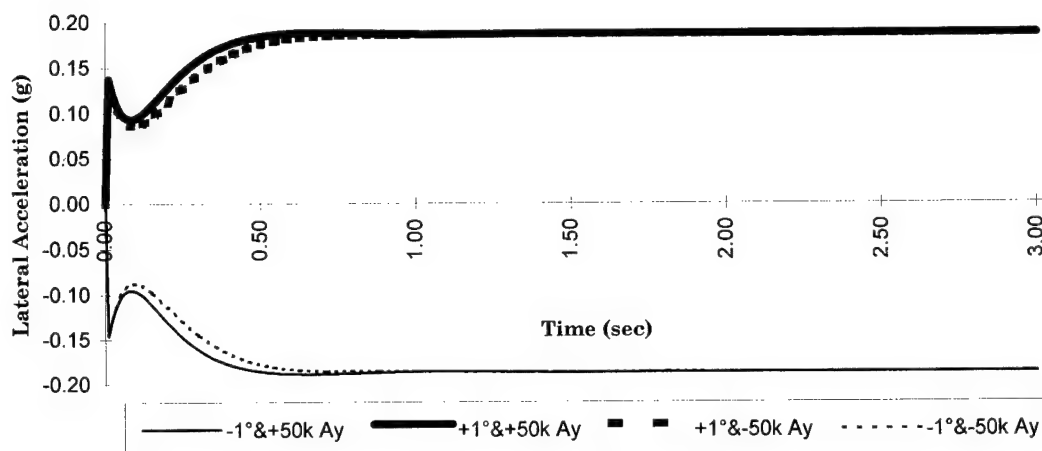


Figure 5.13 Y-Axis alignment - lateral acceleration response for  $+1^\circ$  and  $-1^\circ$  steer angles

### 5.3 Effect on Overall Damping Characteristics

Inclusion of the flywheel in the vehicle system has a dramatic effect on the damping characteristics of the system, especially where the roll degree of freedom is concerned. In the vehicle model, only roll damping is treated as a design parameter, but the coupling of the differential equations of motion ensures that affects will be seen in all vehicle handling measurements. For this reason, the investigation of the effect of the flywheel on the overall damping of the system will be limited to variation of the roll damping design parameter, but the effects on all output parameters will be analyzed.

#### 5.3.1 Variation of Roll Damping

As a design issue, damping is an important factor in the objective and subjective evaluation of the performance of a vehicle. One goal in attempting to optimize the directional response is to minimize the rise and settling times of the essential indices of handling performance. In this case, optimization involves determining the flywheel orientation and flywheel speed range that

provides the quickest response time, and the shortest settling time for the indices of interest.

Often in design, optimization is carried out among a mix of competing interests. Vehicle handling is no exception to this paradox, where handling and ride performance are often at odds with one another during the design and optimization process. To improve handling responsiveness, the designer desires to increase the roll stiffness and roll damping, but these changes come at the expense of increased ride harshness, noise, and vibration (Barak, 1991). Thus far, the flywheel has shown potential for affecting the damped response of the vehicle without the tradeoffs associated with the changes of spring and damping rates already discussed.

In attempting to optimize the rise and settling times of the handling variables of this work, the roll damping of the vehicle was varied from that of the baseline configuration discussed earlier. The baseline values were first adjusted downward to one half their value, then adjusted upward from the baseline in increments of whole values of the baseline damping. The sensitivity of each of the handling indices to roll damping changes was then evaluated over this range. In the plots of the next paragraphs, the independent variable is the non-dimensional angular momentum ratio. The equation for the ratio is:

$$\text{Angular Momentum Ratio} = \frac{I_{fw}\omega}{I_{zz}r}, \quad (5-7)$$

where:

$I_{fw}$  = moment of inertia of the flywheel,

$I_{zz}$  = moment of inertia of the vehicle about the z-axis,

$\omega$  = angular rate of the flywheel,

$r$  = steady state yaw rate of the vehicle for the turn.

The data on the plots correspond to flywheel angular speeds that range from -100,000 rpm to +100,000 rpm. An alternate index would be to use the ratio of kinetic energies of the two bodies. In either case, the goal is to present the data using an index that is applicable across a wider range of vehicle and flywheel combinations than the one investigated in this work.

#### 5.3.1.1 Sideslip Angle

Initially, the relationship between roll damping and sideslip angle shown in Figure 5.14 appears to have some interesting characteristics, but closer analysis of the sideslip angle data reveals the differences are not as significant as they appear. The difference between remaining in the  $\pm 5^\circ$  deadband and leaving it is on the order of  $0.001^\circ$ . The differences are illustrated in Figure 5.15 where the roll damping is varied for a fixed flywheel speed. The system with lower damping does indeed oscillate more, but stays within the deadband, while the more highly damped system oscillates less but goes out of the deadband in the process. Regardless of the reaction, the magnitude of the difference is, for all practical purposes, insignificant, but the positive orientation is clearly favored.

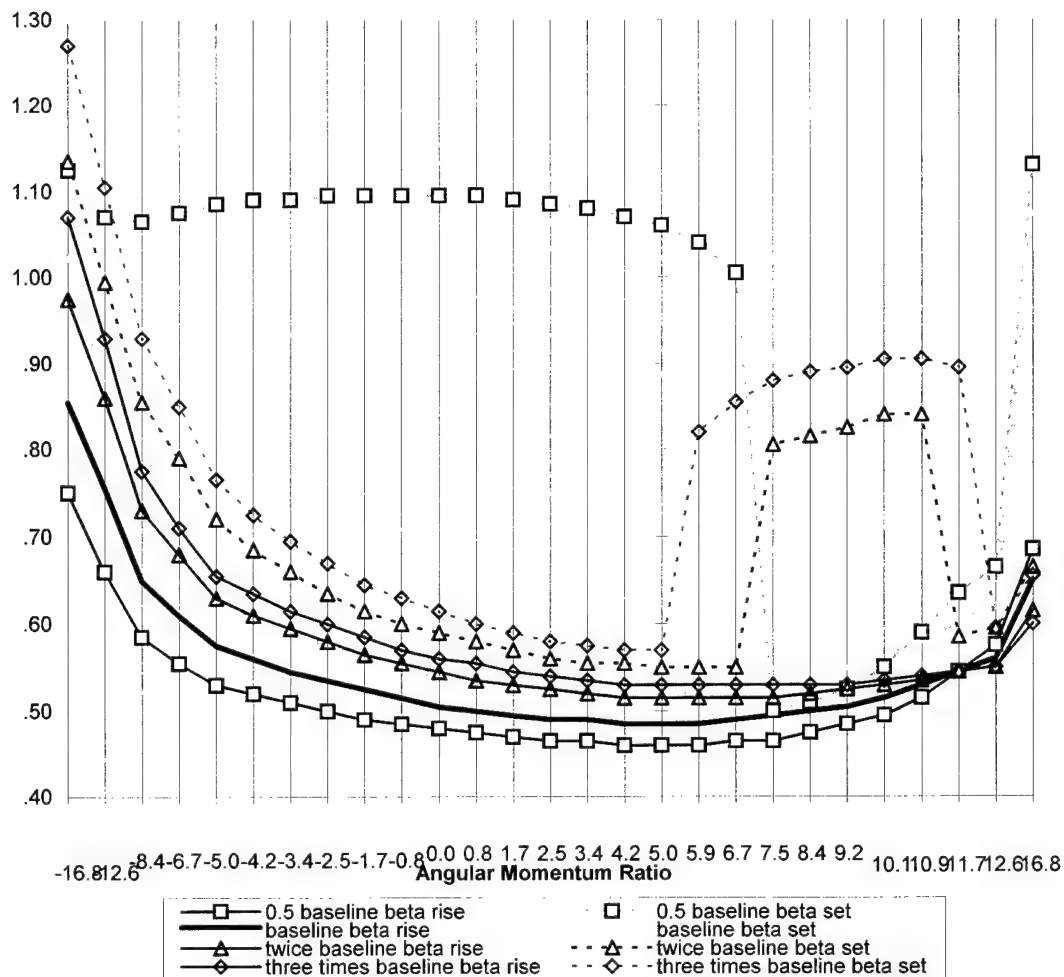


Figure 5.14 Y-Axis alignment - variation of roll damping - sideslip angle response times

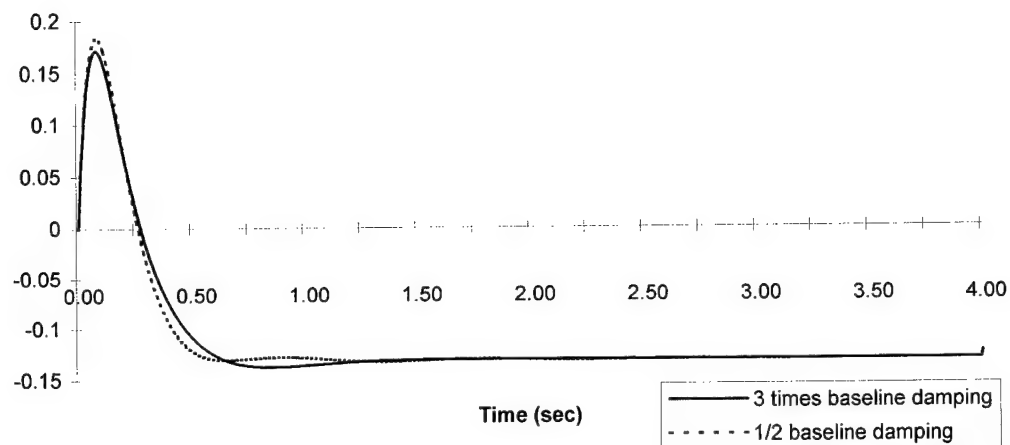


Figure 5.15 Variation of roll damping - sideslip angle illustration of in/out of deadband

#### 5.3.1.2 Yaw Rate

The data in the plot for yaw rate (Figure 5.16) shows that the response times are nearly independent of roll damping, but clearly show a bias toward faster response times for the positive flywheel orientation. In addition, the less damped case produces quicker settling times with the positive flywheel orientation, and longer settling times with negative flywheel orientation. Finally, the outer reaches of the plots show some non-linearity in the relationship between yaw rate and flywheel speed, especially on the side of negative orientation of the flywheel.

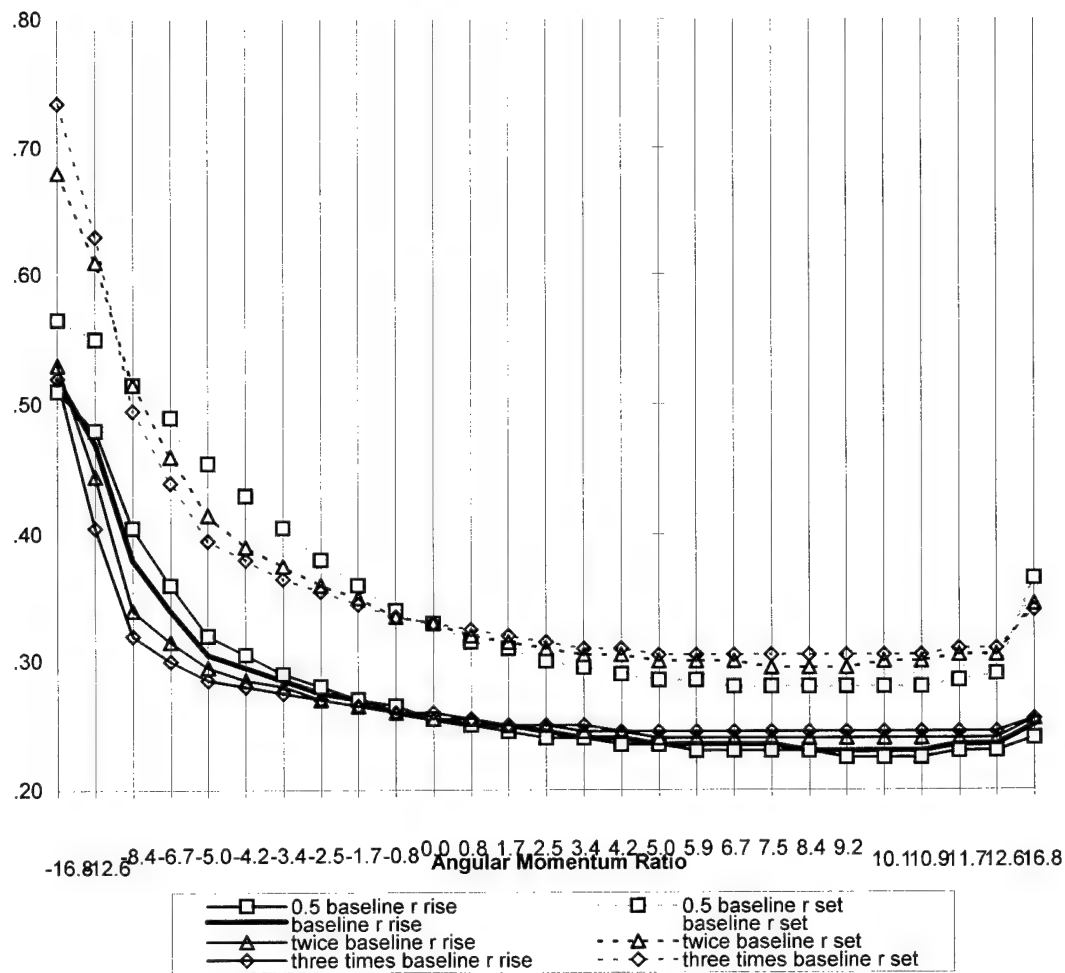


Figure 5.16 Y-Axis alignment - variation of roll damping - yaw rate response times

The reduced settling times for positive orientation of the flywheel are the result of the roll-yaw coupling produced by the flywheel.

### 5.3.1.3 Roll Angle

The roll angle plot shows an interesting result. The data shows that both system response times can be reduced by reducing the value of roll damping in the system, but this is only true for flywheel speeds over a range of 10,000 rpm. This is clearly the result of the presence of the flywheel, as

the system does not respond in the same manner when the flywheel is removed (angular momentum ratio = 0).

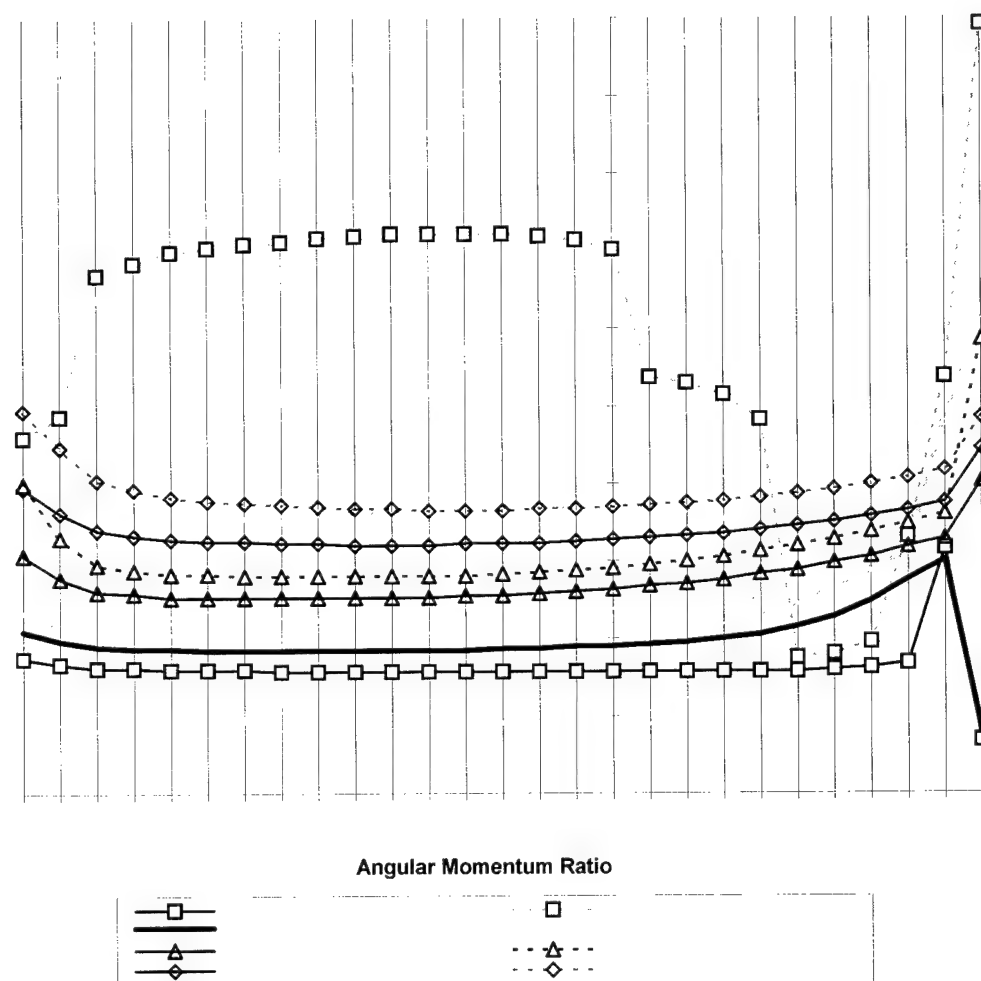


Figure 5.17 Y-Axis alignment - variation of roll damping - roll angle response times

The presence of the flywheel in the system creates a region of critical damping for this configuration of the vehicle system. If the flywheel could be designed so that the principal operating range is within this 10,000 rpm wide range, the roll rate response could be optimized strictly through the use of the flywheel. The draw back to this approach arises when the flywheel is outside this range resulting in a vehicle with very slow response times. From

the flatness of the curves, it is apparent that the roll angle response is relatively insensitive to the flywheel speed.

#### 5.3.1.4 Lateral Acceleration

Lateral acceleration shows a linear relationship between roll damping and response time, with a clear bias toward faster response with the positive orientation of the flywheel. The data show a relationship that favors the lower roll damping value for both rise and settling times, as the oscillations in the data for the less damped case are small enough that they never exceed the  $\pm 5^\circ$  deadband for steady state lateral acceleration.

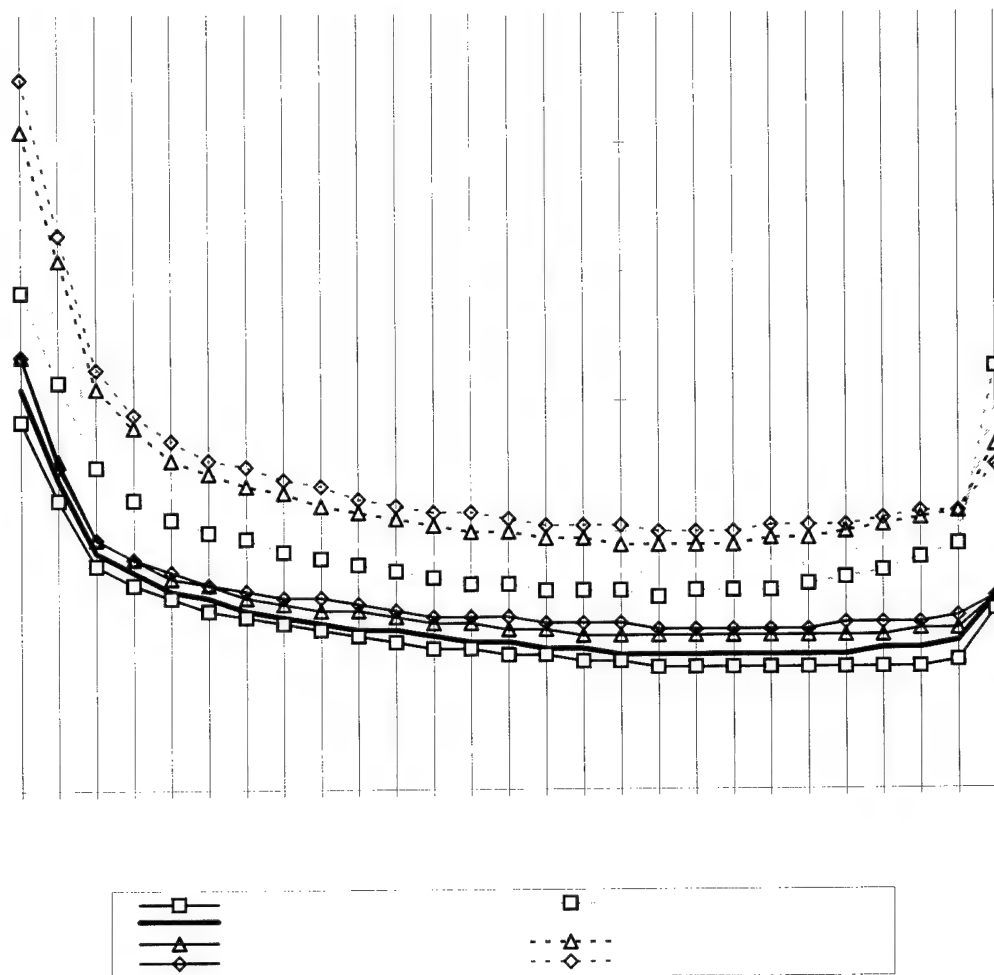


Figure 5.18 Y-Axis alignment - variation of roll damping - lateral acceleration response times

In three out of the four cases analyzed, roll rate, lateral acceleration, and sideslip angle, the reduction of roll damping of the vehicle resulted in optimal response times for the vehicle when subjected to a  $1^\circ$  step steer input. Carrying this result to the extreme, leads to the removal of all roll damping.

### 5.3.2 Roll Damping Removed

The removal of all roll damping allows the roll damping effects of the flywheel to be highlighted. Removing all the roll damping is equivalent to removing the shock absorbers and all other sources of friction in the suspension system. This is obviously an ideal case that can not be recreated in a vehicle, but the results are interesting none the less. When roll damping is removed from the model, the oscillations seen in the degrees of freedom still exhibit a damped response (see Figure 5.5).

The damping exhibited in Figure 5.19 comes as a result of the coupling between roll and yaw that has been described in an earlier section, and is carried out through the tire model at the contact between the tire and the road. As the vehicle turns and oscillates, it scrubs off energy through the non-conservative action of slip at the wheels. The chart above shows the damped oscillations of the roll rate degree of freedom. The decay of the amplitude of oscillation is given by the exponential equation:

$$x = x_1 e^{-\xi \omega_n t} \sin(\omega_d t) \quad (5-8)$$

describes the shape and amplitude of the response of a damped vibratory system. The damping ratio,  $\xi$ , can be calculated using the logarithmic decrement approach:

$$\xi = \frac{1}{2\pi} \ln \left( \frac{x_1}{x_n} \right) \quad (5-9)$$

where:

$x_1$  = amplitude of first peak in interval

$x_n$  = amplitude of last peak in interval

$n$  = number of peaks in the interval

The interval used to compute the logarithmic decrement is not constrained to begin at the first maxima, the interval may begin at any point along the time axis, and may contain as many or as few subsequent peaks as desired.

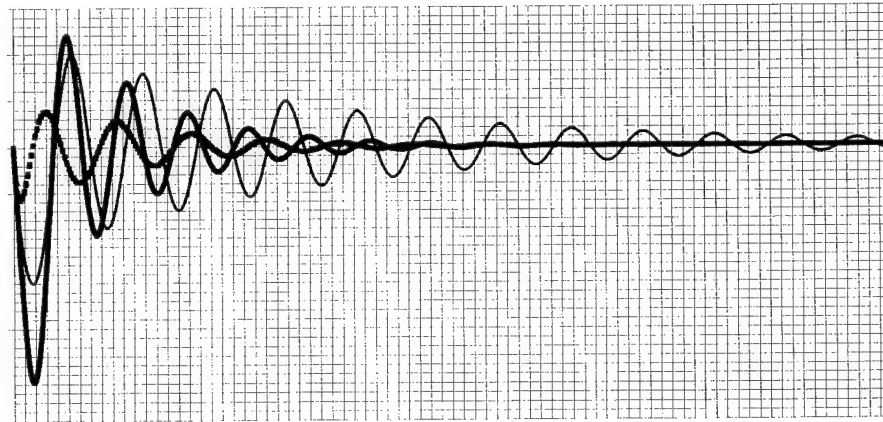


Figure 5.19 Y-Axis alignment - variation of flywheel orientation - roll rate damped response

Roll rate has been chosen for the analysis because of the oscillatory response that it exhibited in section 5.2.3.4.1. Using the logarithmic decrement approach, the damping ratios for the three plots shown in Figure 5.19 are given in Table 5.3.

Table 5.3 Calculated roll rate damping due to flywheel

Flywheel Speed	n	$\xi$	% Change from 0 rpm
+100,000 rpm	6	0.0780	144.16
0 rpm	6	0.0320	0.0
-100,000 rpm	6	0.0819	155.94

#### 5.4 Effect on Understeer Coefficient

Understeer coefficient explains how the steer angle of a vehicle must be changed in response to changes in turn radius or lateral acceleration. The vehicle modeled in this investigation is understeer, with a  $K_{us}$  of approximately 0.5 deg/g. This means that the vehicle will require more steering angle input to maintain a constant radius turn as lateral acceleration is increased. Lateral acceleration is increased by increasing longitudinal velocity of the vehicle, or by decreasing the radius of curvature or the turn.

In general, the understeer coefficient is treated as a steady state measure of vehicle handling, but it has transient response implications as well. The response of a vehicle to steering angle input is composed of reactions at the front and rear wheels that are very distinct from one another. The front wheels receive the initial input from the steering mechanism and begin to generate lateral force based on a build up of slip angle at the front contact patch. This force is transmitted through the linkages and bushings of the front suspension to the chassis. The chassis transmits the input to the rear suspension, and the rear wheels begin to generate lateral force as a result of slip angle at the rear contact patch.

The feel that the vehicle transmits to the driver during this transient period of the maneuver can be quantified by the transient understeer coefficient. The transient understeer coefficient is defined here by the following equation:

$$\frac{\delta}{\delta_{ss}} = \frac{K_{us}}{K_{us} + 1} \quad (5-10)$$

where:

$a_y$  = lateral acceleration

$\alpha_f$  = slip angle at the front

$\alpha_r$  = slip angle at the rear.

The terms used in the calculation are extracted from the results of the simulations. The results of the calculation are shown in Figure 5.20, where it is evident that the addition of the flywheel has a definite effect on the transient values of the understeer coefficient, but almost no effect on the steady state value.

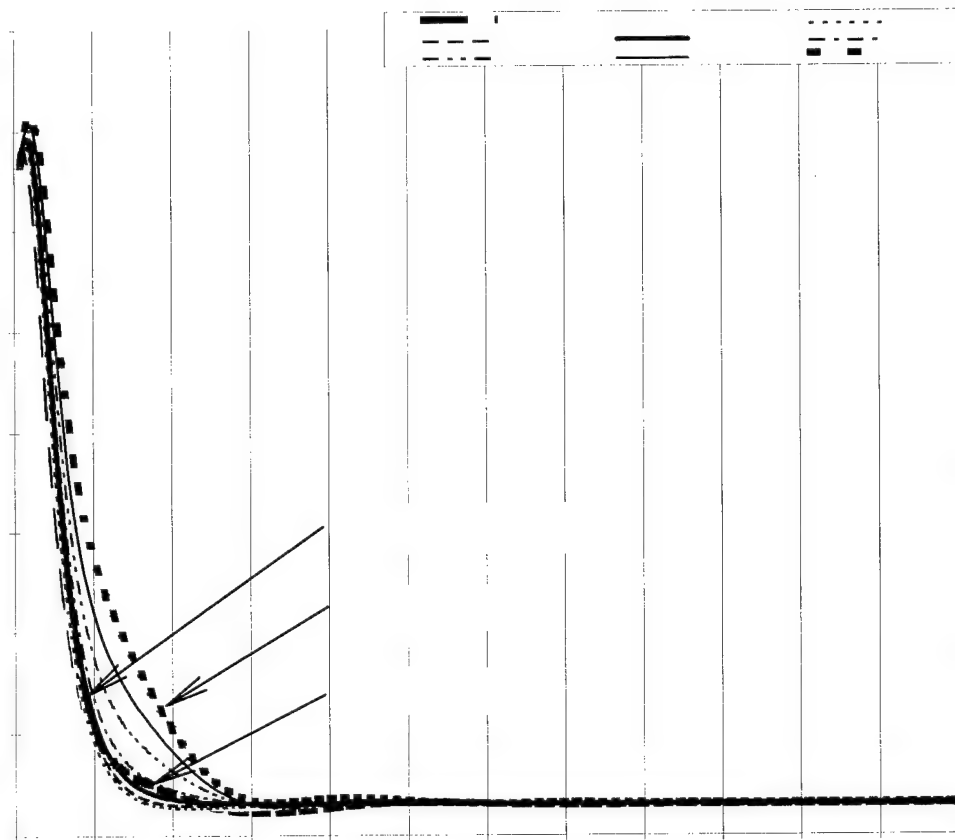


Figure 5.20 Y-Axis alignment - transient understeer coefficient response

As with the other measures of handling, alignment of the spin axis of the flywheel along the  $x$  and  $z$  axes had no apparent effect on the transient understeer coefficient (see Figure 5.21 and Figure 5.22). The  $y$ -axis alignment, on the other hand, had a pronounced effect. Within the  $y$ -axis alignment, the orientation of the flywheel is important in ascertaining the effect of  $K_{us}$ . The positive orientation shows little effect, while the negative orientation tends to raise the transient value of  $K_{us}$ , making the vehicle tend to "push" as the turn is initiated. Push refers to the propensity of a vehicle to continue to move with the original heading for a longer period of time than expected by the driver, and occurs when the slip angle at the rear builds up slowly (the front builds slip instantly with the steer angle). The speed with which the rear wheel builds slip angle is a complex relationship, that may depend upon the roll-yaw coupling of the flywheel, or possibly the damping effect that the flywheel has on roll, and thus lateral weight transfer. The exact relationship is an area worthy of further study.



Figure 5.21 X-Axis alignment - transient understeer coefficient response

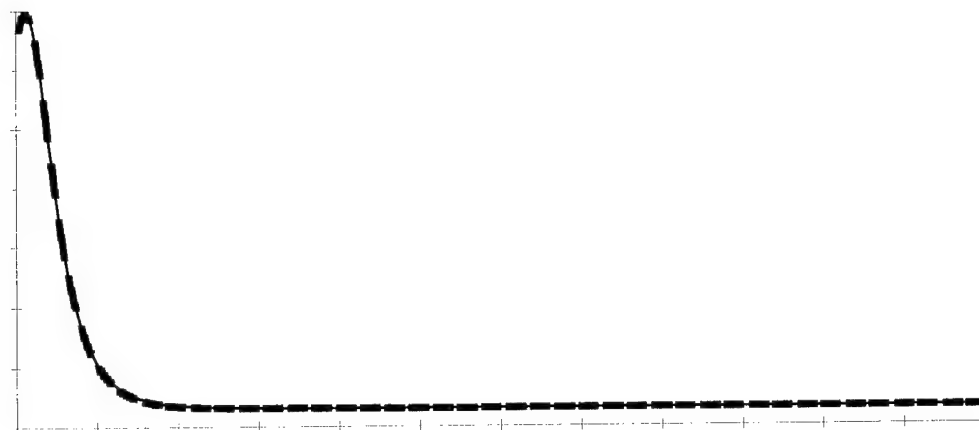


Figure 5.22 Z-Axis alignment - transient understeer coefficient response

### 5.5 Closure

In this chapter, a baseline HEV that uses an energy storage flywheel has been defined, and the results of a handling simulation have been presented for that baseline HEV. The results have been presented based on various orientations of the flywheel within the vehicle, using a full range of flywheel speeds. The data has been analyzed both objectively and subjectively to determine the types of handling effects that could be expected from a HEV of this particular configuration.

Vehicle response data has been presented that is based on various roll stiffness values, as well as various vehicle angular momentum and flywheel angular momentum values. The intent of the presentation method is to put the data in a format that makes it applicable to a broader range of vehicle configurations than the one used in this investigation. The results indicate that alignment of the spin axis of the flywheel with the y-axis of the vehicle significantly effects transient behavior, and can be treated as additional

damping in the system. In addition, the effects of orientation of the flywheel spin axis on rollover has been addressed.

Finally, the effect of the angular momentum of the flywheel on the transient understeer coefficient was investigated. The results indicate that the flywheel contributes significantly to the overall transient response of the vehicle by reducing the responsiveness of the vehicle in the period of time between initiation of a maneuver, and reaching the steady state turn.

## CHAPTER 6

### SUMMARY AND CONCLUSIONS

#### 6.1 Summary

The overall purpose of this thesis was to investigate the vehicle handling implications of including an energy storage flywheel in a hybrid-electric vehicle. The need for this investigation was driven by the desire to understand the nature of the interaction between the angular momentum of the flywheel and vehicle handling.

To clearly understand the problem, it was necessary to review the current state of technology in the field of HEV. This review highlighted the need for continued research and development in a wide range of areas relating to HEV. Paramount to the success of HEV is the development of a reliable and efficient temporary energy storage device. The need for a temporary energy storage device is driven by the desire to recover kinetic energy that would otherwise be lost as heat in the brake system. Thus, regenerative braking is one of the key concepts for making the HEV a viable alternative to the current state of the automotive art.

Three fundamentally different technologies are currently competing to become the primary energy storage device used in future HEV. These technologies are the chemical battery, the ultracapacitor, and the flywheel. The flywheel has shown considerable promise as an energy storage device

because of its high energy density and compact size, especially when compared to the chemical batteries that are currently available. The use of flywheels in personal transportation vehicles has created several safety concerns, including the gyrodynamic effect that results from the precession of a spinning flywheel, the problem of flywheel burst containment, and the interaction of the road and the flywheel through the chassis of the vehicle. The first of these concerns has been the subject of this work.

To understand the dynamic interaction between the vehicle and the flywheel, a model was developed. Model development was preceded by a thorough review of the standard techniques for the development of vehicle and tire models. The importance of the tire model cannot be overstated. The fidelity of the vehicle model is only as good as the model of the interaction between the tire and the road. The tire model provides the forcing function to the vehicle system.

The vehicle is modeled as a four-wheeled system with three degrees of freedom. The degrees of freedom are the sideslip angle, the roll rate, and the yaw rate. Contained in the sideslip degree of freedom is the roll angle, while the sideslip angle gives insight into the relationship between forward and lateral velocity. The model is based on a set of coupled, non-linear, differential equations. The equations are solved numerically using a Runge-Kutta integration scheme. The tire model is based on empirical data derived test data for a *Firestone* P215/70R-14 tire. The model uses a set of five 10<sup>th</sup> order polynomials representing lateral force as a function of slip angle. Each equation is valid for a discrete vertical load on the tire. The vertical load ranges from 400 lb to 2800 lb in 600 lb increments. Wheel loads that fall between these discrete values are interpolated assuming a quadratic relationship.

Validation of the vehicle model is accomplished using two separate methods. The first method involves comparing the analytic solution for the

steady state response of a vehicle against the steady state results obtained from the simulations. The second method compares the simulation results from the bicycle model to the simulation results of the four-wheeled model of this thesis, both vehicle models use a linear tire model in this set of simulations. The tire model is validated by comparing the results generated by the stand-alone tire model against the empirical tire data used to generate the equations of the tire model. Once the validation process was completed, the model was exercised using vehicle design data based on the goals of the Partnership for a New Generation of Vehicles.

The format used to present the results is based on the orientation of the angular momentum vector of the flywheel, and the rotational speed of the flywheel. The angular momentum vector of the flywheel is aligned along the three body-fixed axes of the vehicle, considering both positive and negative orientations in each case. The analysis is focused on qualitatively evaluating the gross effects of flywheel inertia on the handling properties of the vehicle. Each of the indices of vehicle handling performance is evaluated individually. Finally, the effect on overall handling is evaluated through the evaluation of the transient understeer coefficient. This handling performance indicator combines the effects of slip at the wheels with the lateral acceleration to give insight into the nature of the transient response of the vehicle.

## 6.2 Conclusions

Considering the results presented in Chapter 5, many conclusions can be drawn concerning the interaction of the flywheel with the handling properties of the vehicle.

- (1) Aligning the angular momentum vector of the flywheel along the x-axis and along the z-axis has little effect on the overall directional response of

the vehicle. However, these alignments are likely to affect the ride performance of the vehicle.

(2) Aligning the angular momentum vector of the flywheel along the y-axis has a significant effect on several of the measures of handling performance. The measures most affected by the y-axis alignment are roll rate, and roll angle.

(a) Roll Rate Effects:

- Orienting the angular momentum vector along the negative y-axis reduced the roll rate period slightly relative to the baseline vehicle, and increased the roll damping but reduced the roll stiffness.
- Orienting the angular momentum vector along the positive y-axis increased the roll stiffness, and increased the roll damping.

(b) Roll Angle Effects:

- Orienting the angular momentum vector along the positive y-axis reduced the transient and steady state values of roll angle.
- Orienting the angular momentum vector along the negative y-axis dramatically increased the transient and steady state roll angles

(3) The increase in roll angle associated with the negative orientation of the flywheel is of particular interest. Increased roll angles are associated with vehicle rollover. For this reason, the negative orientation of the flywheel is not an attractive option from a vehicle safety point of view.

(4) Aligning the spin axis of the flywheel with the vehicle y-axis introduces damping. Table 6.1 summarizes the results of the study of the effects of this flywheel orientation. In this study, vehicle suspension damping was set to zero to isolate the damping effects of the flywheel.

Clearly the y-axis alignment of the flywheel can have significant effects on the handling of the vehicle, and future studies may provide further insight into other effects as well.

Table 6.1 Qualitative effects of y-axis flywheel alignment

Parameter	Characteristic	Spin Axis Orientation	Effect on Characteristic
Sideslip	Damping	both	increased
	Period	negative positive	decreased increased
Yaw Rate	Damping	both	decreased (weak dependence on flywheel speed)
	Period	negative positive	decreased same
Roll Rate	Damping	both	increased
	Period	negative positive	decreased same
Roll Angle	Damping	both	increased
	Period	negative positive	decreased same
	Stiffness	negative positive	decreased increased
Lateral Acceleration	Damping	both	increased
	Period	negative positive	same increased

### 6.3 Recommendations

One reason for choosing a y-axis alignment might be to simplify the powertrain of the vehicle in which the flywheel is mounted. The

simplification depends upon the way the flywheel will be used. If the flywheel is physically coupled to the drivetrain by gears or a variable ratio transmission, then the flywheel must be aligned with these components, otherwise angled drive gears must be used to incorporate the flywheel into the drivetrain. Front wheel drive is the most prevalent drivetrain configuration in use today. The powertrain is mounted transversely in front wheel drive vehicles, and the flywheel would most conveniently be mounted with its spin axis along the y-axis when used in this situation. In this case, the flywheel should be aligned with the angular momentum vector aligned along the positive y-axis.

The flywheel alignment problem is simplified when the flywheel is used as an electromechanical battery. In this configuration, the only physical connections between the flywheel and the rest of the drivetrain are those required to electrically couple the two systems. In these situations, the spin axis of the flywheel may be aligned in any manner that is consistent with the overall packaging constraints of the vehicle design. The ideal mounting scheme in this situation would be to use a gimbaled mounting system that would allow the gyrodynamic effects of the flywheel on the vehicle to be negated.

#### 6.4 Future Efforts

One area that has not been addressed in this thesis is the effect that noise, vibration and harshness (NVH) have on the flywheel. This is an area of research that must be addressed in order for the flywheel to become a viable energy storage device in HEV. The motivation for investigating NVH and the flywheel is the use of magnetic bearings to mount the flywheel in the containment vessel.

An area of research that would be a direct extension of this work is the investigation of the forces and moments that are imposed on the flywheel during vehicle maneuvers. The force calculations would be based on knowledge of specific flywheel design parameters coupled with the detailed moment calculations provided by the vehicle model of this thesis. A complete understanding of this problem is necessary to prevent the potentially catastrophic consequences of contact between the spinning flywheel and the containment vessel. Knowledge of these imposed forces is also critical to the design of highly efficient magnetic bearings which reduce the parasitic losses.

Addition of the pitch degree of freedom to the vehicle model would be a logical extension of this work into the field of ride simulation. The gyrodynamic effects of the flywheel due to the pitch-roll and pitch-yaw coupling of the flywheel may prove to be of interest in the frequency response area of vehicle ride simulation. The results of this work indicate gyrodynamic damping and stiffness effects occur in roll and yaw and should show similar effects in pitch as well. Thus, inclusion of the pitch degree of freedom would allow a more detailed study of the effects of x-axis and z-axis flywheel alignments.

Another application of this work is to investigate the motion of a gimbaled flywheel assembly as flywheel speed is varied. This study would address the phenomenon of gyroscopic whirl that arises when energy is rapidly added to or removed from the spinning flywheel.

## LIST OF REFERENCES

- Aceves, Salvador M., Smith, J. Ray, 1995, "A Hybrid Vehicle Evaluation Code and Its Application to Vehicle Design," SAE Paper no. 950491, Society of Automotive Engineers, Warrendale, PA.
- Alstead, Chris J., Whitehead, John P., 1994, "Steering and Suspension Development of Road Vehicles, *Vehicle-Road Interaction, ASTM STP 1225*, B.T. Kulakowski, Ed., American Society for Testing and Materials, Philadelphia, 1994, pp. 173-182.
- Anerdi, G., Brusaglino, G., 1994, "Technology Potential of Flywheel Storage and Application Impact on Electric Vehicles," 12th International Electric Vehicle Symposium (EVS-12), v. 1, pp. 37-47.
- Arnold, Ronald N., 1962, "Gyroscopic Vibration Absorbers and Stabilizers," Gyrodynamics, IUTAM Symposium Celerina, August 20-23, 1962, Springer-Verlag, Berlin, GDR.
- Bernard, J. I., Segel, L., Wild, R. E., "Tire Shear Force Generation During Combined Steering and Braking Maneuvers," SAE Paper no. 770852, Society of Automotive Engineers, Warrendale, PA.
- Brooke, Lindsay, 1994, "Patriot Games," *AUTOMOTIVE INDUSTRIES*, February 1994, pp 114-116
- Barak, Pinhas, 1991, "Magic Numbers in Design of Suspensions for Passenger Cars," SAE Paper no. 911921, Society of Automotive Engineers, Warrendale, PA.
- CARB, 1996, Staff Report: "Initial Statement of Rulemaking: Proposed Amendments to the Zero-Emission Vehicle Requirements for passenger cars and light-duty trucks," Feb. 9, 1996, Section 4.3, pg. 21.
- Chen, Fred H., Guenther, Dennis A., 1991, "The effects of Suspension Stiffness on Handling Responses," SAE Paper no. 911928, Society of Automotive Engineers, Warrendale, PA.

- DeLisle, J.E., Ogletree, E.G., Hildebrant, B.M., 1964, "The Application of Gyrostabilizers to Orbiting Vehicles," *Torques and Attitude Sensing in Earth Satellites*, Academic Press, New York, NY.
- Dorf, Richard C., 1989, *Modern Control Systems-5th Edition*, Addison-Wesley Publishing Co., Reading MA.
- Dugoff, H. Fancher, P. S. and Segel, L., 1970, "An analysis of tire traction properties and their influence on vehicle dynamic performance, *SAE Transactions*, Paper 700377.
- Durisek, Nicholas J., Heydinger, Gary J., Chrstos, Jeffery P., Guenther, Dennis A., "Non-Rigid Body Product of Inertia Measurement: Application to Land Vehicles," Transportation Systems American Society of Mechanical Engineers, Dynamic Systems and Control Division (Publication) DSC 54 1994. ASME, New York, NY, USA. p 375-386.
- El-Gindy, M., Ilosvai, L., 1983, "Computer simulation study on a vehicle's directional response in some severe manoeuvres - Part 1: Rapid lane change manoeuvres," *Int. J. of Vehicle Design*, vol. 4, no. 4, pp. 386-401.
- El-Nasher, M. A., 1994, "Computer Tire Simulation for Automobile Handling," SERA-Vol. 2, Safety Engineering and Risk Analysis 1994, American Society of Mechanical Engineers, New York, NY.
- Flanagan, R. C., Keating, M., 1990, "Evaluation of a Flywheel Hybrid Electric Vehicle Drive," IECEC, 1990.
- Flanagan, R. C., Aleong, C., Anderson, W., Olberman, J., 1990, "Design of a Flywheel Surge Power Unit for Electric Vehicle Drives," IECEC, 1990.
- Ford, 1996, "Vehicle Specifications, Ford Taurus," *Ford Motor Company Home Page*, <http://www.ford.com/vehicles/taurus/P51a/index.html>, Accessed 1 Nov. 1996.

- Frik, S., Leister, G., Schwartz, W., 1993, "Simulation of the IAVSD Road Vehicle Benchmark Bombardier Iltis with FASIM, MEDYNA NEWEUL and SIMPACK," *Multibody Computer Codes in Vehicle System Dynamics*, Supplement to *Vehicle Systems Dynamics*, Volume 22, Swets & Zeitlinger, Berwyn, PA.
- Gillespie, Thomas D., 1992, *Fundamentals of Vehicle Dynamics*, SAE Publications Group, Warrendale, PA.
- Hoffman, Joe D., 1992, *Numerical Methods For Engineers And Scientists*, McGraw-Hill, Inc., New York, NY.
- Jayaraman, C. P., Kirk, J. A., Anand, D.K., Anjanappa, M., 1991, "Rotor Dynamics of Flywheel Energy Storage Systems," *Journal of Solar Energy Engineering*, Feb. 1991, Volume 113.
- Jost, Kevin, 1994, "The Patriot's Hybrid-Electric Drivetrain," *AUTOMOTIVE ENGINEERING*, December 1994, pp 30-33.
- Lorentzen, Randy, 1996, "Inside the Dodge Intrepid ESX Hybrid-Drive Sport Sedan of the 21st Century," *MOTOR TREND*, April 1996, pp 30-35.
- Mason, W.T., Kristiansson, U., 1994, "Hybrid EVs versus Pure EVs: Which Gives Greater Benefits?," SAE paper no. 94C017, pp. 135-149.
- MATLAB, 1991, *The Student Edition of MATLAB*, by The MATH WORKS Inc., Natick, MA.
- McDonald, Alan T., 1980, "Simplified Gyrodynamics of Road Vehicles With High-Energy Flywheels," *Proceedings of the 1980 Flywheel Technology Symposium*, Scottsdale, Az, Oct 1980.
- Morse, Phillip R., 1995, "Development and Verification of a Force-Based Roll Center Model for Vehicle Suspensions," Masters Thesis, Purdue University, West Lafayette, IN.

- Pacejka, H.B., Bakker, E., 1993, "The Magic Tyre Formula," *Tyre Models for Vehicle Dynamics Analysis: Proceedings of the 1st International Colloquium on Tyre Models for Vehicle Dynamics Analysis*, ed. Hans B. Pacejka, Swets & Zeitlinger Inc., Berwyn, PA.
- Patil, G. P., 1996, "Alternative Fuels in Future Vehicles," *AUTOMOTIVE ENGINEERING*, Jan. 1996.
- Post, R. F., Bender, D. A., Merritt, B. T., 1994, "Electromechanical Battery Program at the Lawrence Livermore National Laboratory," AIAA Paper no. AIAA-94-4083-CP.
- SAE, "Vehicle Dynamics Terminology," SAE J670e, Society of Automotive Engineers, Warrendale, PA.
- Scarborough, James R., 1958, *The Gyroscope Theory and Applications*, Interscience Publishers, Inc., New York, NY.
- Schreiber, J. G., Shaltens, R. K., Beremand, D. G., 1993, "Evaluation of a Free-Piston Stirling Power Converter for the Ultra-Low Emission Hybrid Vehicle Application," SAE Paper no. 930047, Society of Automotive Engineers, Warrendale, PA.
- Schröder, C., Chung, L., 1995, "Influence of Tire Characteristic Properties on the Vehicle Lateral Transient Response," *Tire Science and Technology*, TSTCA, Vol. 23, No. 2, April-June 1995, pp 72-95.
- Scott, William, B., 1995, "Satellite control Concepts Bolster Civil, Defense Systems," *Aviation Week & Space Technology*, March 6, 1996.
- Segel, Leonard, 1956, "Theoretical Prediction and Experimental Substantiation of the Response of the Automobile to Steering Control," *Research in Automobile Stability and Control*, The Institution of Mechanical Engineers, England, 1956.
- Starkey, John M., 1995, *Fundamentals of Vehicle Dynamics*, Class notes, Purdue University School of Mechanical Engineering, ME 565, West Lafayette, IN.

- Starkey, J. M., "the Effects of Vehicle Design Parameters on Handling Frequency Response Characteristics," *International Journal of Vehicle Design*, Vol. 14, nos. 5/6, pp 497-510.
- Trom, J. D., Lopez, J. L., Vanderploeg, M. J., 1986, "Modeling of a Mid-Size Passenger Car Using Multibody Dynamics Program," ASME Paper 86-DET-39, Presented at the Design Engineering Technical Conference, Oct. 5-8, 1986, Columbus OH.
- van Oosten, J. J. M., Bakker, E., "Determination of Magic Tyre Formula Parameters," *Tyre Models for Vehicle Dynamics Analysis: Proceedings of the 1st International Colloquium on Tyre Models for Vehicle Dynamics Analysis*, ed. Hans B. Pacejka, Swets & Zeitlinger Inc., Berwyn, PA.
- Wipke, Keith, 1994, "Current Hybrid Electric Vehicle Performance Based on Temporal Data from the World's Largest HEV Fleet," *Proceedings of the 12th Intl. Electric Vehicle Symposium*, Anaheim, Ca, December 5-7, 1994
- Wong, J. Y., 1978, *Theory of Ground Vehicles*, Wiley Interscience, New York, NY.
- Yamaguchi, K., Moroto, S., Kobayashi, K., Kawamoto, M., Miyaishi, Y., 1996, "Development of a New Hybrid System - Dual System," SAE Paper no. 960231, Society of Automotive Engineers, Warrendale, PA.